Theoretical studies of EELS in carbon structures

Nobuyuki Fujita

Submitted for the Degree of Master of Philosophy

University of York

Department of Physics

October 2012

Abstract

Graphene nano-ribbons (GNRs) are promising materials for applications in the field of nanotechnology, which requires detailed control of the material at the atomic level. Therefore, a detailed characterisation with atomic resolution is essential. Recently, the improvements of Electron Energy Loss Spectroscopy (EELS) technique made observation of electronic states in a single atom possible. The interpretation of EELS spectra is through fingerprint matching compared to the spectrum from the reference material, however, so far there is no report to indicate the detailed spectral feature based on systematic investigation for the EELS spectra of GNRs. In this project, in order to demonstrate the characteristic spectral features for fingerprint, *ab initio* EELS calculations for GNRs were performed for different atomic sites, edge shapes, ribbon widths and edge modifications. As a result, theoretical EELS spectra showed the different spectral features for each condition. These relations indicate it is possible to convert experimental data into the local atomic arrangement and chemical-bonding states in GNRs.

Contents

List of figures

List of tables

Acknowledgements

I am truly grateful to numerous people who have helped and encouraged me for my study at the University of York.

First, I owe my deep gratitude to my advisor Dr. Matt Probert for all his guidance and support on not only my study but also my life here. He has always been a great example of passionate and inspiring researcher to me.

I would also like to thank Dr. Phil Hasnip for his constant support. He helped me every time with all kind of problems, physical or non-physical.

I have furthermore to thank Professor Jun Yuan. He also helped my research and encouraged me. In particular, I have got a lot of useful advice from an experimental point of view.

I would like to thank Jolyon Aarons. He supported me a lot in my research work. I was not able to proceed my research smoothly without the presence of him.

I gratefully acknowledge financial supports from CANON.

It was a great pleasure for me to spend last two years with wonderful people in this department.

Finally, my deepest gratitude goes to my family.

Declaration

I declare that work presented in this thesis, except otherwise stated, is based on my own research and has not been submitted previously for a degree in this or any other university.

Signed

Nobuyuki Fujita

1. Introduction

1.1. Previous study of GNRs

Graphene is a carbon material that is only one atom thick and the basic structural element of all other graphitic materials such as carbon nanotubes, and fullerenes. If graphene is rounded into a cylindrical shape, it will be a carbon nanotube. If graphene is rolled into a spherical shape, it will be a fullerene. In recent years, the biggest attention is focused on graphene. This is because graphene have the highest mechanical strength [1], extraordinary high thermal conductivity [2] and ultrahigh carrier mobility [3]. In particular, graphene is a zero-gap semiconductor [4] and is expected to be a technological alternative to silicon semiconductors. For semiconducting application, band-gap opening is required. One of the solutions is cutting graphene into narrow strips, which is known as graphene nano-ribbons (GNRs). GNRs are promising materials in the field of nanotechnology and the properties of GNRs are known to be sensitive to local atomic configurations [5] [6] [7]. Therefore elemental identification and electronic state analysis at the atomic scale is becoming increasingly important. So far, the atomic configurations at graphene edges have been investigated by transmission electron microscopy [8] [9] and scanning probe techniques [10], but the electronic properties of these edge states have not yet been determined with atomic resolution.

1.2. State-of-the-art approach to the electronic states

Electron Energy Loss Spectroscopy (EELS) is an effective approach to investigate the electronic structure of carbon materials with high spatial and energy resolution. EELS is a spectroscopic technique to obtain structural, chemical and electronic information about a sample in the STEM (Scanning Transmission Electron Microscope). Figure 1.1 shows a schematic diagram of a STEM-based EELS system. The electron beam passes through the sample and some of the electrons interact with the sample. The total amount of energy loss is measured as Electron Energy Loss Spectrum. Fine structure in an EELS spectrum originates from the transition from a core level to unoccupied states. This is known as Energy Loss Near Edge Structure (ELNES). It includes the detailed information of an electronic structure of a material.

Recently, an experimental study of atom-by-atom EELS measurements for graphene edges was reported [11]. Using low-voltage aberration-corrected STEM, they obtained the single-atom spectrum successfully without damaging the specimen by the electron beam. As a result, the detection of different electronic states in individual carbon atoms has become possible. They showed that the EELS spectrum of each carbon atom depends on the local atomic structure as seen in Figure 1.2(d). In particular, they showed that EELS peaks sensitively reflect the electronic states derived from the local atomic structure in the edge sites. In order to understand these spectra accurately, the support from the theoretical calculations are needed. In particular, comparing several theoretical spectra which have been collected systematically will be an

extremely effective method to interpret the detailed information, such as the atomic structure and electronic states from the spectrum.

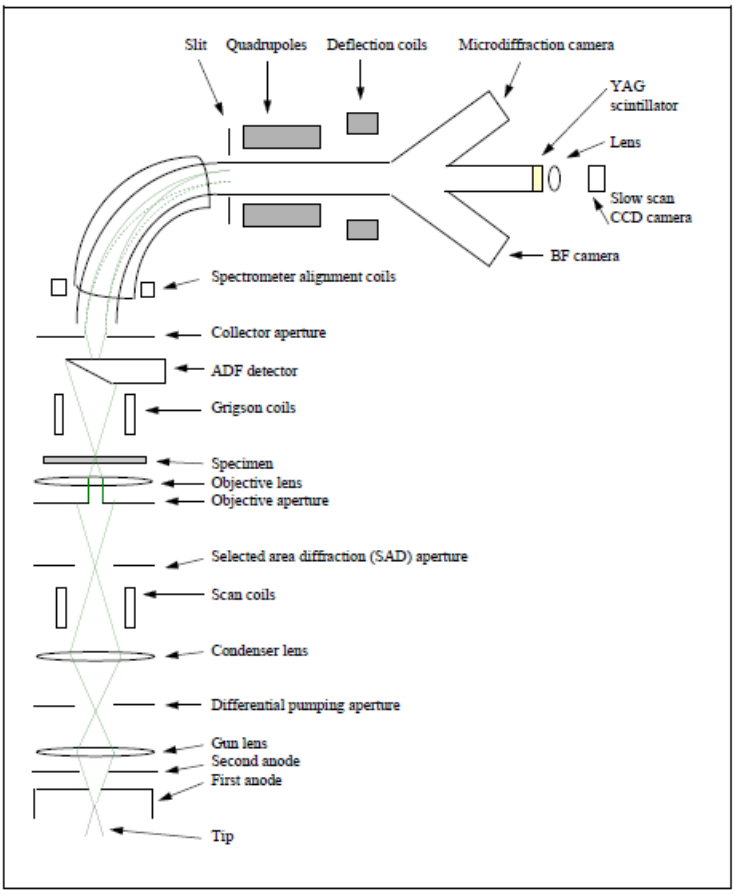

Figure 1.1: Schematic diagram of STEM-based EELS system [12]

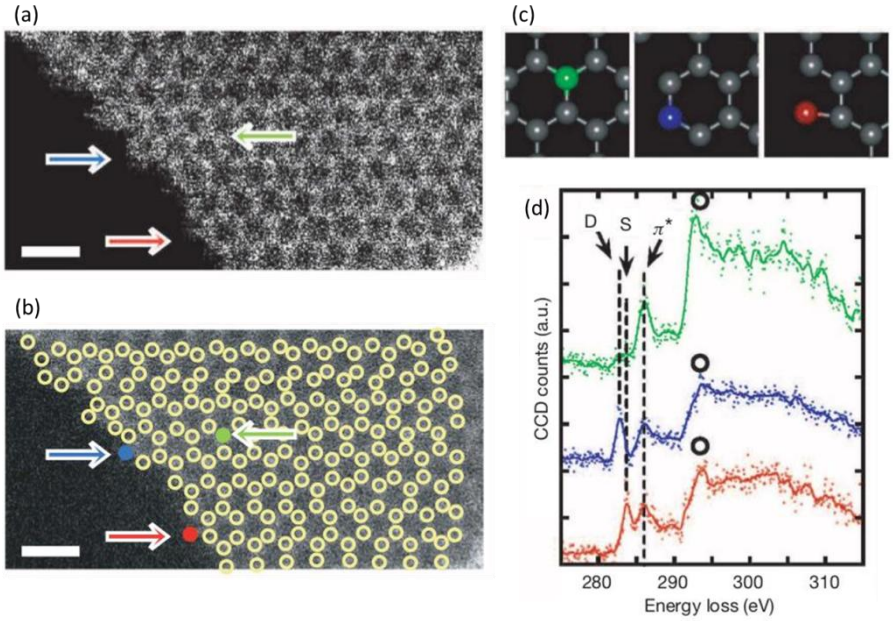

Figure 1.2: Graphene edge spectroscopy [11]. (a) ADF image of single graphene layer at the edge region, and (b)atomic positions are marked by circles in a smoothed image. Scale bars are 0.5nm. (d)ELNES of carbon K(1s) spectra taken at the colour-coordinated atom, respectively. These different states of atomic coordination are marked by coloured arrows in (a) and (b) and illustrated in (c).

1.3. Purpose of this study

In this project, we calculate theoretical EELS by means of the CASTEP first-principles modelling code [13] and show that the spectral feature depend on edge shape, ribbon width, atomic site and chemical modification. Moreover, we clarify that the EELS data obtained systematically can be used as a fingerprint of the GNRs. These data will be able to contribute to the analysis of future experimental work on GNRs and also expected to help the material design of the electronic device based on GNRs.

2. Basic Theory

This chapter outlines the methods required of theoretical EELS calculation. First, the relationship between the EELS signal and the electronic state calculations is discussed. Next, Density Functional Theory (DFT) used for the electronic state calculations is presented. The DFT code used in this thesis is CASTEP, which uses a plane-wave pseudopotential code and employs periodic boundary conditions.

2.1. CASTEP EELS

The EELS spectra are obtained from the partial differential cross section $\frac{d^2\sigma}{d\Omega \mathrm{dE}}$ which is expressed as [14]

$$\frac{d^2\sigma}{d\Omega \mathrm{dE}} = \frac{1}{(\pi e a_0)^2}\frac{1}{q^2} Im\left\{\frac{-1}{\varepsilon(q,\omega)}\right\} \qquad (2.1)$$

where $Im\left\{\frac{-1}{\varepsilon(q,\omega)}\right\}$ represent the loss function including information about the energy loss process for an electron. $\varepsilon(q,\omega)$ is the dielectric function, and q and ω are the momentum and angular frequency of the scattered electron, respectively. $d\Omega$ is the sold angle, e is the electron charge and a_0 is the Bohr radius. The loss function can be described as following:

$$Im\left\{\frac{-1}{\varepsilon(q,\omega)}\right\} = \frac{\varepsilon_2(q,\omega)}{\varepsilon_1(q,\omega)^2 + \varepsilon_2(q,\omega)^2} \tag{2.2}$$

where $\varepsilon_1(q,\omega)$ is the real part and $\varepsilon_2(q,\omega)$ is the imaginary part of the dielectric function. In the energy region of the core-level excitation, $\varepsilon_1 \sim 1$, $\varepsilon_2 \ll 1$ are obtained [15]. Therefore, the loss function is written as following [14]

$$\begin{aligned} Im\left\{\frac{-1}{\varepsilon(q,\omega)}\right\} &= \varepsilon_2(q,\omega) \\ &= \frac{4\pi e^2}{\Omega q^2}\sum_{\sigma}\left|\langle f\left|e^{-iq.r}\right|c\rangle\right|^2 \delta(\hbar\omega - E_f + E_c) \end{aligned} \tag{2.3}$$

where $\langle f\left|e^{-iq.r}\right|c\rangle$ represent transition matrix elements including the core state $|c\rangle$ and the final state $|f\rangle$ on an atomic state. E_c and E_f are the energies of the core state and final states, respectively. Final states and energies are gained from DFT calculation by CASTEP, and the core states are reconstructed using PAW (Projector Augmented Wave) approach [16]. The DFT method will be discussed in the next section.

2.2. Density Functional Theory

Density Functional Theory (DFT) proved by Hohenberg and Kohn [17] could be applied by means of construction of the actual calculation method by Kohn and Sham. The Kohn–Sham equation can be expressed as [18]

$$\left[-\frac{\hbar^2}{2m}\nabla^2 + V_{eff}\right]\varphi = E\varphi \tag{2.4}$$

where V_{eff} is called the Kohn-Sham potential and written as following

$$V_{eff} = V_{ext} + V_H + V_{xc} \tag{2.5}$$

where V_{ext} is the external potential (electron-nuclear interaction), V_H is the Hartree energy (classical electron-electron interactions), V_{xc} is the exchange-correlation energy (quantum electron-electron interactions). V_H and V_{xc} are expressed as following

$$\mathrm{V}_H(r) = \int \frac{\rho(r')}{|r - r'|}\,\mathrm{d}r' \tag{2.6}$$

and

$$\mathrm{V}_{xc} = \frac{\delta E_{xc}}{\delta \rho} \tag{2.7}$$

where $\rho(r')$ is the electronic charge density at a point r', computed as $\rho(r') = |\varphi(r')|^2$, and E_{xc} is the energy of exchange and correlation of an interacting system. It is not simple to express the exchange and correlation rigorously. Therefore, for this part, it would be appropriate to rely on approximations.

2.3. Local Density Approximation

In order to simplify the many-electron system by the density functional method, the exchange-correlation energy must be given. The accurate value of the exchange-correlation energy can be obtained only in the case of homogeneous electron gas (HEG) by means of using Quantum Monte Carlo (QMC) calculations [19]. Therefore the exchange-correlation energy is assumed the following functional forms [18]:

$$E_{ex} = \int \rho(\mathrm{r})\, \epsilon_{ex}(\rho(\mathrm{r}))\mathrm{dr} \tag{2.8}$$

$$\epsilon_{ex}(\rho(\mathrm{r})) = \epsilon_{ex}^{HEG}(\rho(\mathrm{r})) \tag{2.9}$$

where $\rho(\mathrm{r})$ is electronic density, $\epsilon_{ex}(\rho(\mathrm{r}))$ is the exchange-correlation energy at a point r. $\epsilon_{ex}^{HEG}(\rho(\mathrm{r}))$ is the exchange-correlation energy at a point r in the homogeneous electron gas. The Equations 2.8 and 2.9 represent the exchange-correlation energy at a point r is treated as that of the homogeneous electron gas which has the same electron density at a point r. This approximation is called local density approximation (LDA) [20], and at first was considered to work well only in a system where the electron density is slowly varying. However, in practice, the LDA has been outstandingly successful in real systems with inhomogeneous electron density. The reason for the successes and the limitations were discussed in detail by Gunnarsson *et al* [21].

2.4. Bloch's theorem and plane wave basis set

In order to perform the electronic state calculations in solids, a method to handle infinite crystal structure is further required. In the crystal, the distance between atoms is periodic. Therefore, the external potential at a point r felt by the electrons is expressed as follows.

$$\mathrm{V}(r) = \mathrm{V}(r + R) \tag{2.10}$$

where R is the crystal period. In a system with periodic boundary condition, by using the Bloch's theorem [22], it is possible to obtain the solution of the Schrödinger equation. The wave function is written as

$$\varphi_k(r) = e^{ik.r} u_k(r) \tag{2.11}$$

where $u_k(r)$ is a periodic function. Therefore it can be expanded as a set of plane waves

$$u_k(r) = \sum_G c_k(G)\, e^{iG.r} \tag{2.12}$$

where G is the reciprocal lattice vectors. $c_k(G)$ is the Fourier expansion coefficient for the reciprocal lattice vector. By substituting equation 2.12 into equation 2.11, the wavefunction is expressed as follows:

$$\varphi_k(r) = \sum_G c_k(G)\, e^{i(k+G).r} \tag{2.13}$$

Hence the wavefunction is written as a sum of plane waves.

2.5. Cut-off energy

The equation 2.13 expanded by plane waves is the sum for reciprocal lattice vectors G. Ideally, it is desirable to deal with an infinite number of reciprocal lattice vectors, however it is impossible and the sum must be limited by the cutoff energy E_{cut}. E_{cut} is defined

$$\frac{\hbar^2|k+G|^2}{2m} \leq E_{cut} \tag{2.14}$$

This is reasonable because as $|k+G| \to \infty$, $|c_k(G)| \to 0$. (See section 3.2)

2.6. k-point sampling

In the periodic system, the integrals over the infinite system in the real space can be converted into the integrals over the first Brillouin zone in reciprocal space. In this project, the Monkhorst-Pack scheme [23] is used to approximate the integrals in the Brillouin zone by a summation over discrete sampling points, called k-points. (See section 3.4)

2.7. Pseudopotential approximation

In order to further reduce the computational expense of the calculation, CASTEP code uses a pseudopotential method (see section 3.1). The pseudopotential is an approximated potential, which uses a potential function for the valence electron potential without directly dealing with the inner core electrons (=Carbon 1s in this thesis) near the nucleus. This is because in many properties or chemical reactions, inner core electrons do not play an important role. The valence wave function oscillates rapidly and has some nodes in the core region because it must be orthogonal to the core state. However, when a pseudopotential is generated, these nodes are removed. As a result, a smooth and nodeless wave function is obtained, so that the cut-off energy can be reduced significantly. This leads to the reductions of the computational demand of a calculation without affecting the results.

However, in the EELS calculation, the calculation of the core level state is required for the evaluation of the transition matrix element in the equation 2.3. For that reason, the pseudofunction is transformed to the all electron wavefunction using the PAW method. Using the reconstructed wavefunction, the core level can be described, which enable the EELS signal to be calculated.

2.8. Alternative methods of calculating EELS

Besides CASTEP, several codes are known for calculating EELS using DFT. For instance, WIEN2k [24] is an all-electron DFT code and has shown the best agreement with experiment. However, in exchange for the high accuracy, the calculations require the most computational time.

Some codes use the DV-Xα method, as used in the single-atom analysis by Suenaga *et al* [11]. This is less computer-time-consuming than other DFT methods due to using Xα exchange-correlation potential, but on the other hand, the calculation accuracy is sacrificed to some extent. The details of the computational treatments of the DV-Xα method have been reported by Adachi *et al* [25].

In terms of CASTEP, unlike above-mentioned programs, it is not possible to calculate the absolute value of the loss-energy and the chemical shift because of the use of pseudopotentials. However, it is possible to calculate with relatively high speed in spite of being an *ab initio* calculation and taking into account the exchange-correlation potential. Moreover, CASTEP EELS provides results with high accuracy. Che R. Seabourne *et al* [26] have reported that it is possible to obtain the spectra with CASTEP EELS with almost the same level of the accuracy as using WIEN2k.

3. Theoretical Modelling

3.1. Pseudopotentials

In EELS calculations, when using the CASTEP code, an on-the-fly pseudopotential is required for PAW reconstruction. The pseudopotential is generated on-the-fly from a definition string. In order to determine the appropriate string, the pseudopotential convergence and the lattice constant were tested for diamond and graphite models. As a result, the core radius and qc-tuning [27] required for generating these pseudopotentials were determined to be 1.4 Å and 7 , respectively. Table 3.1 shows the results of the tests. The lattice constant calculated by using this pseudopotential agrees with the experimental data [28] [29] very well, and furthermore the pseudopotential possesses sufficiently good convergence, as no artificial ghost states appeared. The string obtained is expressed as follows.

"1|1.4|9.187|11.025|12.862|20N:21L(qc=7)[]"

where the first integer is the angular momentum quantum number of the local channel. The next number is the core radius Rc. The next three integers are the suggested cut-off energies for “coarse”, “medium” and “fine” precision with this pseudopotential. The next section indicates the electrons treated as valence, specified by the principal and orbital angular momentum numbers n and l, i.e. 20:21 means treat 2s and 2p electrons as valence. “N” indicates the norm-conservation.

		Lattice constant (Å)	Error (%)	$dE_{tot}/dlog(E_{cut})$
Diamond		3.550	-0.48	-0.029
Graphite	In-plane	2.454	-0.20	-0.067
	Perpendicular	6.635	-0.11	

Table 3.1: Lattice constants and the lattice constant error in diamond and graphite model. dEtot/dlog(Ecut) represent the pseudopotential convergence.

In this project, the norm-conservation was used because originally a theoretical study by both EELS and Raman has been planned. (The ultrasoft pseudopotentials are not supported in Raman calculation by CASTEP.) 'L' indicates that this state is the local channel. The "qc=7" in round brackets specifies the qc-tuning for the pseudopotential.

Figure 3.1 shows the wavefunctions obtained by the all electron DFT calculations for constructions of pseudowavefunctions and the pseudowavefunctions generated by using the above string. The all electron wavefunction of 2s oscillates inside the core radius Rc. This oscillation maintains the orthogonality between 1s and 2s electrons. Beyond the Rc, the pseudowavefunctions agree with the all electron wavefunctions. Inside Rc, the pseudowavefunctions are smoother than the all electron wavefunction. In this project, we use this string for carbon atom in various structures consistently.

In the case of performing EELS calculations, the pseudopotential for an excited state is needed because the incident electron beams excite electrons in materials. Hence, the excited pseudopotential for carbon atoms excited by incident electron beams is constructed for the atomic configuration $1s^1 2s^2 2p^2$ subtracted electron from 1s level.

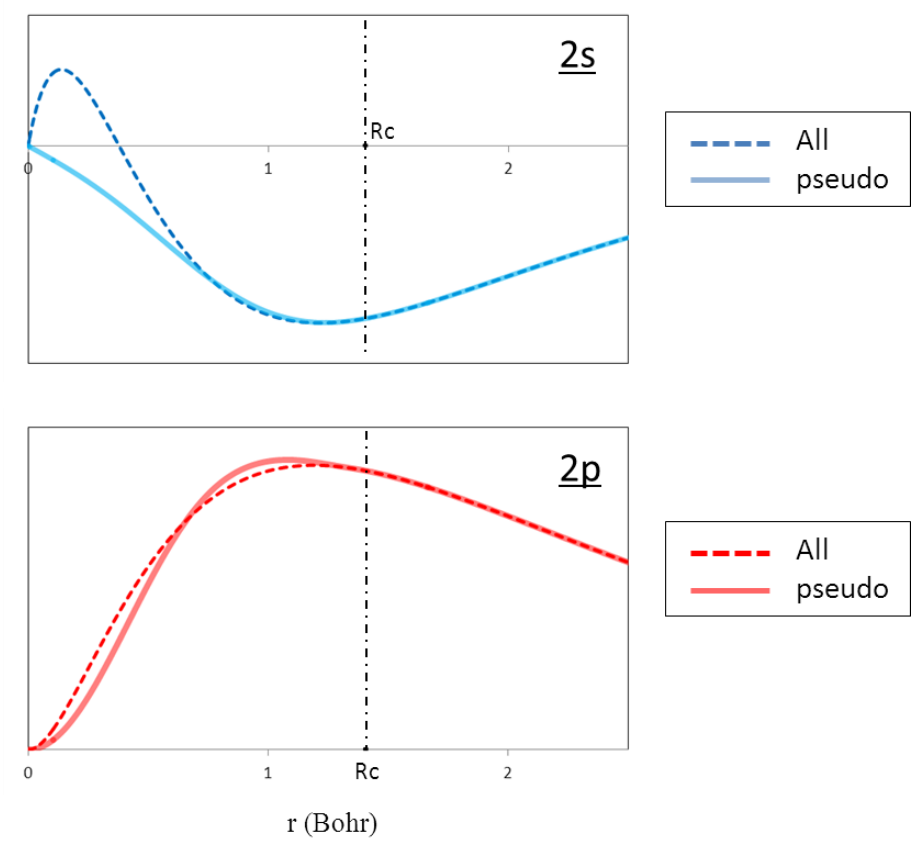

Figure 3.1: All electron and pseudowavefunctions for carbon atom. The core radius Rc=1.4 au.

3.2. Cut off energy

In this section, we present the results of simulations of the lattice constant of graphite and diamond as seen in Figure 3.2(a) (b) and Figure 3.3(a) respectively. Figure 3.2(c) and Figure 3.3(b) show a metric for how well converged the total energy of the simulated cell is with respect to the cut off energy ($dE_{tot}/d\log(E_{cut})$) for graphite and diamond. The simulations were carried out using norm-conserving pseudopotential and LDA approximation. These results show that each lattice constant is in good agreement with experimental data at a level of less than 0.5% error at 700eV and that the total energy is sufficiently converged with respect to cut-off energy at 700eV.

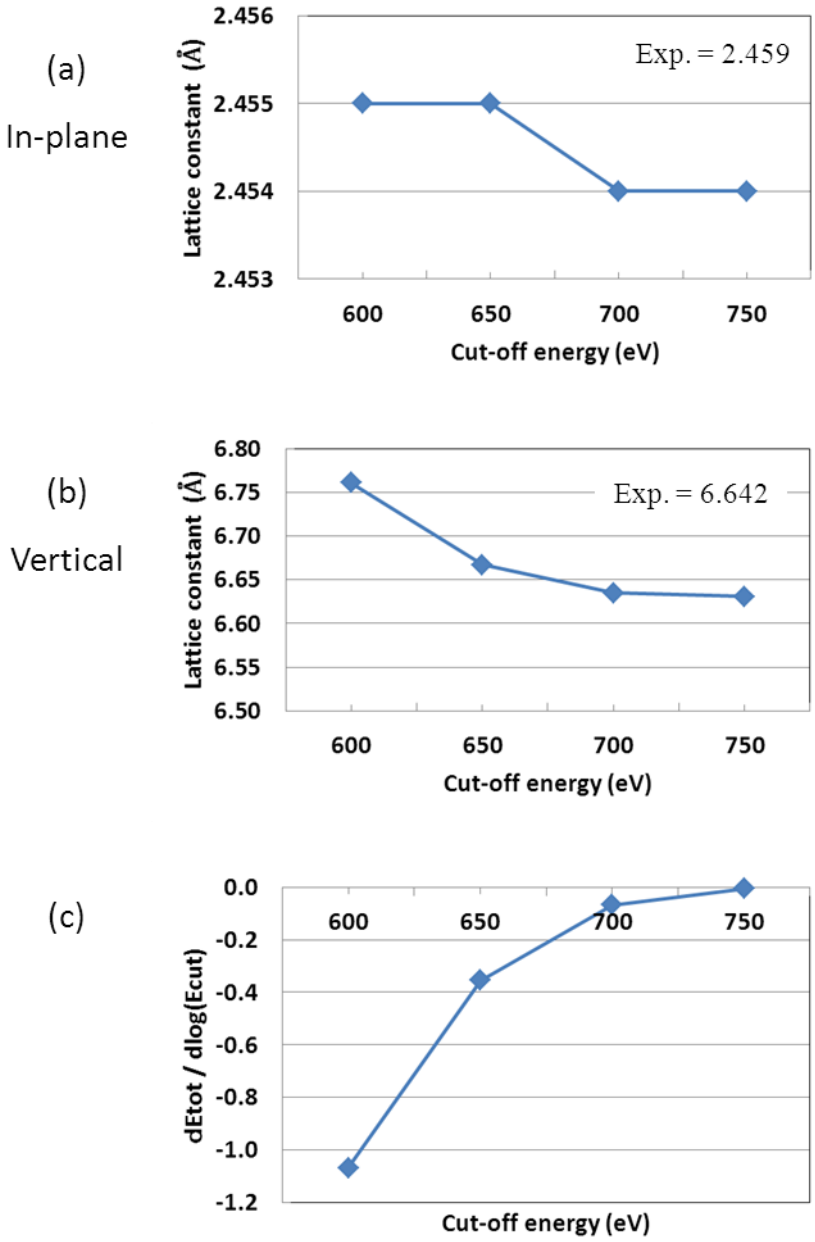

Figure 3.2: Lattice constant of graphite (a) in-plane and (b) along vertical direction for the graphite layer. (c) Metric for how well converged the total energy of the simulated cell is with respect to the cut off energy for graphite.

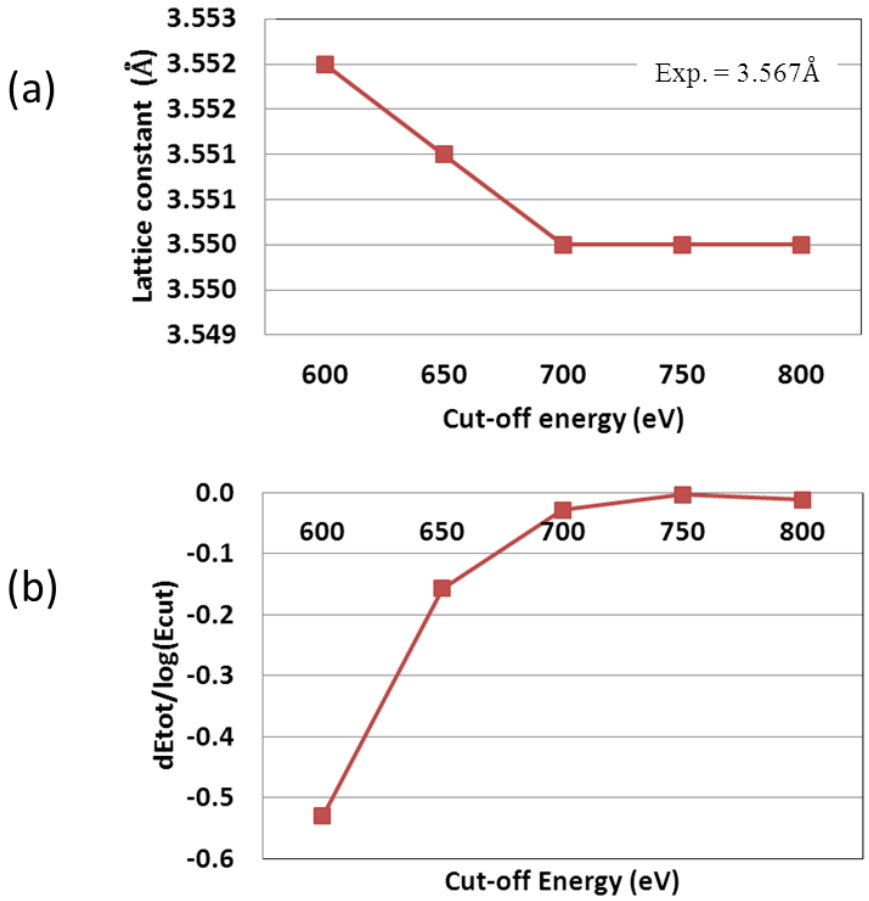

Figure 3.3: (a) Lattice constant of diamond. (b) Metric for how well converged the total energy of the simulated cell is with respect to the cut off energy for diamond.

3.3. Supercell size

This section describes how the size of the supercell was decided. In order to achieve EELS spectra it is necessary to obtain the electronic structure of the excited state. For this purpose, the core hole should be included in the calculation. CASTEP imposes periodic boundary conditions to perform simulations, and it is therefore necessary to make the supercell big enough to minimise the interaction with neighbouring excited atoms. Figure 3.4 shows the illustration of the interactions among excited atoms. To confirm the effect of the interaction, EELS were to be calculated for diamond and graphite for different sizes of supercells. For EELS spectra, all the calculation was performed by CASTEP. For the exchange-correlation functional, the Local Density Approximation (LDA) method was used. The Fermi energy is set to zero. The smearing width is 0.2 eV.

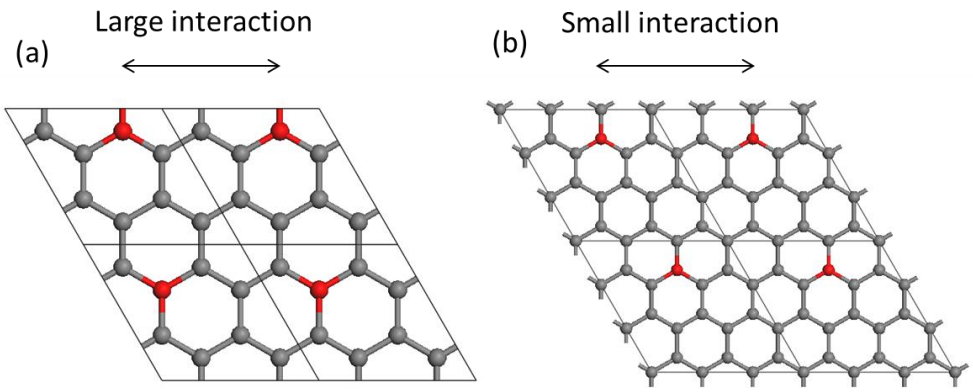

Figure 3.4: Illustration of the interaction among neighbouring excited atoms. The red circles indicate excited atoms.

3.3.1. EELS spectra of carbon in diamond

Figure 3.5(b) shows the EELS spectra of diamond for different sizes of supercells. Figure 3.5(a) shows an experimental EELS spectrum for the sake of comparison, which has two distinct peaks approximately 15eV away from each other and plateau between them. In Figure 3.5(b), the spectrum of the two atom model looks quite different from the others as expected. And then the spectra show a clear trend and converge as the size of the supercell increases. This is because the interaction between neighbouring excited atoms decreases. The spectrum calculated with a 32 atoms supercell shows the features of the experimental spectrum and no significant change for 54 and 64 atoms models. This indicates that the lattice of the 32 atom model is big enough and the size of the lattice is 6.150 Å in each direction. In this case this result shows that the size of supercell needed is approximately 6 Å at least.

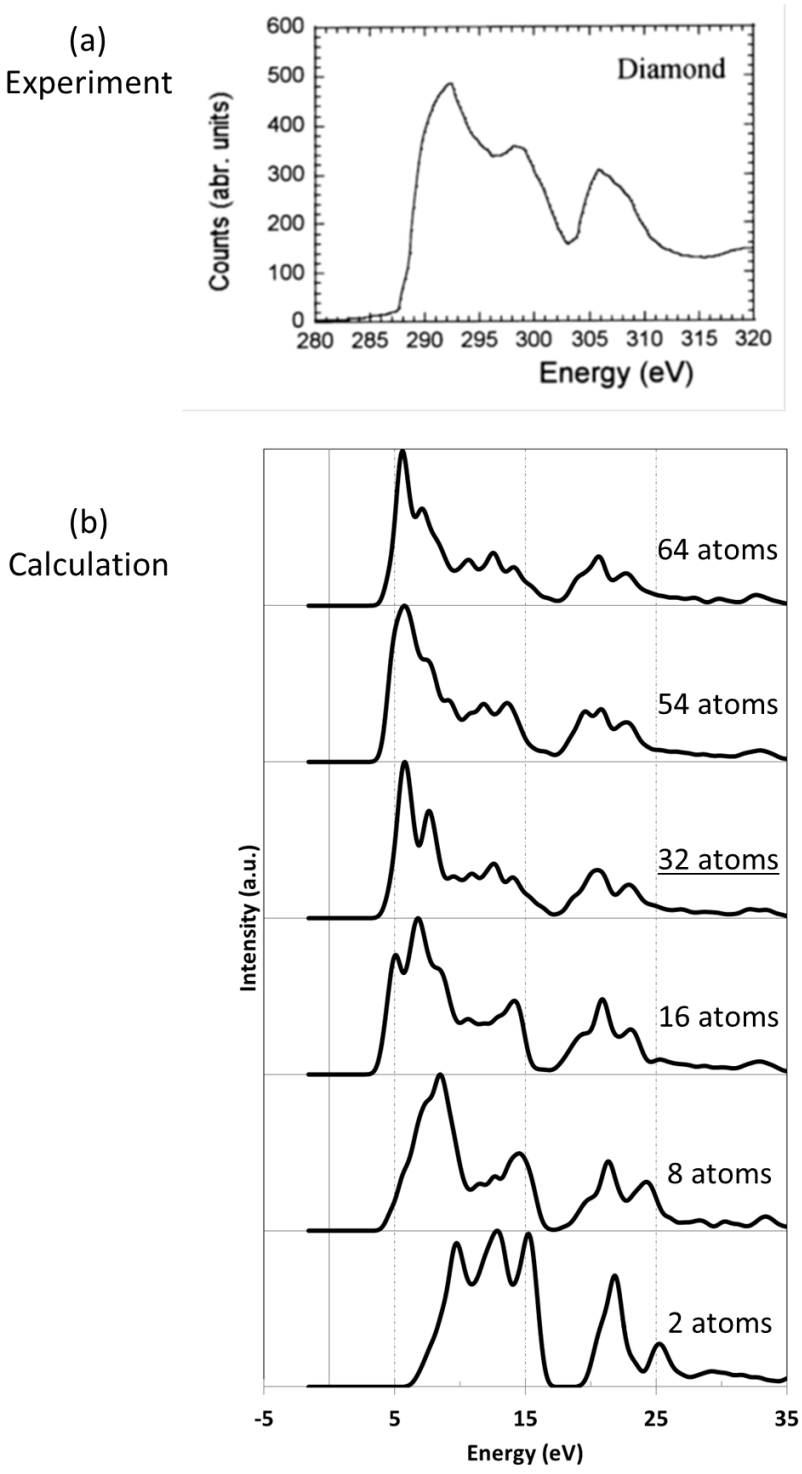

Figure 3.5: (a) Experimental EELS spectrum of diamond taken from [30]. (b) Calculated EELS spectra of carbon in diamond for different supercell size.

3.3.2. EELS spectra of carbon in graphite

Figure 3.6(b) shows the EELS spectra of carbon in graphite for different sizes of supercells. These spectra are remarkably different from the EELS spectra of carbon in diamond, reflecting the differences of the atomic and electronic structures. Figure 3.6(a) shows an experimental EELS spectrum for comparison, which has two main features: the sharp π* peak and the broad σ* peak, including a plateau. The π* peak is caused by transitions from the carbon 1s core level to the anti-bonding state of π bonding and the σ* peak is caused by transitions from the carbon 1s core level to the anti-bonding state of σ bonding. In Figure 3.6(b), these spectra also show a clear trend and converge as the size of the supercell increases. This is because the interaction between neighbouring excited atoms decreases in the same way as the case of diamond. The spectrum calculated with a 36 atom supercell shows the main features and no significant change for 64 and 100 atoms models. This indicates that the lattice of 36 atoms model is big enough and the size of the lattice is 7.363 Å in-plane direction. In this case this result shows that the size of supercell needed is approximately 7 Å at least.

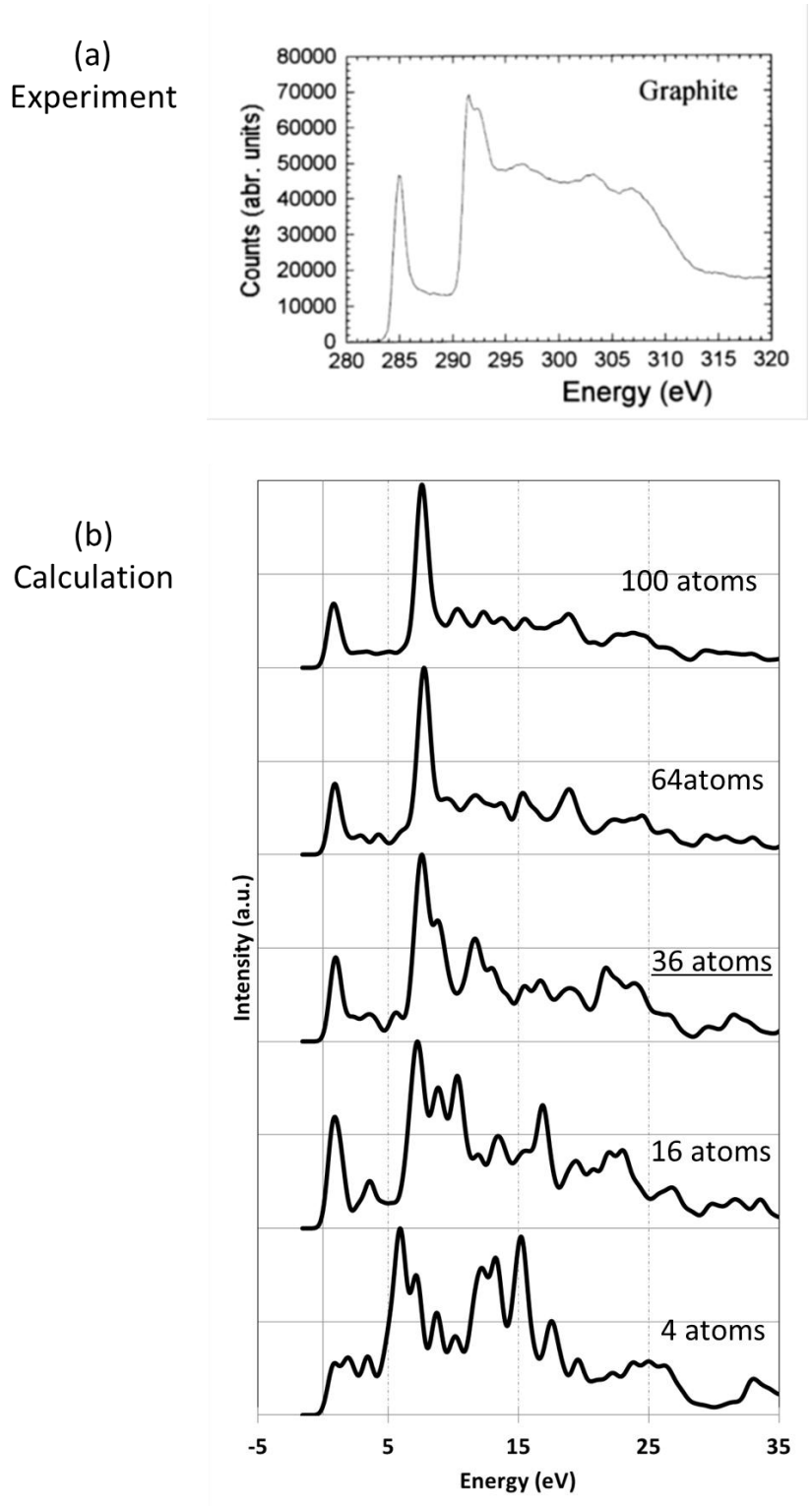

Figure 3.6: (a) Experimental EELS spectrum of graphite taken from [30]. (b) Calculated EELS spectra of carbon in graphite for different supercell size.

3.3.3. Conclusion

In this chapter, EELS calculations with different cell size for diamond and graphite were performed in order to investigate the effect of the interaction between neighbouring excited atoms. As a result, in the EELS calculations for carbon materials, the minimum cell size to ignore the effect of the interaction was more than approximately 7 Å. Hence in all subsequent calculations, the unit cell was always chosen to be larger than this.

3.4. k-point sampling

In order to determine the sampling number of k-point, the EELS calculations for both diamond and graphene were performed. Figure 3.7 displays a series of EELS spectra calculated for a 54-atom diamond model for different numbers of k-points. Figure 3.8 shows the structural model of graphene and Figure 3.9 displays a series of EELS spectra calculated for the graphene model for different numbers of k-points. For the 54-atom diamond model, the convergence of the EELS spectrum is complete by a 6x6x6 k-point mesh with k-point spacing of $0.020 \times 2\pi Å^{-1}$. For the 18-atom graphene model, the convergence of the EELS spectrum is achieved by a 8x8x1 k-point mesh with k-point spacing of $0.020 \times 2\pi Å^{-1}$. From these results, the k-point spacing required for EELS calculations of carbon materials is preferably less than $0.020 \times 2\pi Å^{-1}$.

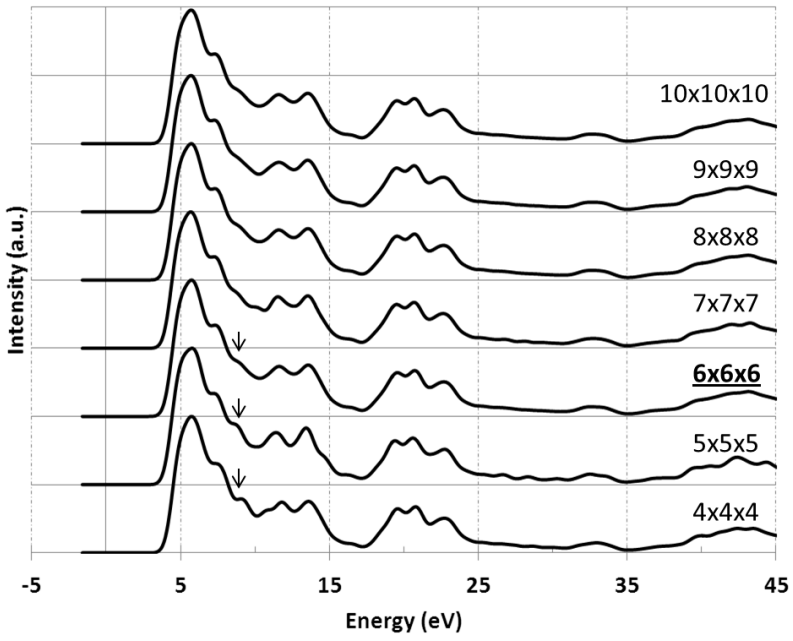

Figure 3.7: EELS spectra of 54-atom diamond model.

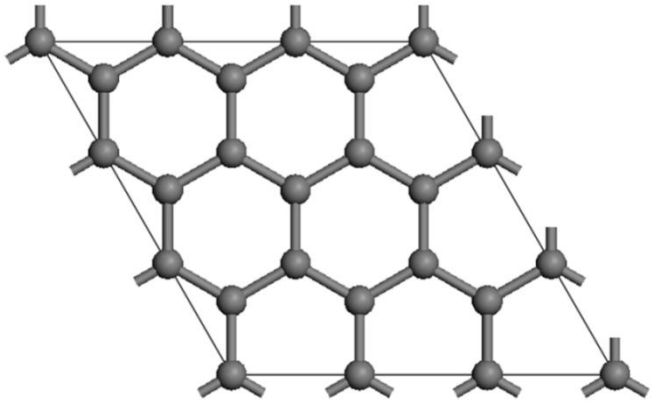

Figure 3.8: Structural model of graphene. (3x3 supercell of graphene)

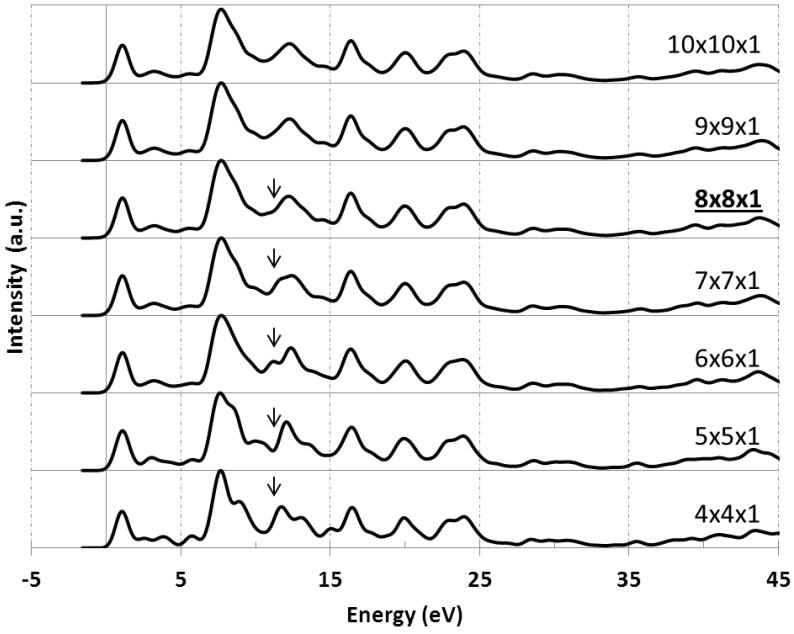

Figure 3.9: EELS spectra of graphene for different numbers of k-points.

4. Atomistic structure and magnetism of GNRs

Graphene nano-ribbons are divided into two classes. Figure 5.1 shows GNRs with (a) armchair (AGNR) and (b) zigzag edge (ZGNR). The width N of a ribbon is commonly measured by the number of dimers or zigzag lines [31]. Several theoretical investigations of the edge structure and the stability in GNRs have been carried out and the most stable structures were reported [32] [33]. However, in the experiments, the GNRs which are not the most stable have been observed as well, including non-passivated edge structure [8].

Therefore, in this section, we will focus on the clean zigzag and armchair edge as the basic structure at first, and then reveal the features at the atomic level. In addition, we also investigate the effect on both the structure and the magnetism by the edge modification such as hydrogen modification, reconstructed edges and the Klein edge.

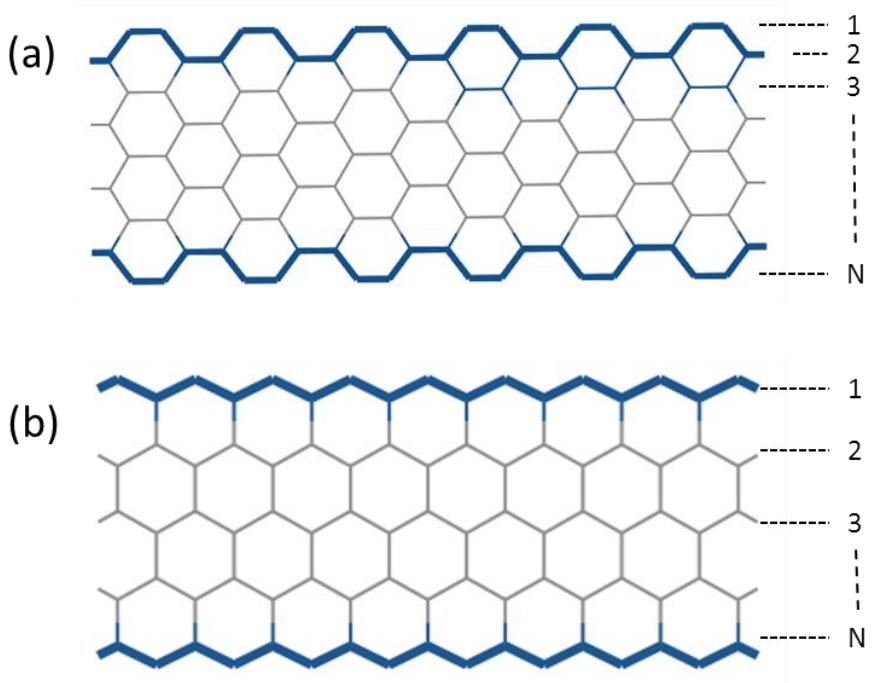

Figure 4.1: Graphene nano-ribbons with (a) armchair and (b) zigzag edge for width N.

4.1. Armchair GNRs

In this section, the features of the atomistic structures of AGNRs with and without hydrogen passivation are reported. AGNRs do not show the magnetic structures regardless of the edge modification.

4.1.1. Non-passivation

Figure 4.2 shows the relaxed structures of the ribbon width with N=5-9. In these structures, each grey spheres represents the position of carbon atoms. Solid lines represent σ bonds. A carbon atom in the interior region of GNRs has two interchain bonds and one intrachain bond with its nearest neighbours. At the edge atom, it has one intrachain bond and one interchain bond. The edge relaxation contracts the intrachain bonds at the edge by 0.18 Å compared to the bond in the bulk. The bond length is reduced to 1.23 Å, which is close to the triple bond of acetylene (1.21 Å). The presence of triple bonds at the edge of armchair ribbons have been reported in previous studies [34], therefore it is considered reasonable to presume that these short bonds are triple bonds. This structural change is independent of the ribbon width investigated for N=5 to 9. This effect comes from the lack of a bonding counterpart in an interchain bond, which generates both the dangling bond of σ orbital at the edge and the nonbonding part of the π orbital at the edge. Figure 4.3 shows the bond-length change from the edge to internal site in 9-AGNR. The blue circle indicates intrachain bond length and the red triangle indicates the interchain-bond length. The dashed line indicates the bond length in graphene. The horizontal axis is the bond number which is indicated at N=9 ribbon in Figure 4.2. Moving away from the edge, the short bond at the edge, especially interchain bond, converges to the bond of bulk graphene rapidly.

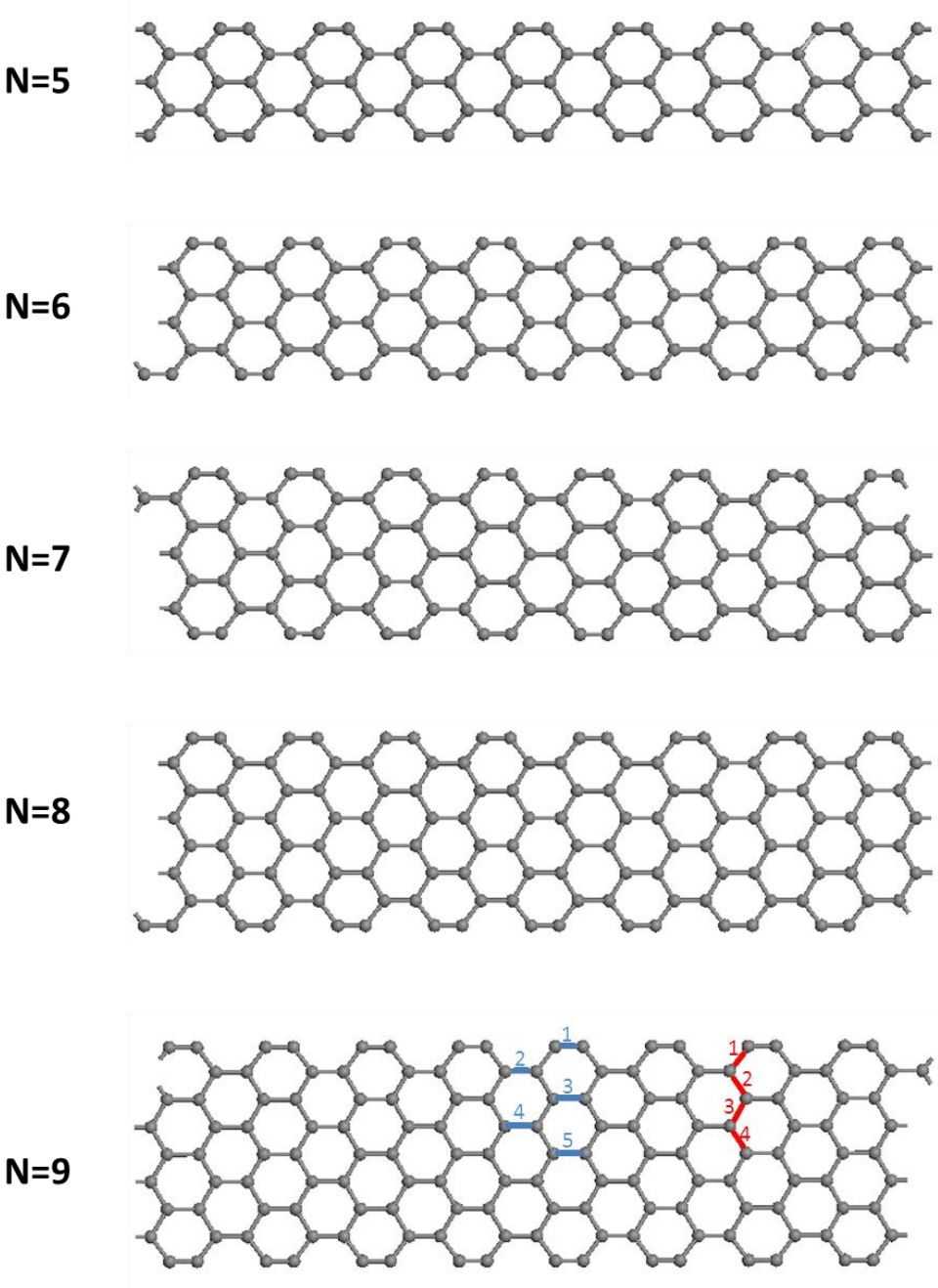

Figure 4.2: The relaxed structure of N-AGNR. In N=9 the blue numeral indicate the bond number of intrachain bonds and the red numeral indicates the bond number of interchain bonds.

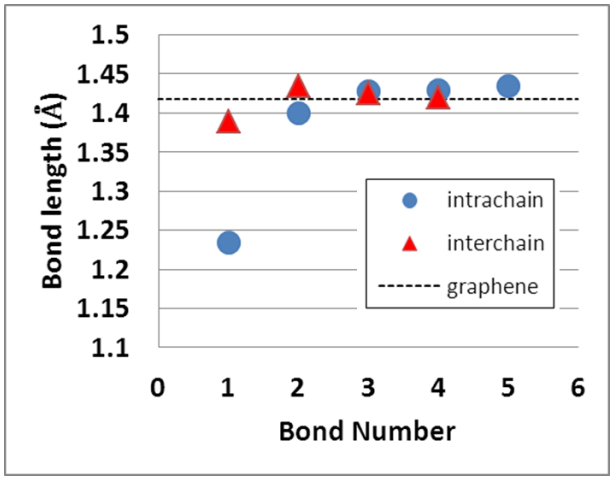

Figure 4.3: The bond-length change from the edge to internal site in 9-AGNR. The blue circle indicates intrachain bond length and the red triangle indicates interchain bond length. The dashed line indicates the bond length in bulk graphene.

4.1.2. Hydrogen passivation

Figure 4.4 shows the relaxed structures of (a) mono-hydrogenated 5-AGNR, (b) dihydrogenated 5-AGNR, and (c) the side view of dihydrogenated 5-AGNR. Dark circle denote carbon atoms and open circles represent hydrogen atoms. Solid lines represent a section of a unit cell in plane with the ribbons. The two edges of the each structure have the same configurations. The mono-hydrogenated GNRs are in-plane and each edge carbon atom is bonded to a hydrogen atom. Compared to the edge interchain bonds of the non-passivated AGNR, the length of the edge interchain bonds of the mono-hydrogenated AGNR is expanded to 1.37 Å, which is close to the double bond of ethylene (1.34 Å). In the dihydrogenated GNRs, each edge carbon atom form sp3 hybridised orbitals instead of sp2 hybridised orbitals and has bonds with two hydrogen atoms and two neighboring carbon atoms. The plane which two hydrogen atoms and one edge carbon atom make is perpendicular to the graphene sheet.

The length of the edge interchain bonds of the dihydrogenated AGNR is expanded to 1.53 Å, which is close to the single bond of ethane (1.52 Å).

Figure 4.5 shows the computed total-energy differences of the system:

$$\Delta E = E_n^{total} - E_0^{total} \tag{4.1}$$

$$E_n^{total} = E_{ribbon} + (4 - 2n)E_{hydrogen} \tag{4.2}$$

where E_{ribbon} is the energy of the unit cell of GNRs including passivated hydrogen atoms, $(4-2n)E_{hydrogen}$ is the energy in the hydrogen reservoir and the notation n means the number of hydrogen atoms per each edge atom. In case of adding three or more hydrogen atoms to an edge carbon atom we confirmed hydrogen-desorption occur. In the unit cell, there are four edge carbon atoms, therefore the maximum hydrogen molecules in the reservoir are set to four. $E_{hydrogen}$ is the energy of the isolated hydrogen molecule (=-30.962 eV). The system contains 10 carbon atoms and 8 hydrogen atoms. E_{total} can be used to determine the stability of hydrogen passivation. By the hydrogenation on the edge carbon atom of non-passivated AGNR, total energy of hydrogenated AGNRs is stabilized energetically. In this system, the most stable structure is found to be dihydrogenated AGNRs.

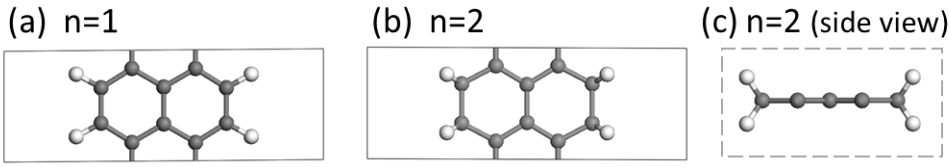

Figure 4.4: The structure of (a) mono-hydrogenated 5-AGNR, (b) dihydrogenated 5-AGNR and (c) the side view of dihydrogenated 5-AGNR.

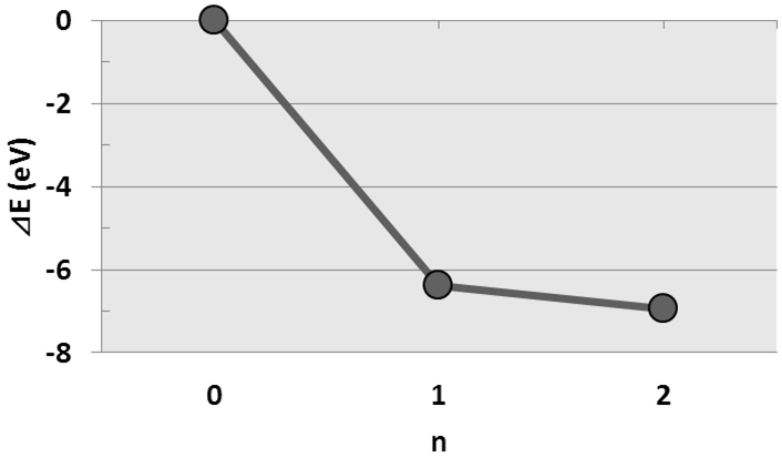

Figure 4.5: The total-energy differences of the system including both AGNR consisted of 10 carbon atoms and 8 hydrogen atoms.

4.2. Zigzag GNRs

In this section, the features of the atomistic structures of ZGNRs with non-passivation, self-passivation, hydrogen passivation and Klein edge are reported. Especially, in terms of hydrogen modification, energetic stability is reported.

4.2.1. Non-passivation

The structural relaxation with spin polarisation is performed in the ribbon width with N=3-7. Figure 4.6 shows the relaxed structures of N-ZGNR. A carbon atom in the interior region of GNRs has two intrachain bonds and one interchain bond with its nearest neighbours. At the edge atom, it has only intrachain bonds. The edge relaxation contracts the intrachain bonds at the edge by 0.04 Å compared to the bond in the bulk. As a result, interchain bonds expand. This structural change is independent of the ribbon width with N=3 to 7. This effect comes from the lack of a bonding counterpart in an interchain bond, which generates both the dangling bond of σ orbital at the edge and the nonbonding part of the π orbital at the edge. Figure 4.6 shows the bond-length change from the edge to internal site in 7-ZGNR. The blue circle indicates intrachain-bond length and the red triangle indicates the interchain-bond length. The dashed line indicates the bond length in bulk graphene. The horizontal axis is the bond number which is indicated at N=7 ribbon in Figure 4.6. Moving away from the edge, both the short bond of the intrachain bond and the long bond of interchain bond converge to the bond of bulk graphene rapidly.

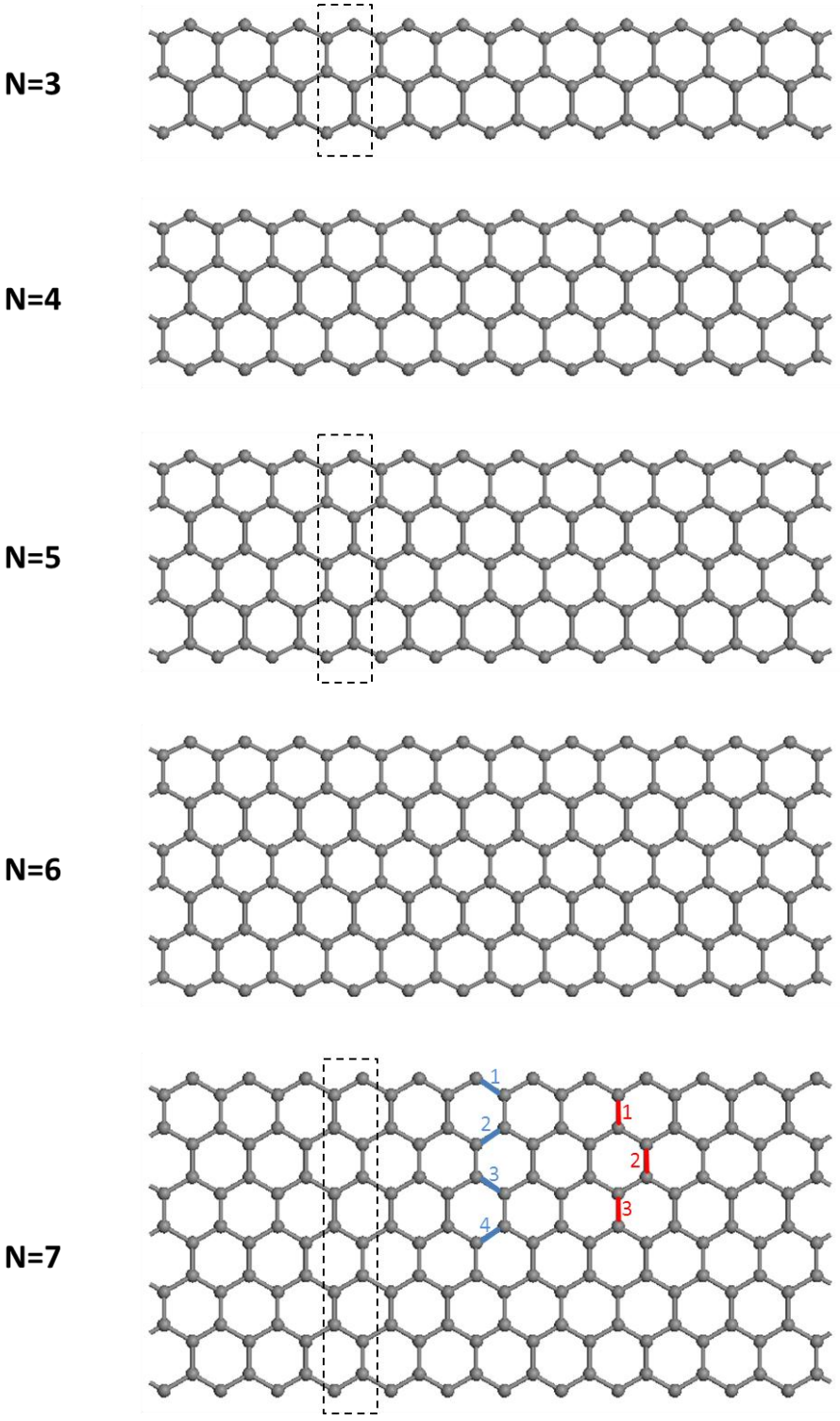

Figure 4.6: The relaxed structure of N-ZGNR. In N=7 the blue numeral indicates the bond number of intrachain bonds and the red numeral indicates the bond number of interchain bonds. The dashed lines indicate the unit cells.

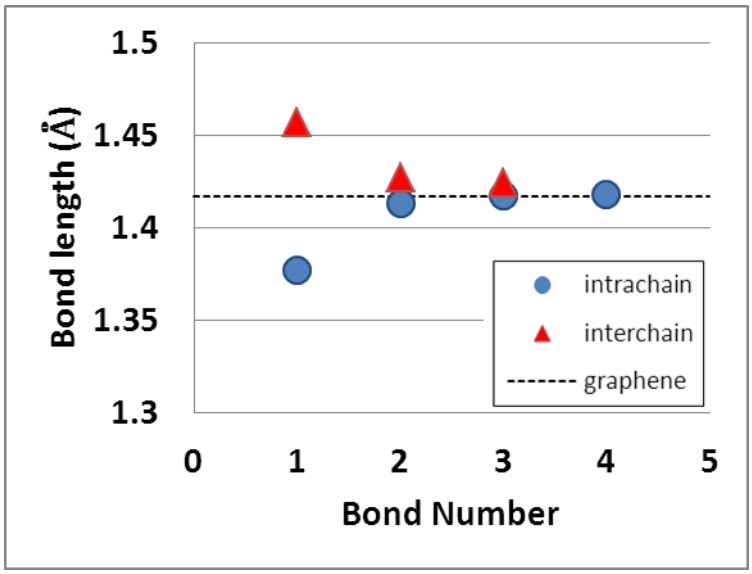

Figure 4.7: The bond-length change from the edge to internal site in 7-ZGNR. The blue circle indicates intrachain bond length and the red triangle indicates interchain bond length. The dashed line indicates the bond length in bulk graphene.

	N=3	N=5	N=7
⊿E (eV/edge carbon atom)	-0.09	-0.11	-0.11
Integrated absolute spin density (electrons/a_0^3)	2.556	2.741	2.801

Table 4.1: Stabilised Energy by spin polarisation ⊿E and integrated spin density for ribbon width N = 3, 5, 7. The spin densities are for the unit cells shown in Figure 4.6.

Regarding spin polarisation, the different spin configurations and the relative energies are investigated. As a result the spin moment on the carbon atoms on one edge are found to be antialigned to the spin moment on the opposite edge and it is energetically favourable. The total magnetisation of the ribbon is zero and the spin configuration is an antiferromagnetic (AF). Figure 4.8 shows the isovalue surface of the spin density in 3, 5 and 7-ZGNRs. The isovalue is 0.06 electrons/a_0^3, where $\boldsymbol{a_0}$ is Bohr radius. The spin-polarised electronic states localise on the both edges and the spin configurations are independent of the ribbon width. Table 4.1 shows the stabilised energy per edge carbon atom by spin polarisation ΔE and the integrated spin density. This magnetic order stabilised the energy by approximately 0.1 eV per edge carbon atom within the ribbon width N=3-7. The integrated spin density shows the dependence on the ribbon width and increase slightly as the widths become wider.

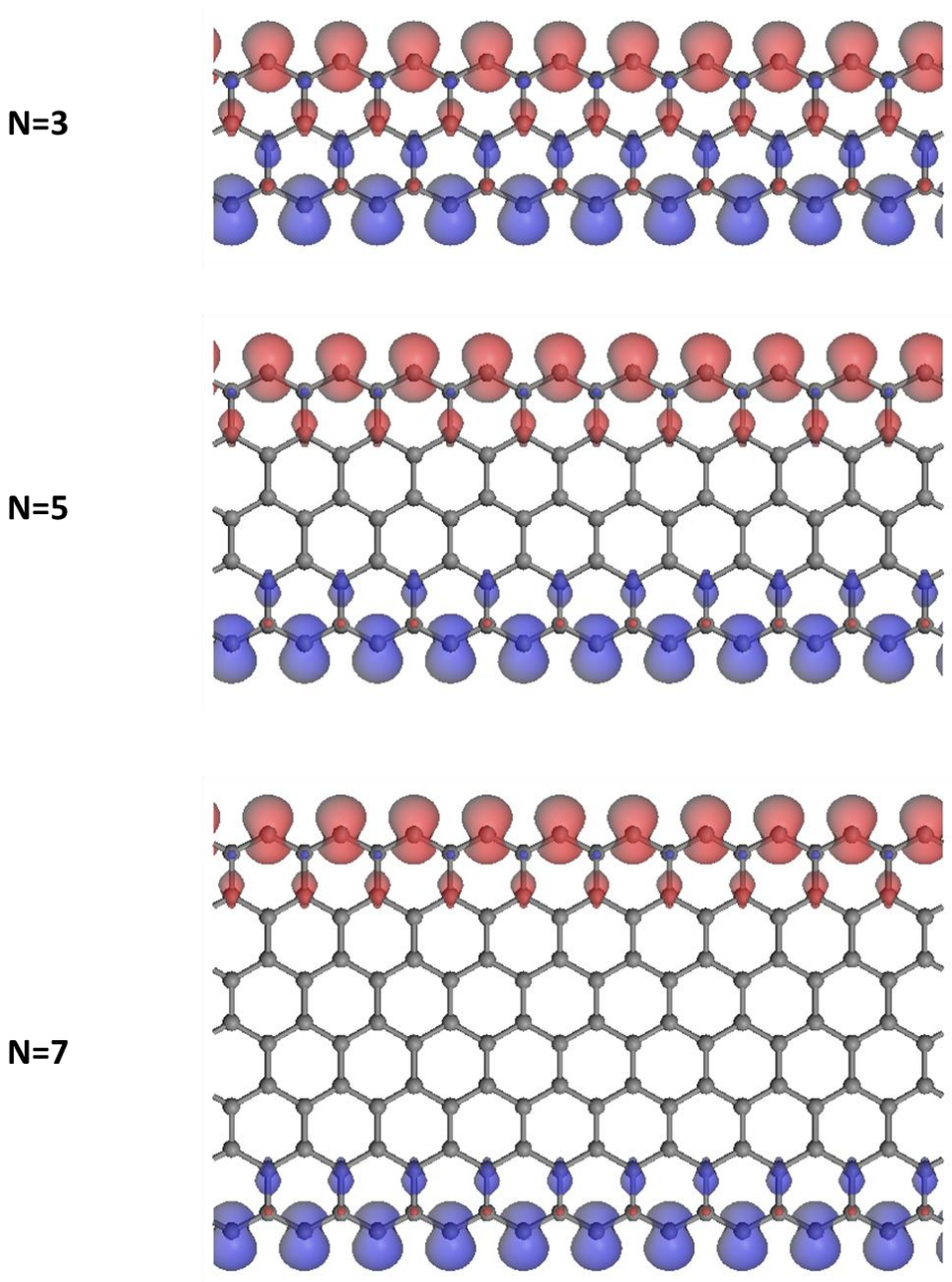

Figure 4.8: Isovalue surface of the spin density calculated from spin-polarised simulation in AGNR with different widths N=3, 5, 7. The isovalue is 0.06 electrons/a_0^3. Colour code: red, α spin density; blue, β spin density.

4.2.2. Self-passivation

From the energetic point of view, two neighbouring hexagons of the bare zigzag edge may reconstruct and transform to the structure of a pentagon and a heptagon. This edge structure is known as Stone-Wales (SW) defect [35] and energetically favourable over the bare zigzag edge [36] [37]. Figure 4.9 shows the relaxed structure of 7-GNR with (a) bare zigzag edge and (b) reconstructed edge. The structural relaxations on reconstructed ZGNR are performed in the ribbon width with N=3-7. These structures are stabilised in non-magnetic ground state and by 0.4 eV per edge carbon atom. The edge structures have triple bonds in the armrests as well as bare AGNRs. The length of the bond is 1.24 Å independent of the ribbon width investigated N=3-7. The structure of reconstructed ZGNR is favourable due to the presence of these triple bonds instead of dangling bonds in bare zigzag edges.

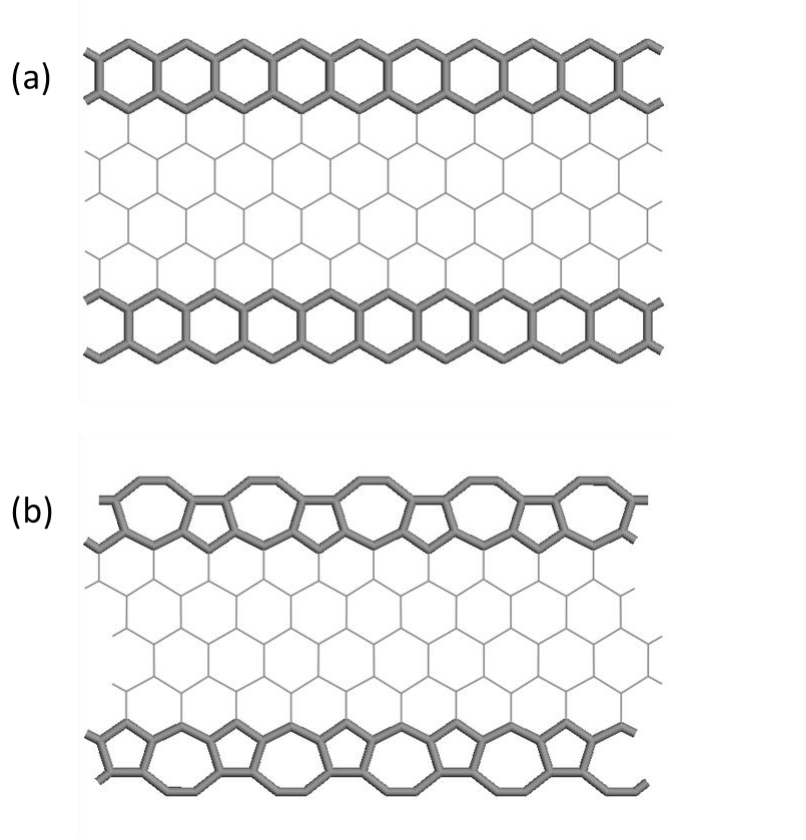

Figure 4.9: Schematics of 7-GNRs with (a) bare zigzag edge and (b) reconstructed edge.

4.2.3. Hydrogen passivation

Figure 4.10 shows (Left) the relaxed structures and (Right) spin density plot (Isovalue is 0.06 electrons/a_0^3) of (a) non-passivated 5-ZGNR as a reference (b) mono-hydrogenated 5-ZGNR, (c) dihydrogenated 5-ZGNR, and (d) the side view of dihydrogenated 5-ZGNR. The two edges of the each structure have the same configurations. The mono-hydrogenated GNRs are in-plane and each edge carbon atom is bonded to a hydrogen atom. In the dihydrogenated GNRs, each carbon edge atom has bonds with two hydrogen atoms and two neighboring carbon atoms. The plane which

two hydrogen atoms and one carbon atom make is perpendicular to the graphene sheet.

Regarding spin polarisation, the different spin configurations and the relative energies are investigated. As a result, in mono-hydrogenated 5-ZGNR, the spin moment on the C atoms on one edge are antialigned to the spin moment on the opposite edge same as non-passivated ZGNRs. The total magnetisation of the ribbon is zero and the spin configuration is an antiferromagnetic (AF). The dihydrogenated 5-ZGNR is found to be non-magnetic. The decreasing trend of spin density with the number of the addition of hydrogen is confirmed clearly. Table 4.2 shows the stabilised energy per edge carbon atom by spin polarisation ⊿E and the integrated spin density.

Figure 4.11 shows the computed total-energy differences of the system given by equation 4.1. In the present case, total energy of the system is described below.

$$E_n^{total} = E_{ribbon} + (2-n)E_{hydrogen} \tag{4.3}$$

where E_{ribbon} is the energy of the unit cell of GNRs including passivated hydrogen atoms, $(2-n)E_{hydrogen}$ is the energy in the hydrogen reservoir and the notation n means the number of hydrogen atoms per each edge atom. In case of adding three or more hydrogen atoms to an edge carbon atom we confirmed the hydrogen-desorption occur. In the unit cell, there are two edge carbon atoms, therefore the maximum hydrogen molecules in the reservoir are set to two. $E_{hydrogen}$ is the energy of hydrogen molecule (=-30.962 eV). The system contains 10 carbon atoms and 4 hydrogen atoms. E_{total} can be used to determine the stability of hydrogen passivation. By

the hydrogenation on the edge carbon atom of non-passivated ZGNR, total energy of hydrogenated ZGNRs is stabilized energetically. In this system, the most stable structure is dihydrogenated ZGNRs.

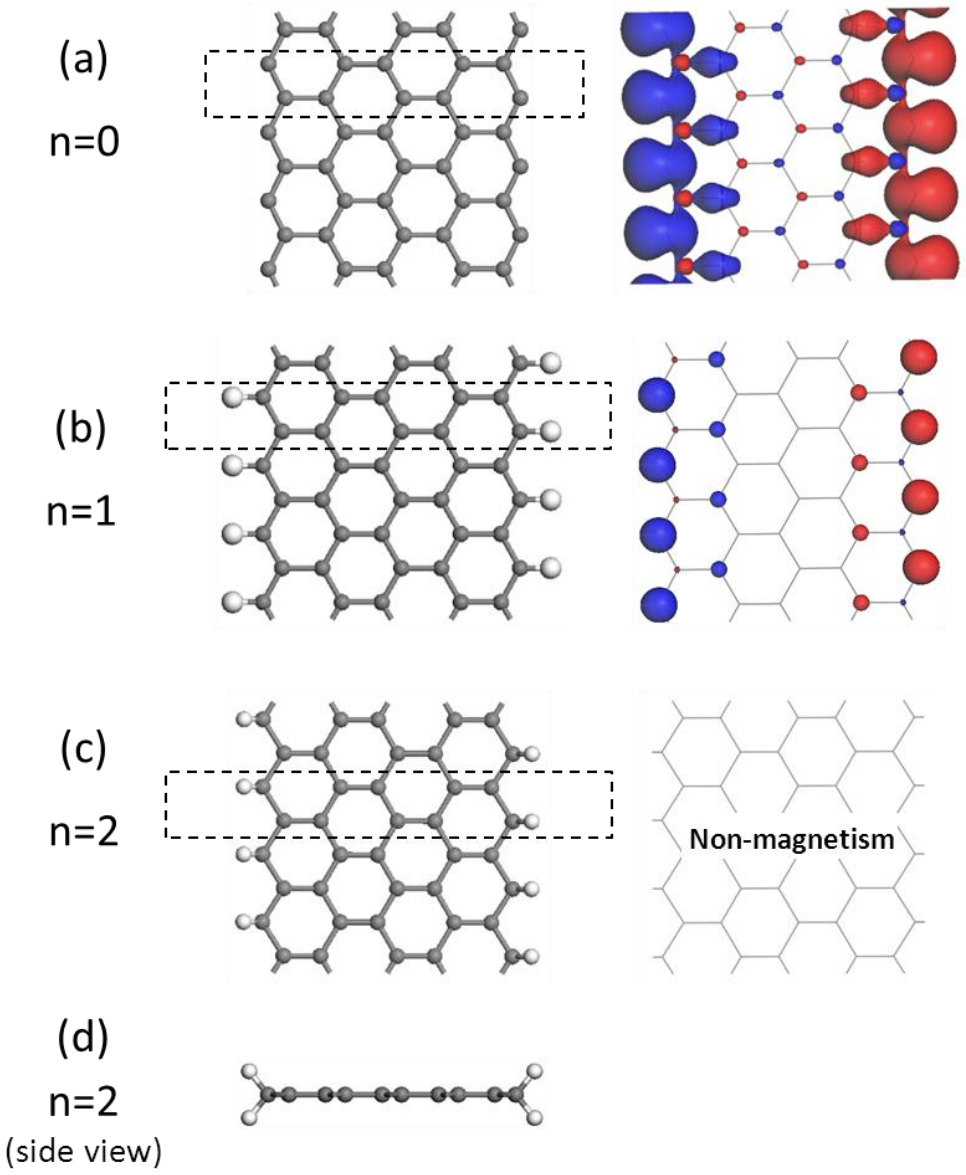

Figure 4.10: (Left) Atomic configurations and (Right) spin density plot (Isovalue is 0.03 electrons/a_0^3) for 5-ZGNRs with (a)Non-passivation as a reference, (b) Mono-hydrogenation, (c)Di-hydrogenation, and (d)side view of atomic configuration of di-hydrogenated 5-ZGNR. Dashed lines represent a section of a unit cell in the ribbon plane. α (β) spin are represented by red (blue).

	n=0	n=1	n=2
⊿E (eV/edge C atom)	-0.11	-0.11	0
Integrated absolute spin density (electrons/a_0^3)	2.741	0.585	0
Magnetism	AFM	AFM	Non-magnetism

Table 4.2: Stabilised energies by spin polarisation ⊿E and integrated spin density for the different number of hydrogen atoms added on the edge carbon atom. The spin densities are for the unit cells shown in Figure 4.10.

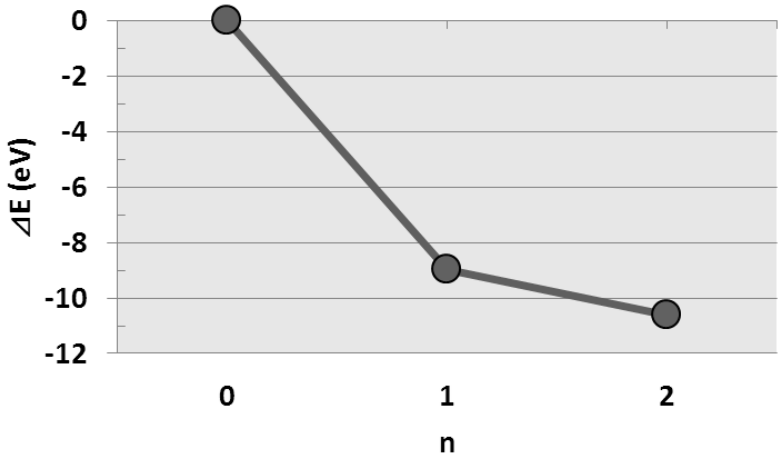

Figure 4.11: The total-energy differences of the system including both ZGNR consisted of 10 carbon atoms and 4 hydrogen atoms.

4.2.4. Klein edge GNRs

Klein edge [38] is defined as an atomic configuration of zigzag edge which each carbon atom is bonded to an additional carbon atom. Klein edge has been experimentally identified by different techniques, such as high resolution transmission electron microscopy [8], scanning tunnelling microscopy [39], and atom-resolved EELS spectroscopy [11]. Figure 4.12 (a) shows schematics of GNR with the bare Klein edge. The bare Klein edge is not favoured energetically because the edge atoms have dangling bonds. Figure 4.12 (b) shows the reconstructed Klein edge in which geometry optimisation is performed with the bare Klein edge structure. The two neighbouring bare Klein edges transform a five-membered ring including the triple bond at the armrest. As a result, this edge reconstruction is found to lower its energy by 0.35 eV/atom.

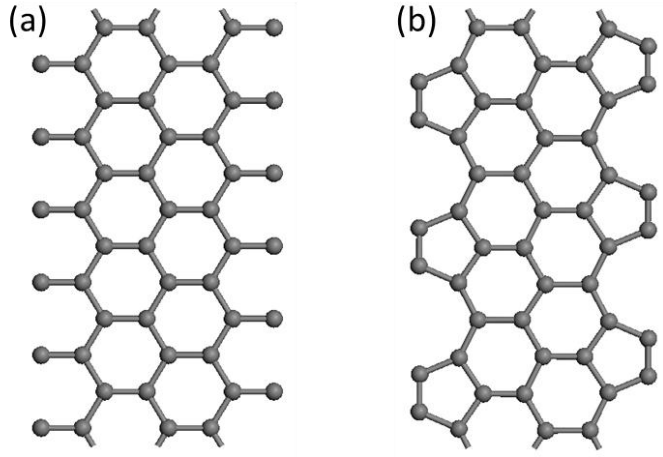

Figure 4.12: Schematics of GNRs with (a) bare Klein edge and (b) reconstructed edge.

Figure 4.13 shows the relaxed structures of GNRs with (a) mono-hydrogenated Klein edge, (c) dihydrogenated Klein edge and (e) trihydrogenated Klein edge. (b), (d), (f) show the side view of (a), (c), (e), respectively. Figure 4.14 shows the computed total-energy differences of the system for the case of hydrogen passivation given by equation 4.1. In the present case, total energy of the system is described below. :

$$E_n^{total} = E_{ribbon} + (4-n)E_{hydrogen} \qquad (4.4)$$

where E_{ribbon} is the energy of the unit cell of GNRs including passivated hydrogen atoms, $(4-n)E_{hydrogen}$ is the energy in the hydrogen reservoir and the notation n means the number of hydrogen atoms per each edge atom. In case of adding four hydrogen atoms to an edge carbon atom we confirmed it is energetically unfavorable. In the unit cell, there are two edge carbon atoms, therefore the maximum hydrogen molecules in the reservoir are set to four. $E_{hydrogen}$ is the energy of hydrogen molecule (=-30.962 eV). The system contains 8 carbon and 8 hydrogen atoms. E_n^{total} can be used to determine the stability of hydrogen passivation. In this system, the most stable structure is trihydrogenated Klein edge structure, which stabilised in non-magnetic ground state.

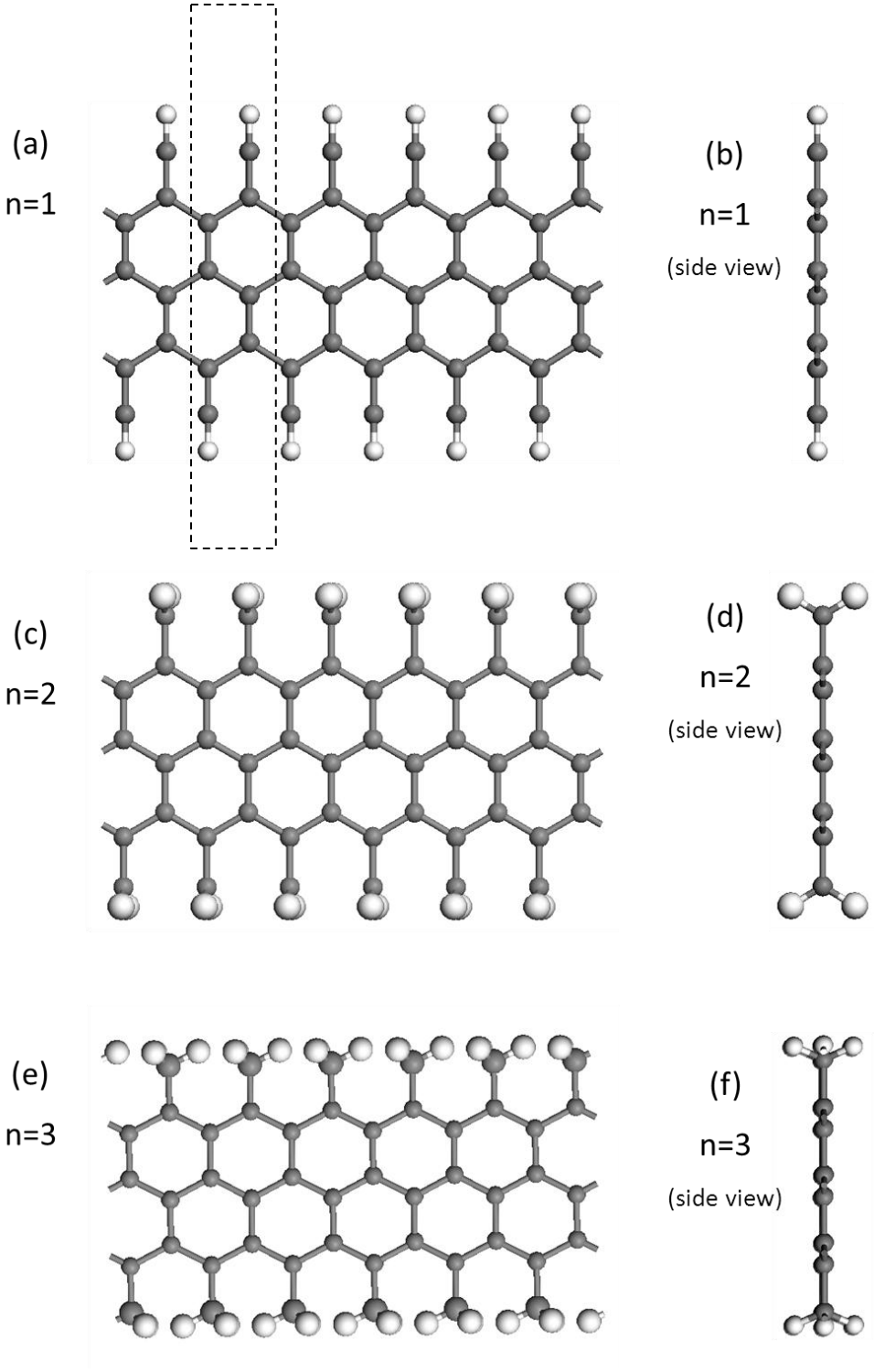

Figure 4.13: Schematics of GNRs with (a) mono-hydrogenated Klein edge, (c) dihydrogenated Klein edge and (e) trihydrogenated Klein edge. (b), (d), (f) show the side view of (a), (c), (e), respectively. Dashed line represents a section of a unit cell in the ribbon plane.

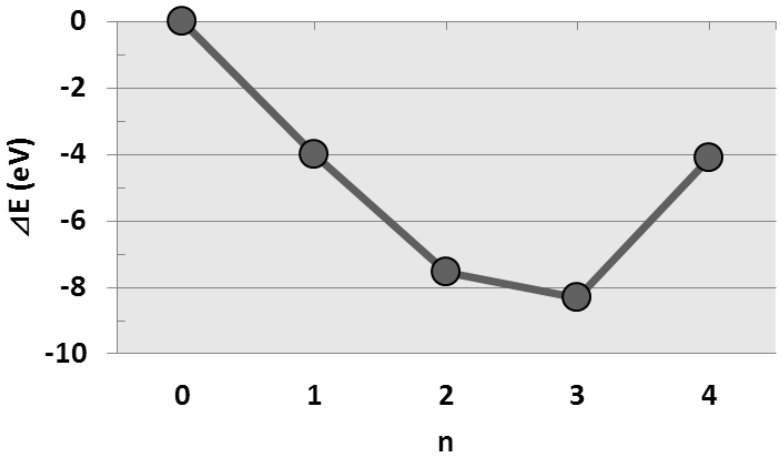

Figure 4.14: The total-energy differences of the system including both GNR consisted of 8 carbon atoms and 8 hydrogen atoms.

4.3. Conclusions

In conclusion, we have reported the systematic study of atomic structures of GNRs. *Ab initio* DFT calculations indicate that the ribbon edges are stabilised by full saturation of all carbon dangling bonds in each system such as armchair and zigzag. In order to compare these different edge structures, the edge energy is defined

$$\mathrm{E}_{edge} = \frac{E_{total} - N_c E_{total}^{at(graphene)} - N_H E_{total}^{at(H2)}}{\mathrm{N}_c^{edge}} \qquad (2.15)$$

where N_c, N_H, N_c^{edge} are the number of carbon atoms, hydrogen atoms, and edge carbon atoms per unit cell, respectively. E_{total} is the total energy per unit cell in the ground state.

$E_{total}^{at(graphene)}$ = -158.530 eV/atom and $E_{total}^{at(H2)}$ = -15.481 eV/atom are total energies of a carbon atom in garphene and a hydrogen atom in the H_2 molecule. These edge energies can compare with different structures and previous data [32] [33] [36] [7]. Figure 4.15 shows the edge energies of the ribbons without hydrogen atoms. Energies are plotted as a function of the ribbon widths. These energies are nearly independent of the ribbon widths and the energetic stabilities can be determined by the edge shape. Energy of zigzag ribbons is approximately 1 eV higher than the others. This can be understood that zigzag edges have dangling bonds and the others have triple bonds instead of dangling bonds. Table 4.3 shows the summary of the edge energies and magnetism for all different edge shapes within this work and Figure 4.16 shows the corresponding edge energies in a graph for easy comparison. These results indicate that the armchair ribbon by two hydrogen atoms is the most stable within this work. With regard to magnetic properties, only ZGNRs unsaturated by hydrogen exhibit the magnetism (antiferromagnetism).

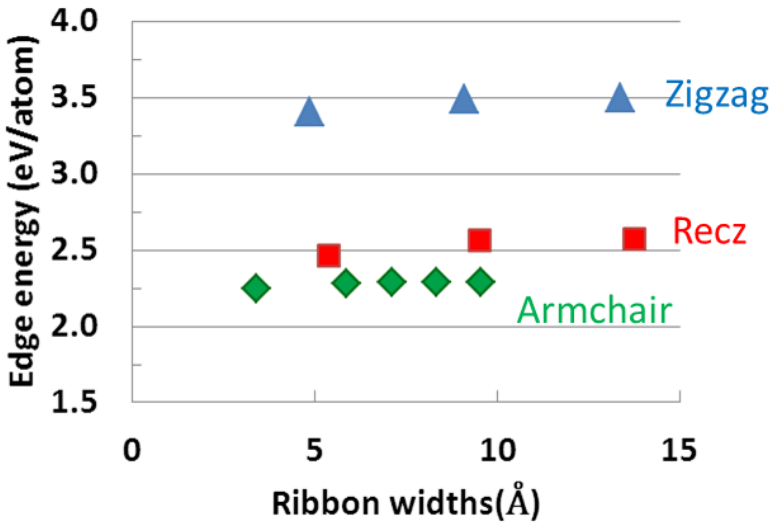

Figure 4.15: The edge energies of the ribbons without hydrogen passivation. Energies are plotted as a function of the ribbon widths. Zigazag, Recz and Armchair represent ZGNRs, reconstructed ZGNRs and AGNRs, respectively.

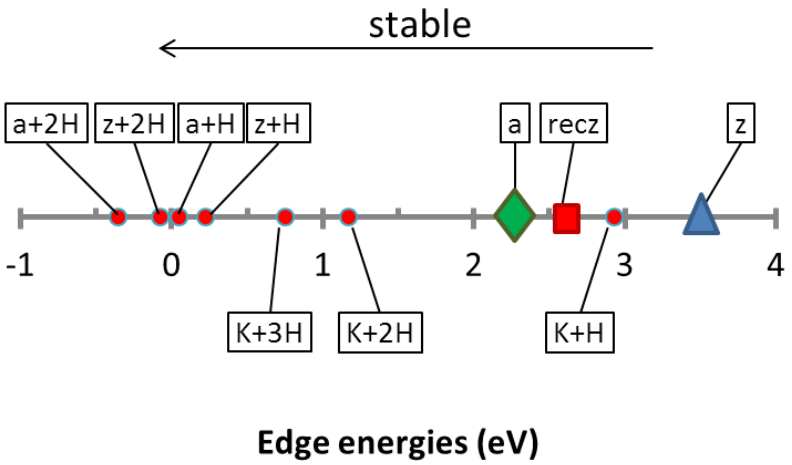

Figure 4.16: The edge energies of the ribbons for all structure within this work. K, z, a, recz represent GNRs with Klein edge, zigzag edge, armchair edge, reconstructed zigzag edge, respectively. H represent hydrogen atoms added on an edge carbon atoms. The small edge energy indicates that the edge formation is more stable.

	Edge energy (eV/atom)	Magnetism
Zigzag	3.469	AF
Zigzag+H	0.223	AF
Zigzag+2H	-0.078	Non
Armchair	2.287	Non
Armchair+H	0.050	Non
Armchair+2H	-0.357	Non
Reconstructed Zigzag	2.574	Non
Klein+H	2.928	Non
Klein+2H	1.166	Non
Klein+3H	0.753	Non

Table 4.3: Summary of the edge energies and magnetism. Edge energies are calculated by dividing the total energy by the number of edge carbon atoms. The small edge energy indicates that the edge formation is more stable.

5. Electronic structure and EELS spectra of GNRs

In this chapter, we will focus our attention on the unoccupied electronic states of GNRs. As shown in chapter 4, the atomistic structures of GNRs are optimised for the different edge structures and modifications. This section deals with the theoretical EELS for GNRs which were relaxed. In particular, we have investigated the dependence of the edge structure, including armchair, zigzag, and Klein edges, the core excitation on the different atomic sites, and the passivation, which has been examined for different width N.

In addition, in order to understand electronic state in detail, we report the polarised EELS which are obtain by polarising the orientation of the incident electron beam. Since GNRs are anisotropic materials, it is strongly reflected in the high-directionality of its orbitals. It is therefore possible to discuss the origin of some EELS features in terms of σ* and π* orbitals.

For the conditions of EELS calculations, all the calculation in this work was performed by CASTEP. For the exchange-correlation functional, the Local Density Approximation (LDA) method was used. For each GNRs model, based on the results of the Chapter 3, the ribbon length is built more than 7 Å and the layers were separated by 7 Å vacuum spaces and along the ribbon width direction, over 5 Å vacuum spaces was installed (see Appendix B). The Brillouin zones of the GNR unit cell are sampled by

Monkhorst-Pack grids of the form 1 x k x 1, which k is set so that the maximum spacing between k points in the periodic direction y is $0.020 \times 2\pi Å^{-1}$. For EELS spectra, the Fermi energy was set to zero and smearing width is 0.2 eV. The intensity of spectra were normalised by using the area in the range of approximately 0-60eV.

5.1. Armchair GNRs (AGNRs)

The theoretical EELS calculations are performed for different ribbon width with non-passivation and hydrogen passivation in AGNRs. In this section, we report the calculated EELS spectra and the dependence on the atomic site, ribbon width and the edge modification.

5.1.1. Non-passivation

The relaxed structures of non-passivated AGNRs with different width N = 5-9 were showed in Figure 4.2. The characteristic feature is a triple bond which eliminates the dangling bond at the edge. First, by performing EELS calculations systematically, we demonstrate the relationship between the EELS spectrum and the ribbon width. Next, we pay attention to the edge structure which is characteristic of non-passivated AGNRs, and analyse in detail.

5.1.1.1. Ribbon width

Figure 5.1 shows the results of total EELS spectra with 5 different ribbon widths. Each spectrum is obtained by averaging the corresponding spectra for the symmetry-independent carbon atoms, and the chemical shifts are not taken into account in the individual spectra. As a consequence, the total spectra may contain about 2eV ambiguity at most [40]. The top plot indicates the calculated EELS spectrum of an infinite sheet of graphene for reference purposes. The features of each curve converge slowly to the EELS spectrum of the graphene sheet as the ribbon width becomes wider. Therefore, in the spectra of the ribbons, the second peaks around 2 eV and the peaks around 7-11 eV can be identified as the π^* peaks and σ^* peaks respectively. Note that the first peak around 0 eV appears in EELS spectra for all ribbon widths although there are no similar signal below the π^* peak graphene. These peaks can be predicted to come from the edge carbon atoms because these first peaks are the new feature in the ribbons and also the intensities of these peaks decrease as the ribbon width become wider. Next, we will focus on the ribbon width N=9 as an example AGNR in order to undertake the detailed analysis. (The atomic resolved EELS spectra of N=5-8 are shown in Appendix A.)

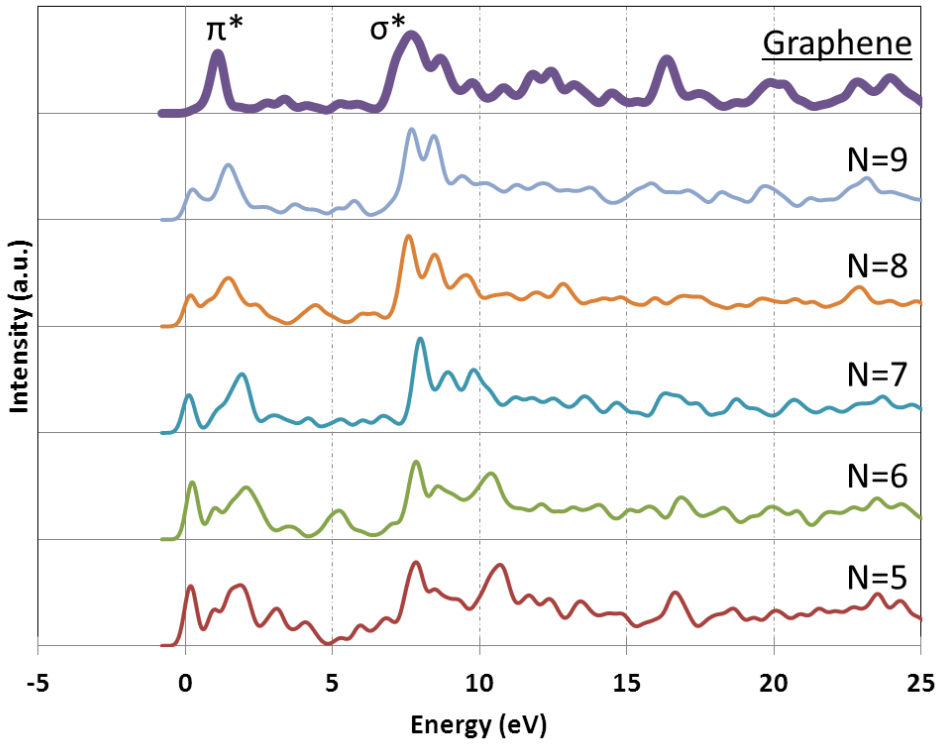

Figure 5.1: EELS spectra of AGNRs for various widths N=5-9. The top line is the EELS spectrum of an infinite sheet of graphene.

5.1.1.2. Atomic resolved and polarised spectroscopy

Figure 5.2 shows (a) the relaxed structure of the non-passivated 9-AGNR and (b) the atomic resolved EELS spectra. In this case, independent EELS calculations were performed with the core-hole inserted into one of the five distinct atoms in different environments (labelled by the number 1 to 5). The EELS calculations were performed for each atom. Each spectrum was normalised by the area under the EELS spectra so that total integrated EELS =1. A total spectrum is obtained by averaging over

the individual spectra. Figure 5.3 shows the results of EELS calculations with polarised electric field and orientation in the direction of the (a) X, (b) Y and (c) Z-axis respectively. In bulk graphene, only when the direction of applied electric field is in plane of graphene sheet, transition into the anti-bonding states of σ symmetry in X-Y plane can be allowed. When the direction of applied electric field is Z axis, transition into the anti-bonding states of π symmetry is allowed. However, non-passivated AGNRs have the triple bonds at the edge and are expected to be allowed to transition into the anti-bonding states of π symmetry in the X-Y plane. In Figure 5.2, the four peaks are labelled by P1 to P4 in the total spectrum. These atomic resolved spectra show the first peak at the edge carbon atom (labelled by the number 1) makes a big contribution to the peak P1 in the total spectrum. In Figure 5.3, this first peak from the edge atom is observed in (a) X-direction. Therefore this peak can be assigned to the transition into the anti-bonding π state of the triple bonds in X-Y plane. The peak corresponding to the peak P2 is present in the spectra of each atom and appears in the (c) Z-direction. Therefore the peak P2 can be assigned to π* peak. In Figure 5.3, the peaks P3 and P4 mainly appear in the (a) X-direction and (b) Y-direction, respectively. Therefore these peaks can be assigned to σ* peak. Particularly, considering the polarisation direction, the peaks P3 and P4 mostly come from the interchain and the intrachain bonds, respectively.

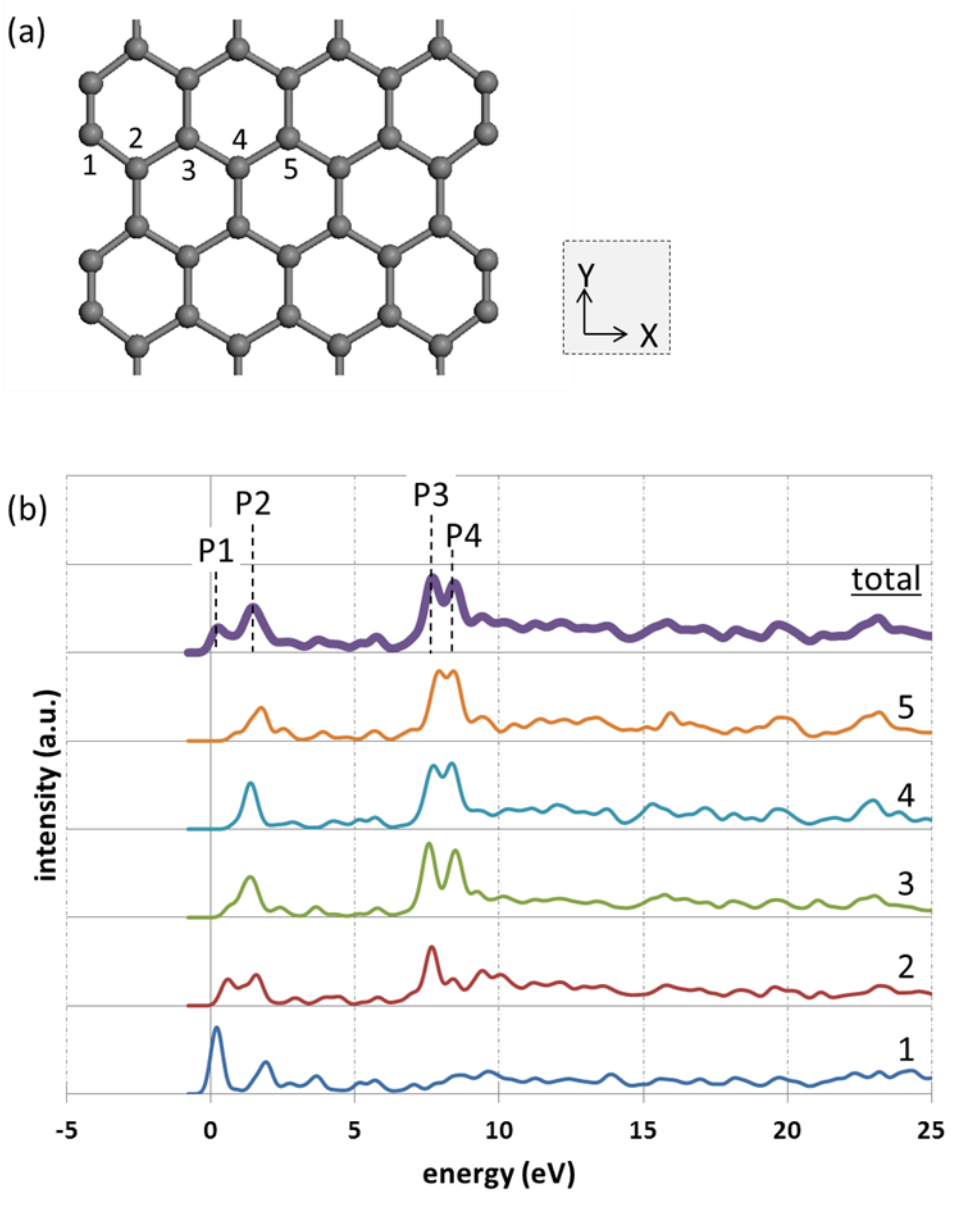

Figure 5.2: (a) The relaxed structure of non-passivated 9-AGNR and (b) EELS spectrum for each core-hole atom. The top plot shows the total spectrum averaged over all possible core-hole sites.

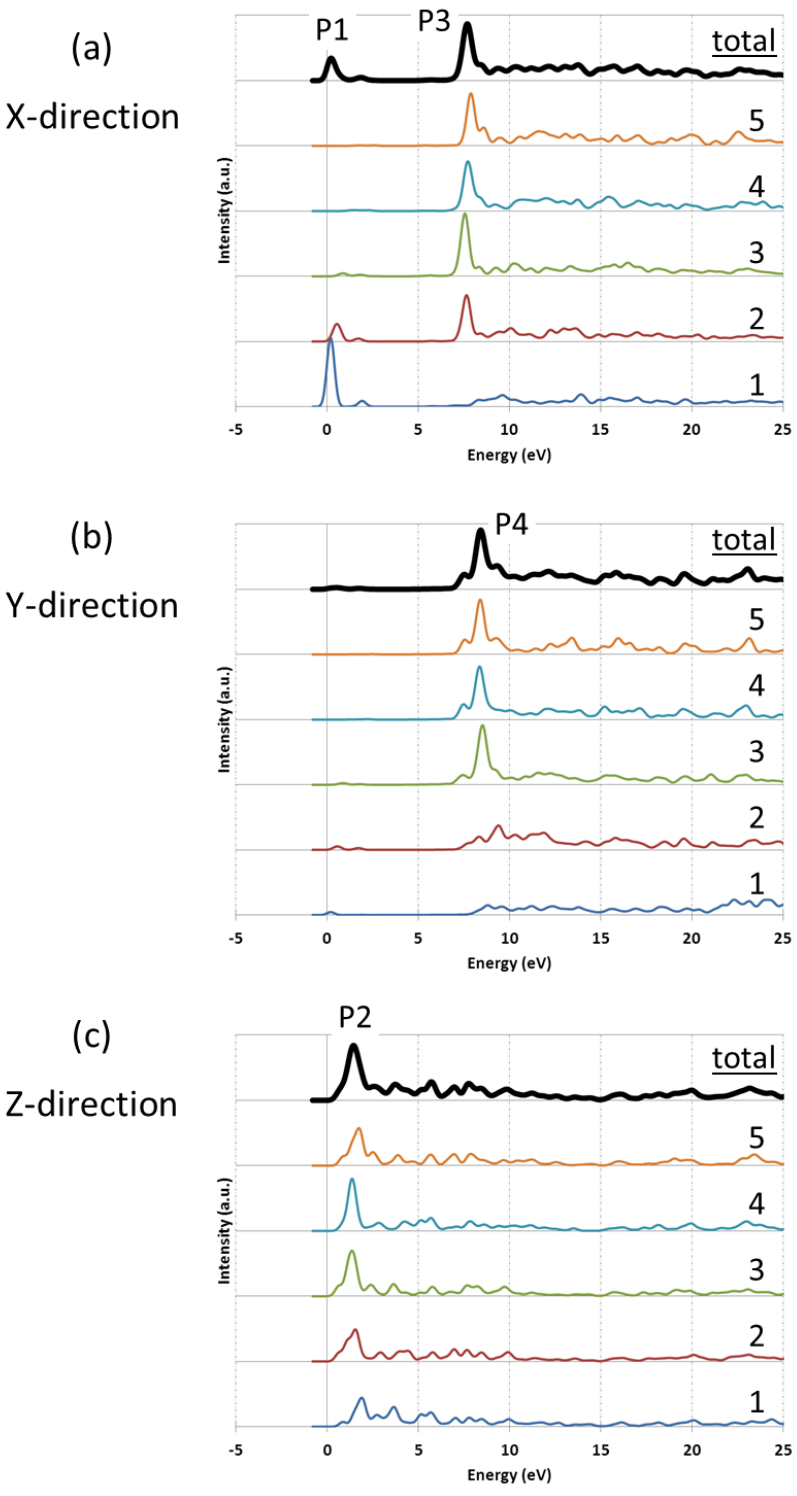

Figure 5.3: Polarised EELS spectra with the direction (a) X-axis, (b) Y-axis, (c) Z-axis. The top plots show the total spectra averaged over all possible core-hole sites.

5.1.2. Hydrogen passivation

The relaxed structures of AGNRs with the different number of hydrogen atoms bonded to the edge carbon atom are shown in Figure 4.4. In this section, by performing EELS calculations systematically, we demonstrate the effect of hydrogen modification at the edge on the EELS spectra, and analyse the results in terms of the electronic states.

Figure 5.4 shows the total spectra of two different widths in mono-hydrogenated AGNRs. The π^* and σ^* peak are clearly observed. By contrast with the case of bare AGNRs, the spectral dependence on ribbon width is extremely small. The EELS spectrum largely reflects the state of the edge structure in the narrow ribbon because the proportion of the edge structure is relatively large. However, in the hydrogenated AGNR, the spectral change is small even in a narrow ribbon N = 5. This can be understood from the fact that the distortion of the hexagonal structure at the edge is small because the triple bond is eliminated by the addition of hydrogen atom.

Figure 5.5 shows the total EELS spectra of 8-AGNR with non-passivation for reference purposes, mono-hydrogenation and di-hydrogenation. The number of hydrogen atoms bonded to each edge carbon atom has a dramatic influence on the EELS spectra. Each spectrum can be clearly distinguished. Especially, the first peak at the non-passivated ribbon is destroyed by adding hydrogen atom on the edge carbon atom. In di-hydrogenated ribbon, two prominent peaks appear between π^* and σ^* peaks. They are also identifiable features. In order to proceed with a detailed analysis, we focus on atom-resolved EELS spectra in each spectrum.

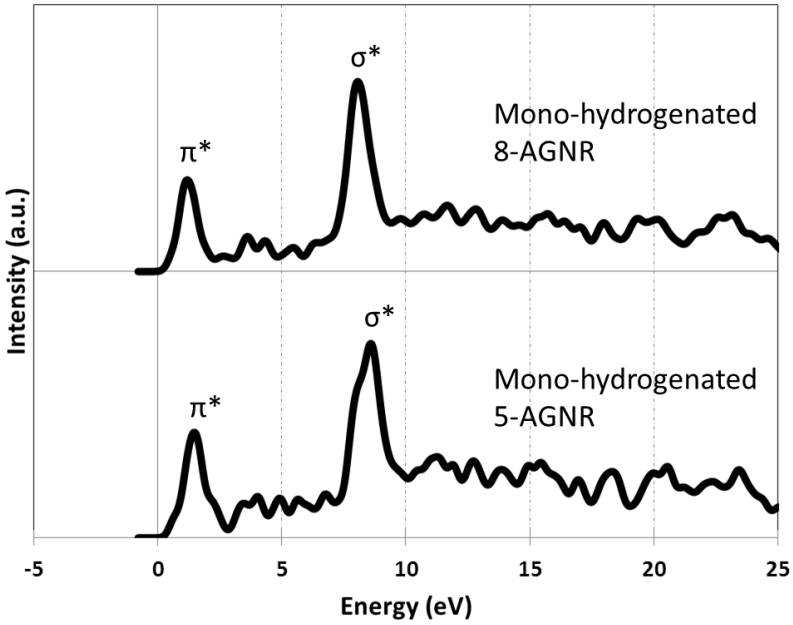

Figure 5.4: Total EELS spectra of 5 and 8-AGNR with mono-hydrogenation.

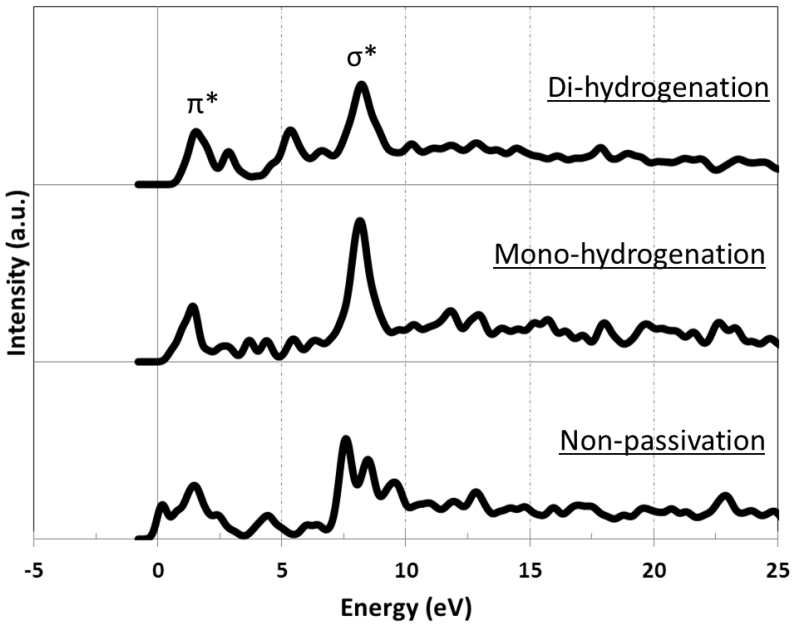

Figure 5.5: Total EELS spectra of 8-AGNR with non-passivation for reference purposes, mono-hydrogenation and di-hydrogenation.

5.1.2.1. Mono-hydrogenation

Figure 5.6 (a) shows the relaxed structure of mono-hydrogenated 5-AGNR. The three distinct atomic sites in different environments of this supercell are labelled as 1, 2 and 3. The X and Y-axes are in-plane and the Z-axis is perpendicular to the graphene nano-ribbons. (b) shows the results of EELS calculations for core-hole on atoms labelled 1, 2 and 3 with unpolarised electric field. The top plot is the total EELS spectrum which is obtained by averaging over the individual spectra.

Figure 5.7 (a), (b) and (c) show the results of EELS calculations for core-hole on 1, 2 and 3 with polarised electric field and the orientation in the direction of the X, Y and Z-axis respectively. When the direction of applied electric field is X and Y axis, transition into the σ* orbitals is allowed. When the direction of applied electric field is Z axis, transition into the anti-bonding states of π* orbitals is allowed. The σ* peaks in Figure 5.6 (b) obtained from the different atomic sites can be observed in X and Y direction in Figure 5.7 as expected. The peaks below σ* peak, approximately below 7eV, are shown in Figure 5.7 (c). Due to polarisation in the Z-direction, these peaks can be assigned to a transition into the anti-bonding π* states. However, in this area, a new peak which isn't observed in bare AGNR appears at approximately 4 eV in X and Y-direction as seen in Figure 5.7 (a)(b). These peaks are assigned to the σ* of bonding between carbon and hydrogen atoms because it is a new feature at the edge carbon atom and appears only in X-Y plane.

Figure 5.8 shows the projected density-of-states (PDOS) for excited edge carbon atom in hydrogen passivated 5-AGNR. In order to compare the peaks, the atom-resolved EELS spectrum for the same atom is shown in the upper plot. As seen in Eq 2.1 and 2.3, the

EELS signal is proportional to a product of the DOS term and the transition matrix element. Therefore the DOS make a strong contribution to the EELS spectra. Moreover, only the p density-of -states needs to be considered in this thesis due to the dipole selection rule. In Figure 5.8 the EELS spectrum reflects the peak separations and intensities of p orbitals in PDOS very well. This indicates that from the experimental point of view, EELS can probe the unoccupied PDOS directly, and from the theoretical point of view, the further information of the EELS peak can be obtained by reference to the PDOS.

Below approximately 3 eV in PDOS, these bands are contributed by the only p orbitals. Above approximately 3 eV, these bands are contributed by hybrid orbitals formed by the mixture of s and p orbitals. Namely, in the EELS spectrum, the peaks below approximately 3 eV are the transition into the anti-bonding π^* states composed of only p orbitals and the two large peaks above approximately 3 eV are the transition into the anti-bonding σ^* states composed of hybrid orbitals formed by the mixture of s and p orbitals. These data of unoccupied electronic states indicates the origins of the EELS peaks clearly and shows that there is good evidence that the peak assignments are reasonable.

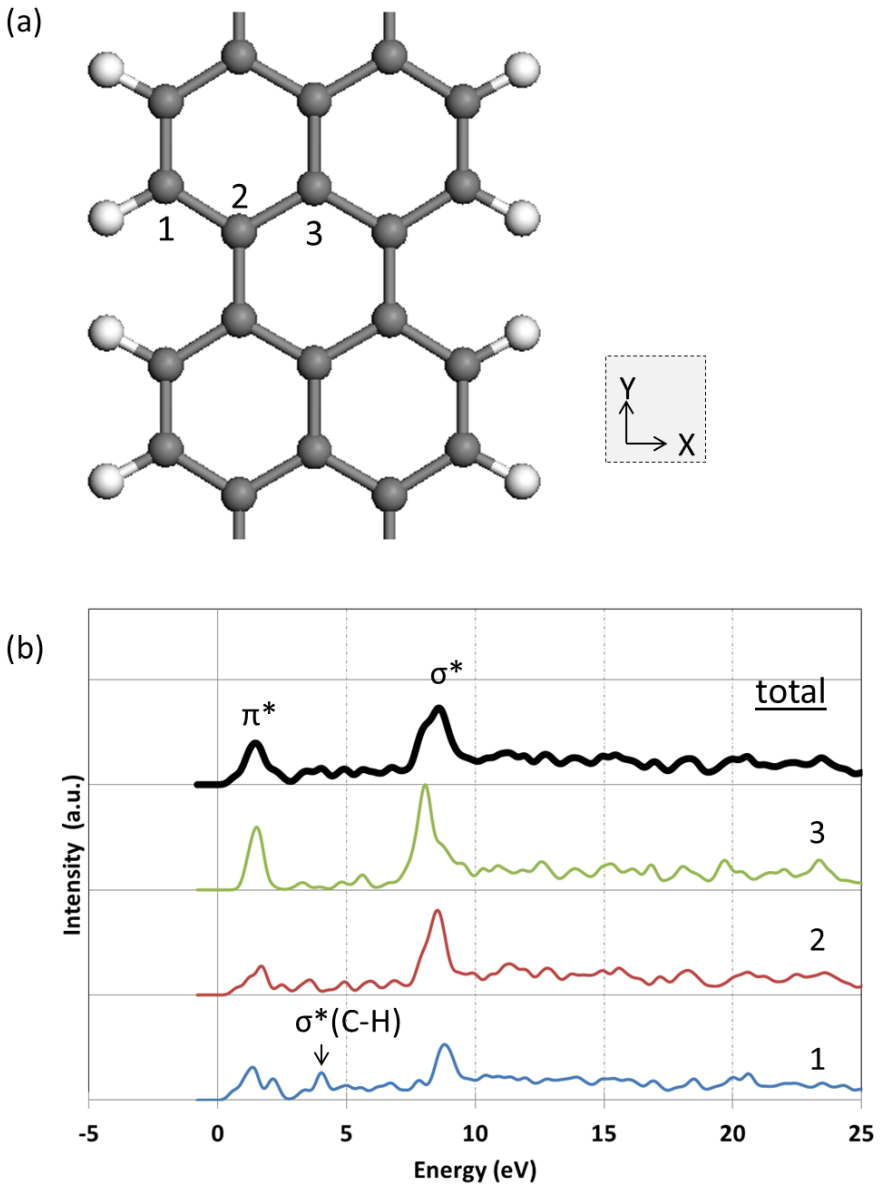

Figure 5.6: (a) A relaxed structure of mono-hydrogenated 5-AGNR (b) the atom-resolved EELS spectrum. The top line shows the total spectrum averaged over all possible core-hole sites.

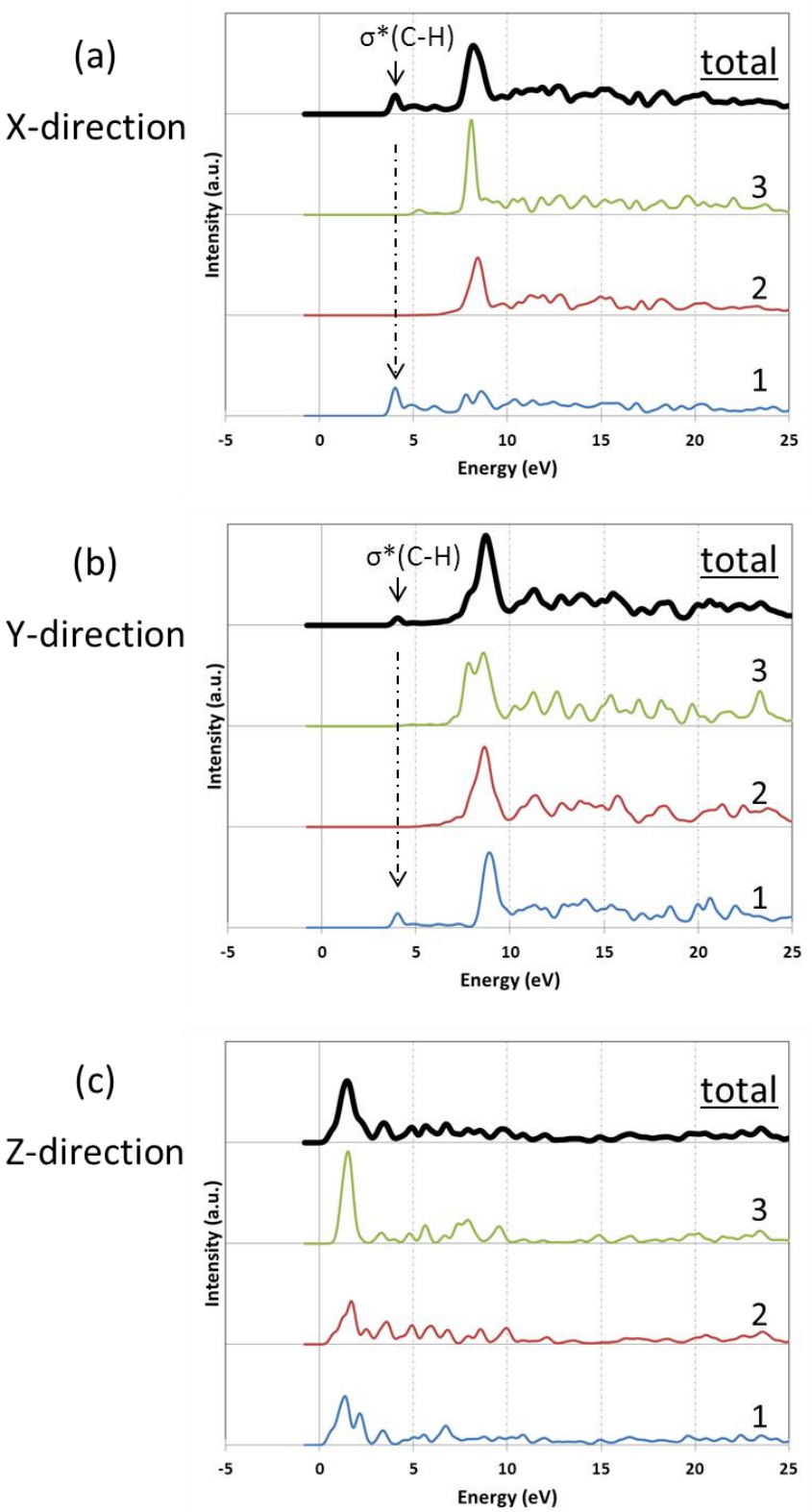

Figure 5.7: Polarised EELS spectra with (a) X-axis, (b) Y-axis, (c) Z-axis. The top plots show the total spectra averaged over all possible core-hole sites.

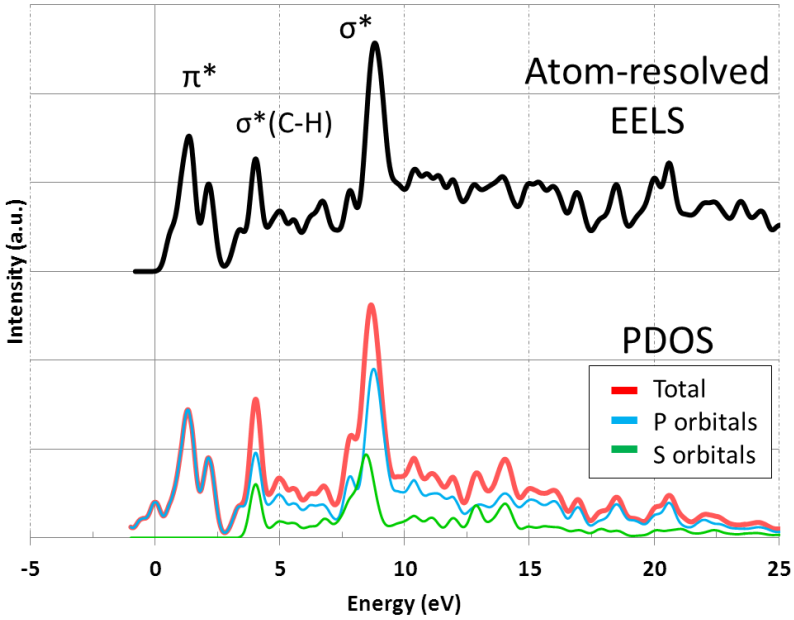

Figure 5.8: (Above) Theoretical EELS spectrum and (Below) projected density-of-states (PDOS) for excited edge carbon atom in mono-hydrogenated 5-AGNR.

5.1.2.2. Di-hydrogenation

Figure 5.9 shows (a) the relaxed structure of the di-hydrogen passivated 8-AGNR and (b) the atomic resolved EELS spectra. In this case, independent core-holes were inserted into four distinct atomic sites in different environments. The EELS calculations were performed for each atomic site. Each spectrum was normalised by the area under the EELS spectra so that total integrated EELS =1. A total spectrum is obtained by averaging over the individual spectra. Figure 5.10 shows the results of EELS calculations with polarised electric field and orientation in the direction of the (a) X, (b) Y and (c) Z-axis respectively.

The π* and σ* peaks are clearly observed in the total EELS spectrum as seen in Figure 5.9(b). As expected, these peaks also can be seen in the direction of Z axis and X-Y plane in Figure 5.10, respectively. The two peaks between π* and σ* peak are labelled by A1 and A2 in the total spectrum. These peaks mainly come from the edge site atom. In the spectrum at the edge carbon atom, the π* peak vanishes due to the sp3 carbon atom bonded to two hydrogen and two carbon atoms. Then, instead of the π* peak, the double peak is observed around 2.5eV. These peaks also can be seen in all three directions of X, Y and Z, respectively in Figure 5.10. These directions correspond to the orientations of two C-H bonds connected to the edge carbon atom. Moreover these peaks are not seen in the spectra of non-passivated AGNRs, therefore this double peak is attributed to σ* peak of C-H bonding. In the total spectrum, this double peak corresponds to the shoulder of the π* peak and the peak A1. Around 5.3eV, in the spectrum of edge carbon atom, a prominent peak corresponding to A2 appears. This peak is attributed to the σ* peak of the edge carbon atom because the peak is mainly seen in X and Y direction in Figure 5.10, and has red-shifted from 2.9eV at the other atomic sites. This shift can be understood by the fact that the bond length at the edge site becomes longer due to the hydrogen saturation on the edge carbon atom.

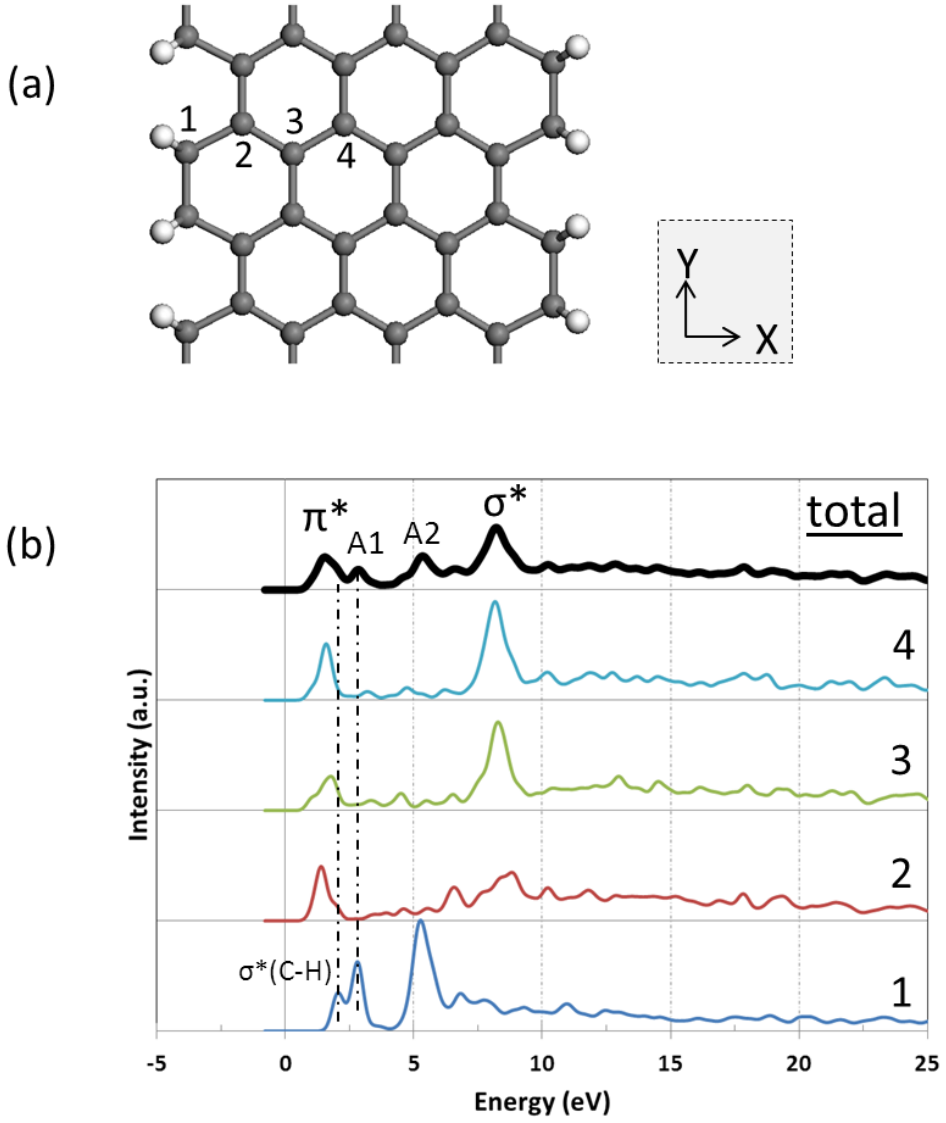

Figure 5.9: (a) Relaxed structure of di-hydrogenated 8-AGNR (b) the atom-resolved EELS spectra. The top plot shows the total spectrum averaged over all possible core-hole sites.

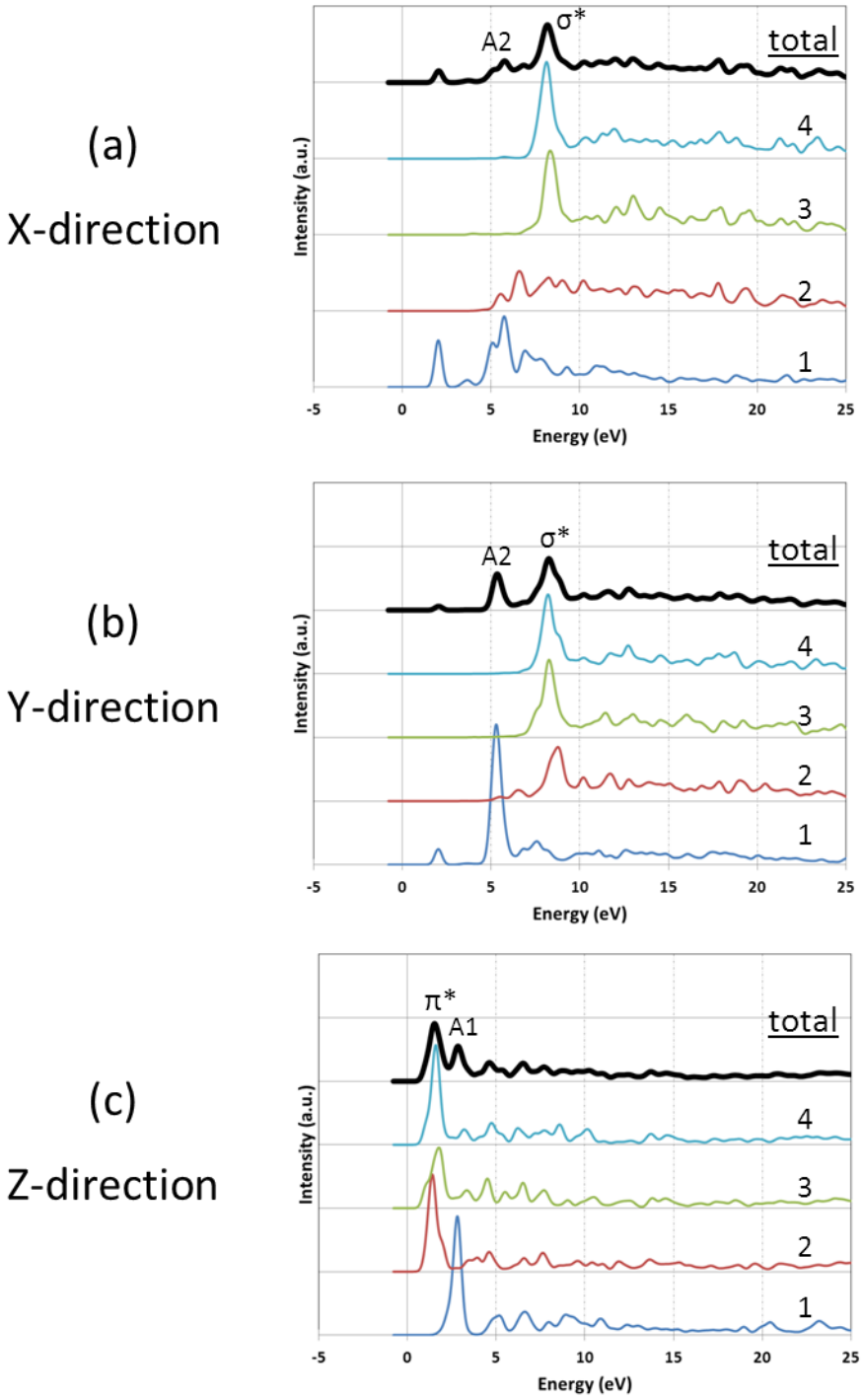

Figure 5.10: Polarised EELS spectra of di-hydrogenated 8-AGNR with (a) X-axis, (b) Y-axis, (c) Z-axis. The top plots show the total spectra averaged over all possible core-hole sites.

5.2. Zigzag GNRs (ZGNRs)

The theoretical EELS calculations are performed for different ribbon width with non-passivation, self-passivation, hydrogen passivation and Klein edge in ZGNRs. In this section, we report the calculated EELS spectra and the dependence on the atomic site, ribbon width and the edge modification.

In chapter 4, it was confirmed that the magnetism in ZGNRs with non-passivation and mono-hydrogen passivation emerge. However, the effect of spin polarisation on EELS spectra was very small. Figure 5.11 displays the EELS spectra for the edge atom in non-passivated 4-ZGNRs as an example. The solid red line and the black dashed line represent EELS with non-spin-polarisation and spin-polarisation, respectively. These two spectra are almost identical although some small discrepancy exists. Therefore, the EELS calculations in this chapter don't include the spin polarisation.

5.2.1. Non-passivation

The relaxed structures of non-passivated ZGNRs with different width N = 3-7 are shown in Figure 4.6. The characteristic is the dangling bond at the edge. The edge carbon atoms of bare ZGNRs are more active than that of bare AGNRs due to the presence of this dangling bond. First, by performing EELS calculations systematically, we demonstrate the relationship between the EELS spectrum and the ribbon width. Next, we pay attention to the edge structure which is characteristic of non-passivated ZGNRs, and analyse in detail.

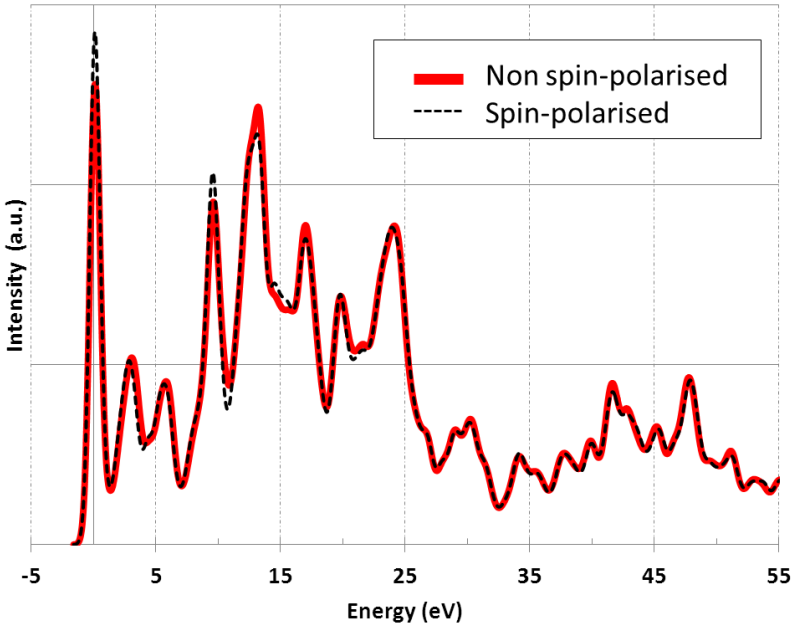

Figure 5.11: The EELS spectra for the edge atom in non-passivated 4-ZGNRs. The solid red line and the black dashed line represent EELS with non-spin-polarisation and spin-polarisation, respectively.

5.2.1.1. Ribbon width

Figure 6.7 shows the total EELS spectra calculated for four different widths. The top plot indicates the calculated EELS spectrum of graphene for reference purposes. Unlike the AGNRs case, the total EELS spectra of ZGNRs converge slowly to the EELS spectrum of graphene as the ribbon width becomes wider. This could be understood as the strong effect of the dangling bonds at the edge. In the spectra of the ribbons, the peaks at approximately 1-2 eV and the peaks around 7-11 eV can be identified as the π^* peaks and σ^* peaks respectively. Note that the first peak around 0 eV appears in EELS spectra for all ribbon widths although there is no similar signal below the π^* peak in graphene. These peaks can be

predicted to come from the edge carbon atoms because these first peaks are the new feature in the ribbons and also the intensities of these peaks relatively decrease as the ribbon width become wider. Next, we will focus on the ribbon width N=4 as an example ZGNR in order to undertake the detailed analysis. (The atomic resolved EELS spectra of N=3 and 5-8 are shown in Appendix A.)

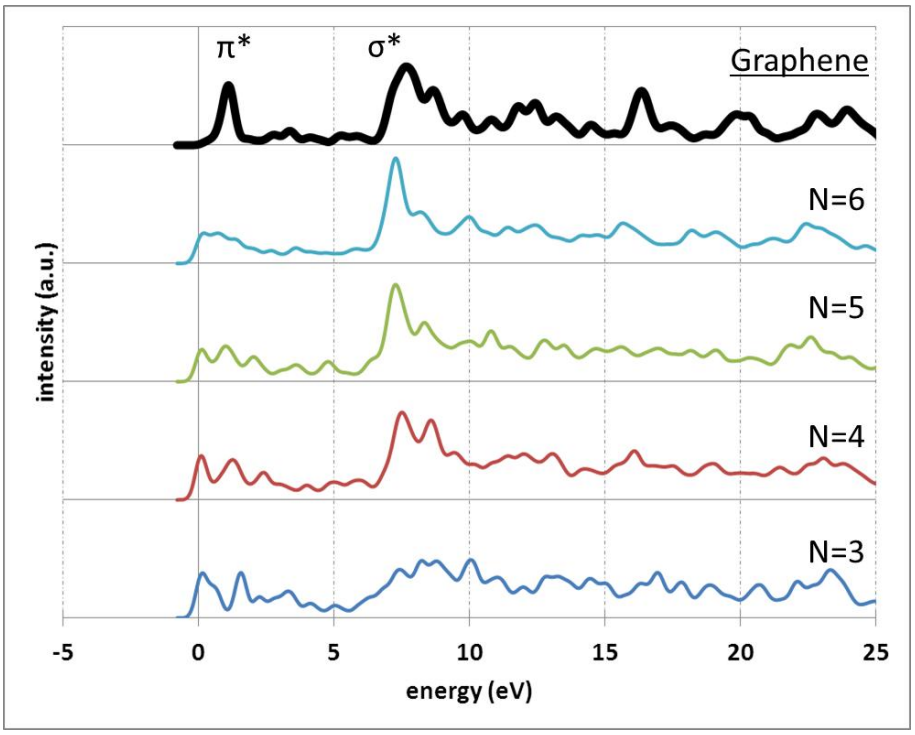

Figure 5.12: EELS spectra of ZGNRs with different widths N=3-6. The top line is the EELS spectrum of graphene sheet.

5.2.1.2. Atomic resolved and Polarised spectroscopy

Figure 5.13 shows (a) the relaxed structure of the non-passivated 4-ZGNR and (b) the atomic resolved EELS spectra. In this case, independent core-holes insert into one of the four distinct atoms in different environments. The EELS calculations were performed with the each excited atom labelled by the number 1 to 4. Each spectrum was normalised by the area under the EELS spectra so that total integrated EELS =1. A total spectrum is obtained by averaging over the individual spectra. Figure 5.14 shows the results of EELS calculations with polarised electric field and orientation in the direction of the (a) X, (b) Y and (c) Z-axis respectively. In bulk graphene, when the direction of applied electric field is X and Y axis, transition into the anti-bonding states of σ symmetry are allowed. When the direction of the applied electric field is Z axis, transitions into the anti-bonding states of π symmetry are allowed.

In Figure 5.13, the atomic resolved spectrum shows the first peak at edge carbon atom makes a large contribution to the first peak in the total spectrum as expected. For non-passivated ZGNR, the presence of the edge state and dangling bond state in the vicinity of the Fermi energy was reported [34]. Therefore this peak can be assigned to the transition into the unoccupied state which is a mixture of the edge state and the dangling bond state. In Figure 5.14, this first peak at the edge atom is mainly observed in (c) Z-direction. However, a small peak is also observed in (a) X-direction and (b) Y-direction. These peaks in X-Y plane can be assigned to the transition into unoccupied dangling bond state because they disappear completely by terminating dangling bonds with hydrogen atoms as seen in Figure 5.19 (a) and (b). The peaks around 2 to 6 eV are present in the spectra of each site and appear in the (c) Z-

direction. Therefore these peaks can be assigned to π* peak. The peaks around 7 to 10 eV appear in the (a) X-direction and (b) Y-direction. Therefore these peaks can be assigned to σ* peak.

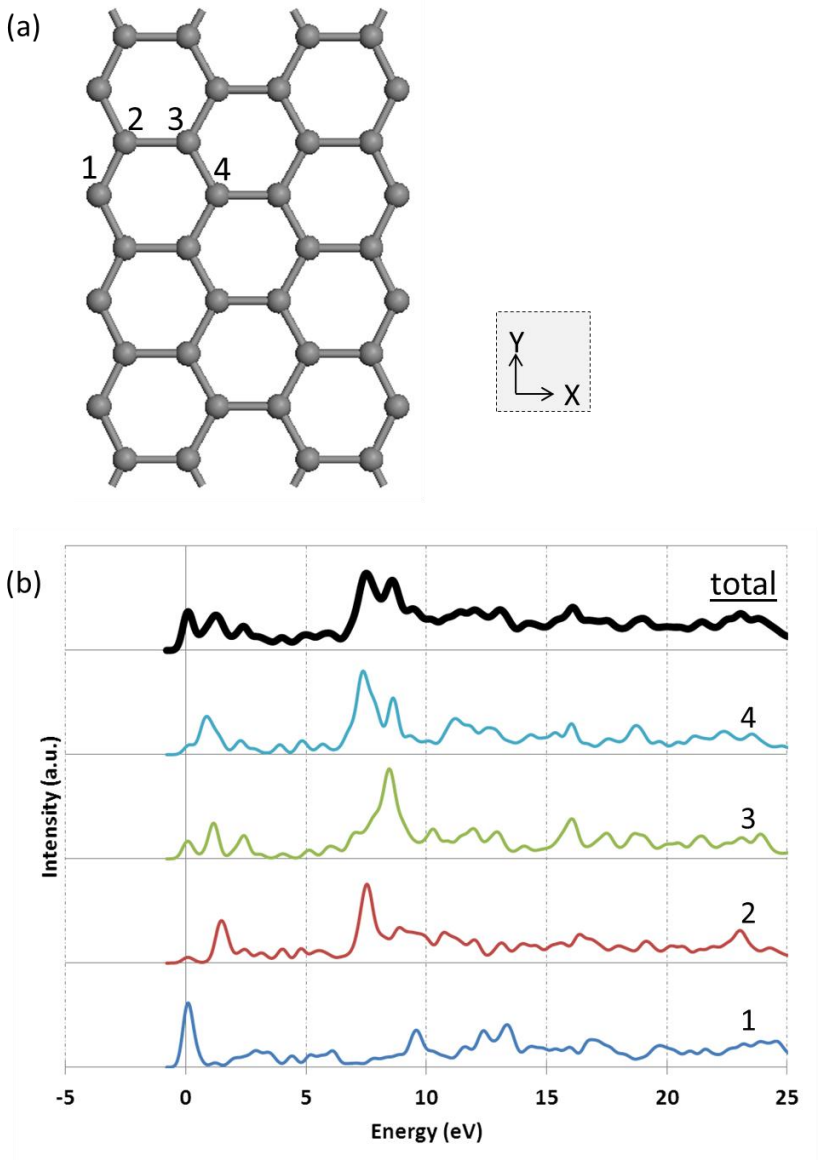

Figure 5.13: (a) The relaxed structure of non-passivated 4-ZGNR and (b) EELS spectrum for each core-hole atom. The top plot shows the total spectrum averaged over all possible core-hole sites.

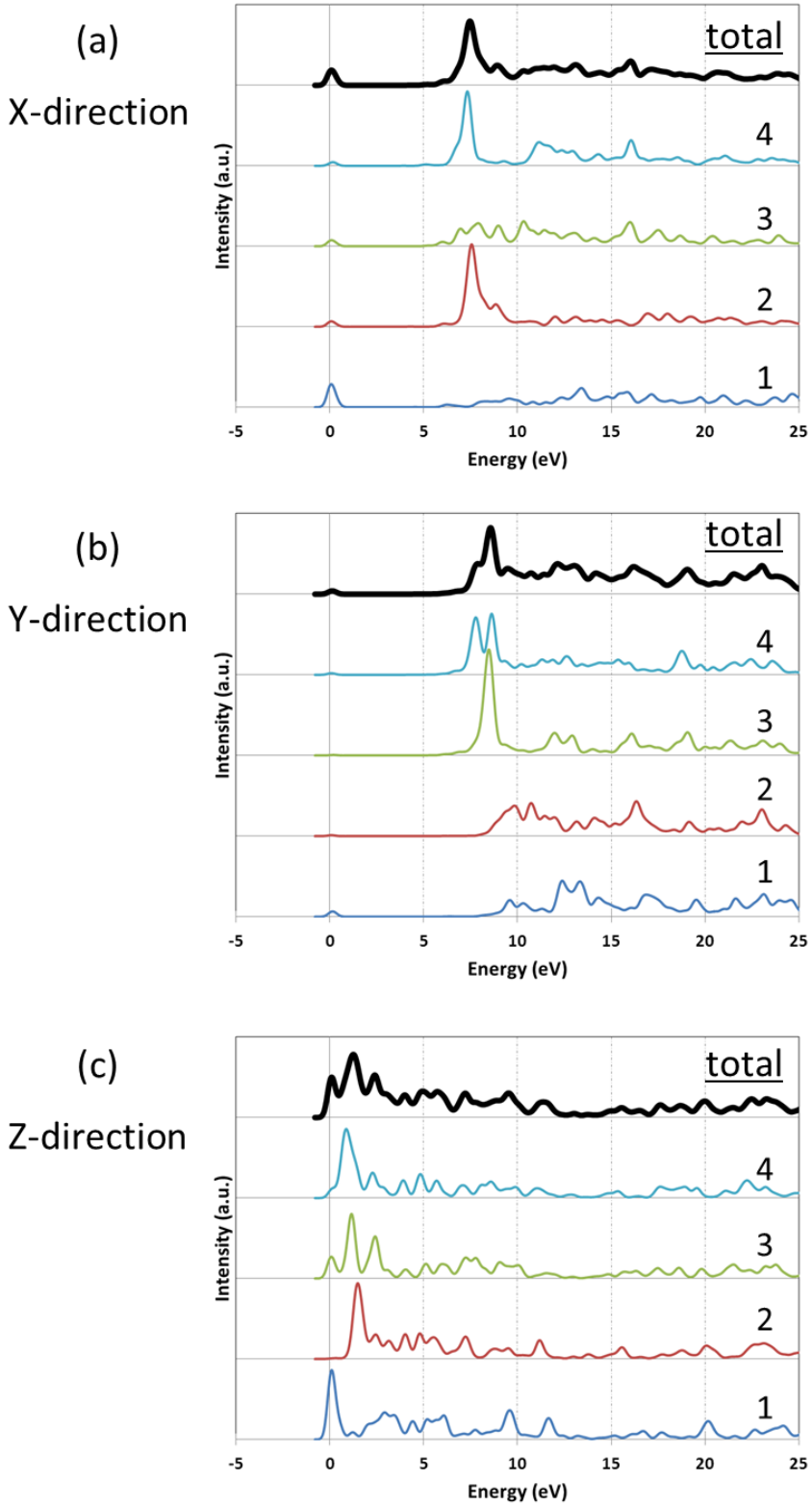

Figure 5.14: (a) Polarised EELS spectra with (a) X-axis, (b) Y-axis and (c) Z-axis. The top plots show the total spectra averaged over all possible core-hole sites.

5.2.2. Self-passivation

Figure 5.15(a) shows the relaxed structure of a reconstructed 5-ZGNR. The ten carbon atoms in different environments of this supercell are labelled as number 1 to 10. The X and Y-axes are in-plane and the Z-axis is perpendicular to the graphene nano-ribbon. Figure 5.15(b) shows the results of independent EELS calculations for atoms 1 to 10 with unpolarised electric field. The top plot is the total EELS spectrum which was obtained by averaging over the individual spectra. Figure 5.16 (a), (b) and (c) show the results of independent EELS calculations for atoms 1 to 10, now with a polarising electric field oriented in the direction of the X, Y and Z-axis respectively. The top plot is the total polarised EELS spectrum for each orientation which was obtained by averaging over the individual site-resolved spectra.

In Figure 5.15 (b), the four peaks are labelled by S1 to S4 in the total spectrum. The features of this curve are very similar to the spectrum of non-passivated AGNRs. These atomic resolved spectra show the first peak at the edge carbon atom make a big contribution to the peak S1 at the total spectrum. In Figure 5.16, this first peak at the edge atom is observed in the X-direction. Therefore this peak can be assigned to the transition into anti-bonding π^* state of the triple bonds in X-Y plane. The peaks corresponding to the peak S2 are present in the spectra for a core-hole at all atomic sites and appear in the Z-direction polarised spectrum as shown in Figure 5.16 (c). Therefore the peak P2 can be assigned to be a π^* peak. The peaks S3 and S4 appear in the Figure 5.16 for X-direction polarisation and for Y-direction polarisation. Therefore the peaks S3 and S4 can be assigned to be σ^* peaks and in particular, the peak S4 has a large contribution from inner carbon atoms labelled 4 to 7.

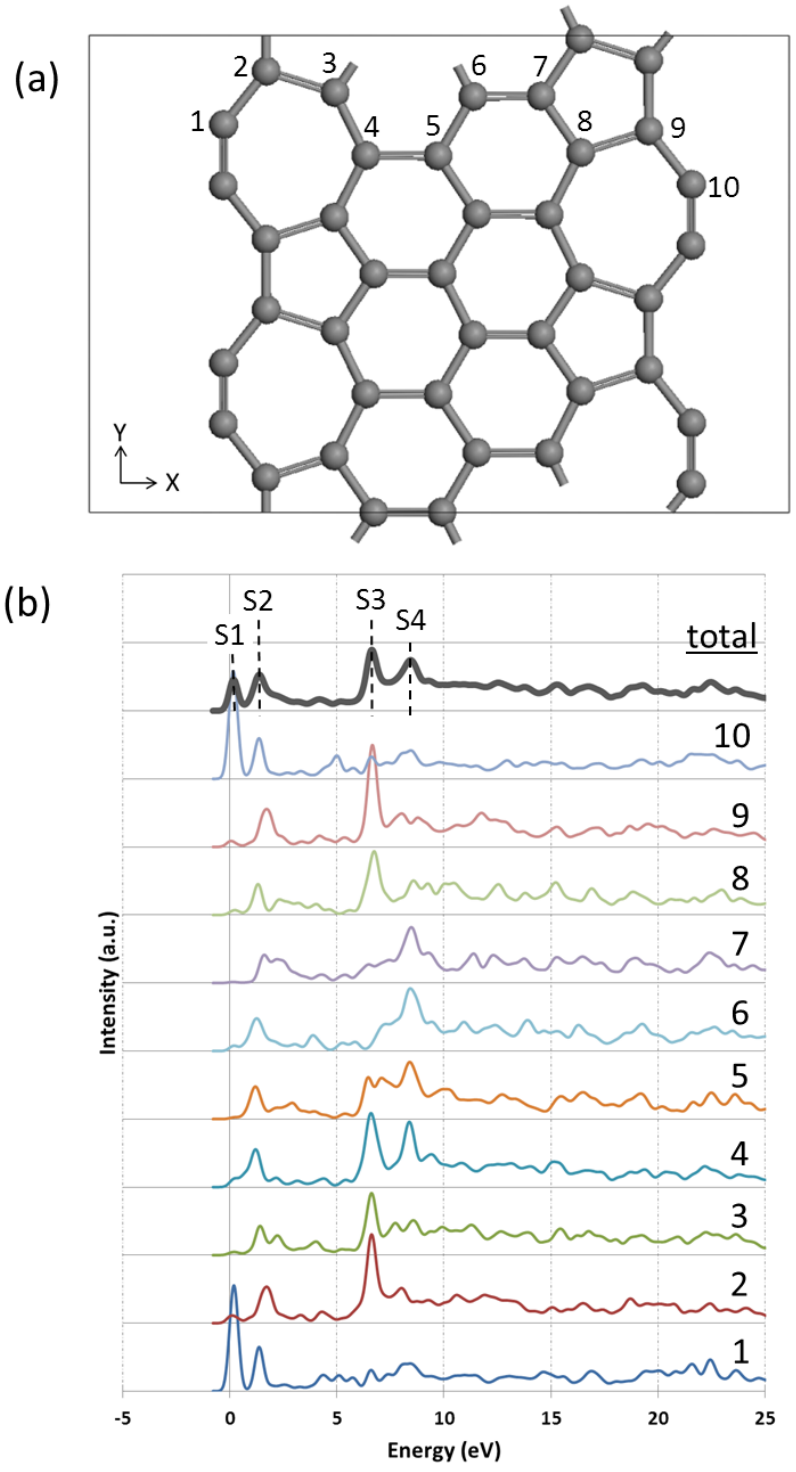

Figure 5.15: (a) A relaxed structure of reconstructed 5-ZGNR and (b) the atom-resolved EELS spectra. The top plot shows the total spectrum averaged over all possible core-hole sites.

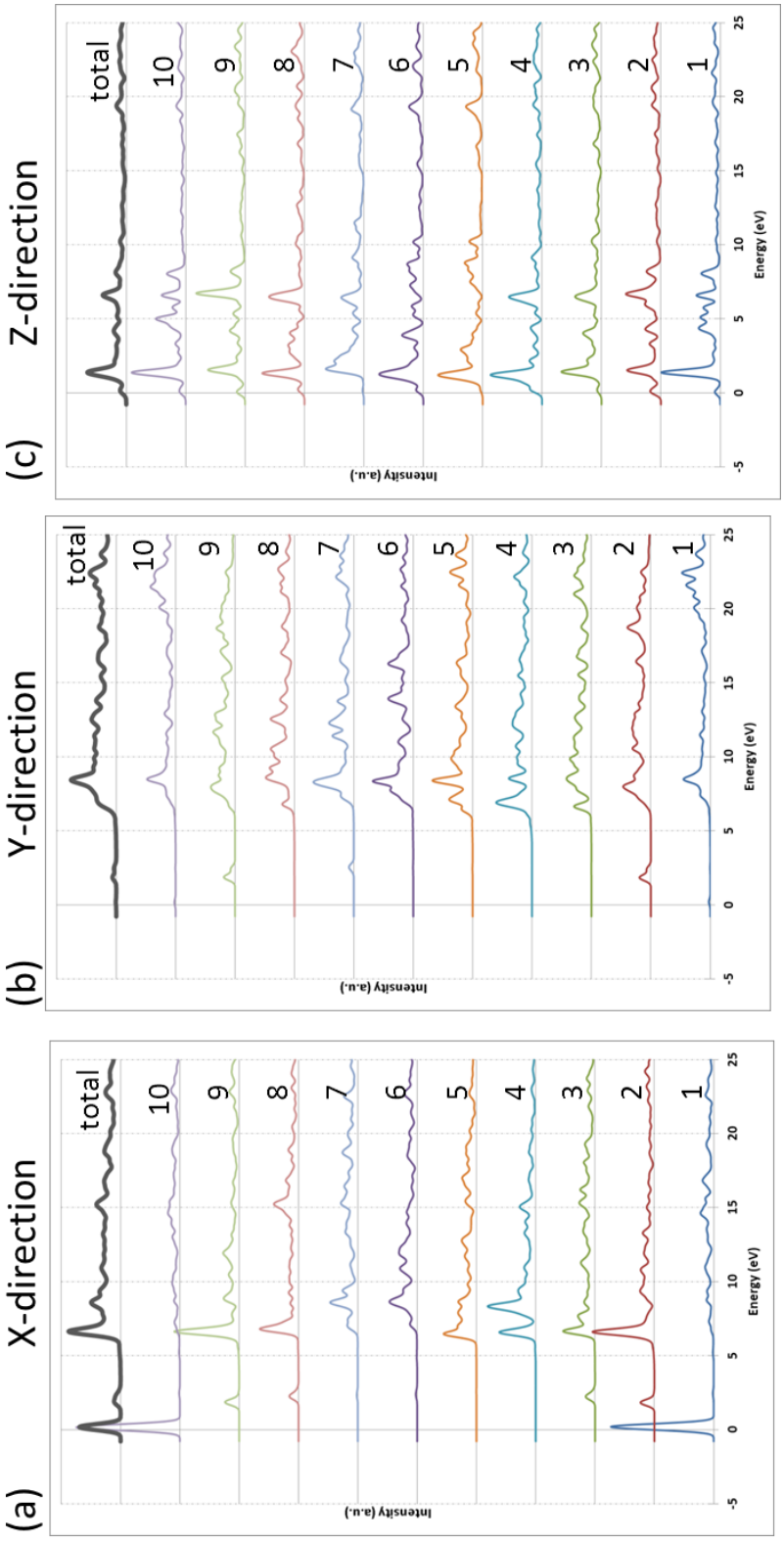

Figure 5.16: Polarised EELS spectra with (a) X-axis, (b) Y-axis, (c) Z-axis. The top plots show the total spectrum averaged over all possible core-hole sites.

5.2.3. Hydrogen passivation

The relaxed structures of ZGNRs with the different number of hydrogen atoms bonded to the edge carbon atom are shown in Figure 4.10. In this section, by performing EELS calculations systematically, we demonstrate the effect of hydrogen modification at the edge on the EELS spectra, and analyse the results in terms of the electronic states.

Figure 5.17 shows the total EELS spectra of 3-ZGNR with non-passivation for reference purposes, mono-hydrogenation and di-hydrogenation. The number of hydrogen atoms bonded to each edge carbon atom has a dramatic influence on the EELS spectra. Each spectrum can be clearly distinguished. Especially, the first peak at the non-passivated ribbon is greatly decreased by mono-hydrogenation. Additionally, the first peak vanishes completely by adding one more hydrogen atom on mono-hydrogenated edge carbon atom. In di-hydrogenated ribbon, two prominent peaks appear between π^* and σ^* peaks. They are also identifiable features. In order to proceed with a detailed analysis, we focus on atom-resolved EELS spectra in each spectrum.

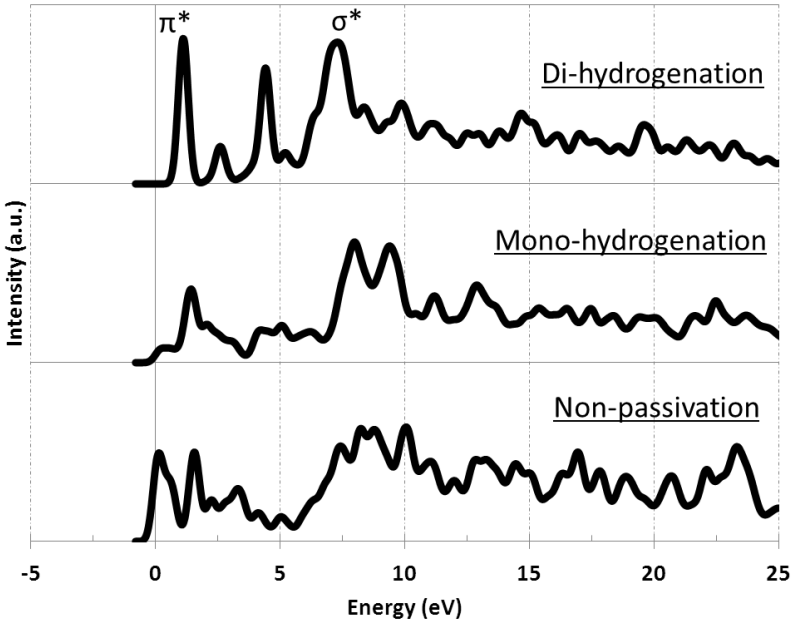

Figure 5.17: Total EELS spectra of 3-ZGNR with non-passivation for reference purposes, mono-hydrogenation and di-hydrogenation.

5.2.3.1. Mono-hydrogenation

Figure 5.18 shows (a) the relaxed structure of the monohydrogen passivated 3-ZGNR and (b) the atomic resolved EELS spectra. In this case, the independent core-holes are inserted into three distinct atomic sites in different environments. The EELS calculations were performed for each atomic site. Each spectrum was normalised by the area under the EELS spectra so that total integrated EELS =1. A total spectrum is obtained by averaging over the individual site resolved spectra. Figure 5.19 shows the polarised results of EELS calculations with the polarised electric field oriented in the direction of the (a) X, (b) Y and (c) Z-axis respectively. In graphene sheet, when the direction of applied electric field is X and Y axis, transition into the anti-bonding σ* states are allowed. When

the direction of applied electric field is Z axis, transitions into the anti-bonding π* states are allowed.

The π* and σ* peak are clearly observed in the total EELS spectrum as seen in Figure 5.18. These peaks also can be seen in the polarised spectra for directions of Z axis and X-Y plane in Figure 5.19, respectively. The peak below π* peak in total spectrum is considered the transition into the unoccupied edge state and the intensity is extremely reduced due to the elimination of dangling bonds by hydrogen passivation. The peaks (dashed circle) between the π* and σ* peaks are labelled "M" in the total spectrum in Figure 5.18. These M-peaks are predicted to be attributable to the transition into C-H anti-bonding state, because these peaks are not present in non-passivated ZGNRs. However, the atom-resolved EELS spectra show that these M-peaks also relate to two sites, other than the edge atom where hydrogen atoms have been added. Hence, the M-peaks cannot be assigned to pure σ*(C-H). Here, we focus on the polarised EELS in order to perform a detailed analysis of these peaks. In Figure 5.19 (a) X-direction, the peaks (dashed circle) belonging to the same area as the M-peaks are observed at the edge atom. These peaks can be attributed to pure σ*(C-H) due to the direction of C-H bonding and are the identifiable feature for monohydrogenated GNRs. Meanwhile the peaks belonging to the same area as the M-peaks are observed at all three site in Figure 5.19 (c) Z-direction. These peaks are considered attributable to π* peaks due to the direction of polarisation. Based on the above analysis, the peaks, labelled "M" in the total spectrum can be assigned to the unoccupied mixture state of π* and σ*(C-H).

Figure 5.20 shows the projected density-of-states (PDOS) for excited edge carbon atom in monohydrogen passivated 3-ZGNR. In order to compare the peaks, the atom-resolved EELS spectrum for the same atom is shown in the upper plot. As discussed in the

previous section 5.1.2, by reference to PDOS, the origins of π* and two σ* peaks can be confirmed by atomic orbitals, and the validity of the peak assignments can be supported.

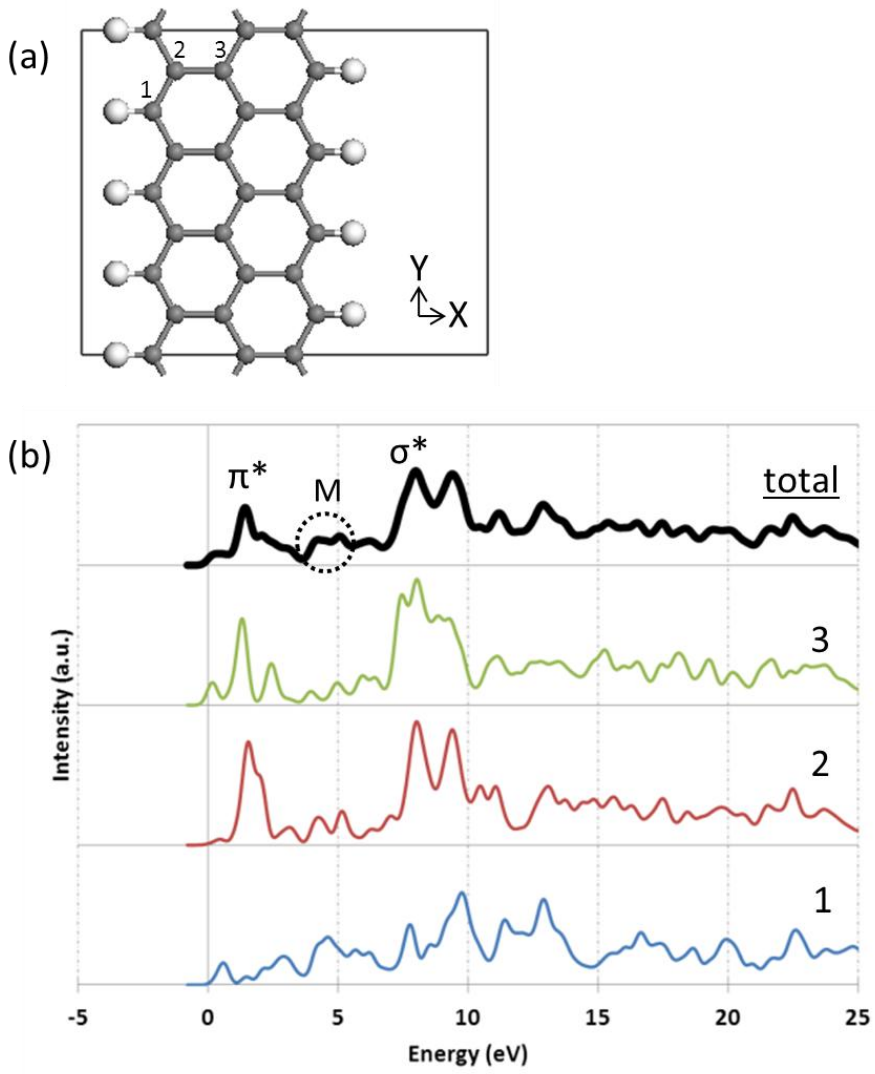

Figure 5.18: (a) A relaxed structure of mono-hydrogen passivated 3-ZGNR and (b) the atom-resolved EELS spectra. The top plot shows the total spectrum averaged over all possible core-hole sites.

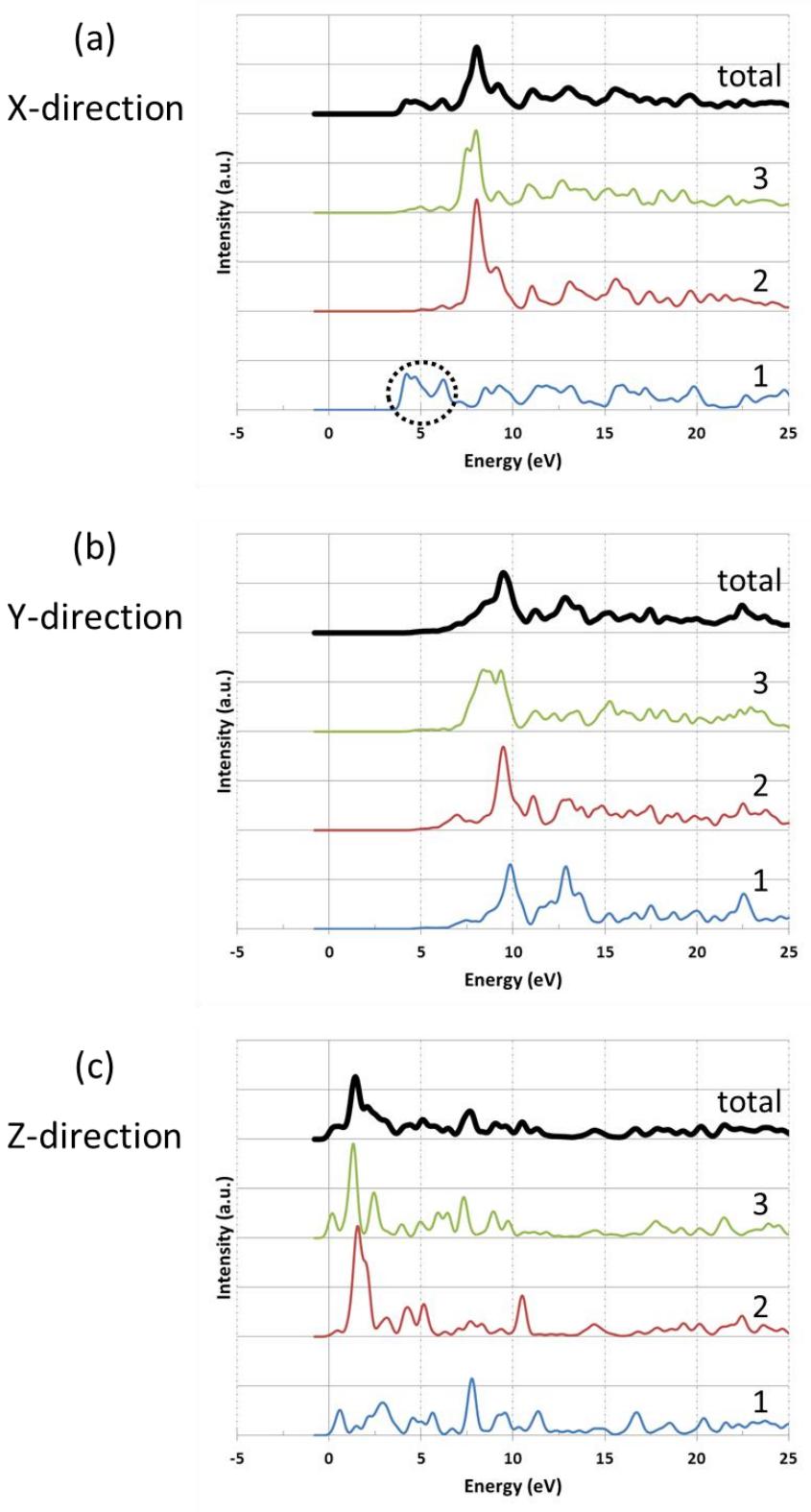

Figure 5.19: Polarised EELS spectra of monohydrogenated 5-ZGNR with (a) X-axis, (b) Y-axis, (c) Z-axis. The top plot shows the total spectrum averaged over all possible core-hole sites. The dashed circle indicates pure σ*(C-H) peaks.

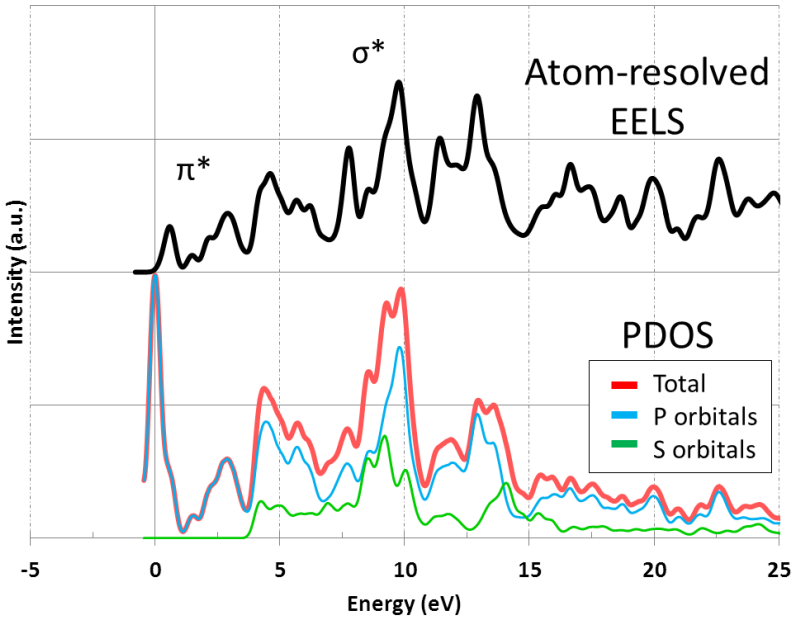

Figure 5.20: (Above) Theoretical EELS spectrum and (Below) projected density-of-states (PDOS) for excited edge carbon atom in mono-hydrogen passivated 3-ZGNR.

5.2.3.2. Di-hydrogenation

Figure 5.21 shows (a) the relaxed structure of the dihydrogen passivated 3-ZGNR and (b) the atomic resolved EELS spectra. In this case, independent core-holes were inserted into three distinct atomic sites in different environments. The EELS calculations were performed for each atomic site. Each spectrum was normalised by the area under the EELS spectra so that total integrated EELS =1. A total spectrum is obtained by averaging over the individual spectra. Figure 5.22 shows the results of EELS calculations with polarised electric field and orientation in the direction of the (a) X, (b) Y and (c) Z-axis respectively.

The π* and σ* peaks are clearly observed in the total EELS spectrum as seen in Figure 5.21. These peaks also can be seen in the direction of Z axis and X-Y plane in Figure 5.22, respectively. The two peaks between π* and σ* peak are labelled by D1 and D2 in the total spectrum. These peaks mainly come from the edge site atom. The π* peak vanishes at the edge site due to the sp3 carbon atom bonded to two hydrogen and two carbon atoms. The two prominent peaks corresponding to D1 and D2 appear below the σ* peak. These peaks can be seen in (a) X-direction and (c) Z-direction in Figure 5.22. These directions correspond to the directions of two C-H bonds connected to the edge carbon atom and assigned to σ*(C-H) peak. The D1 peak is also related to two inner carbon sites although the contribution is small. The corresponding peaks at these atoms are observed only in Figure 5.22 (c) Z-direction. Therefore, these peaks can be assigned to split π* peak. Judging from these results, the D1 peak in total spectrum can be assigned to the unoccupied mixture state of π* and σ*(C-H). The D2 peak can be assigned to pure σ*(C-H) peak.

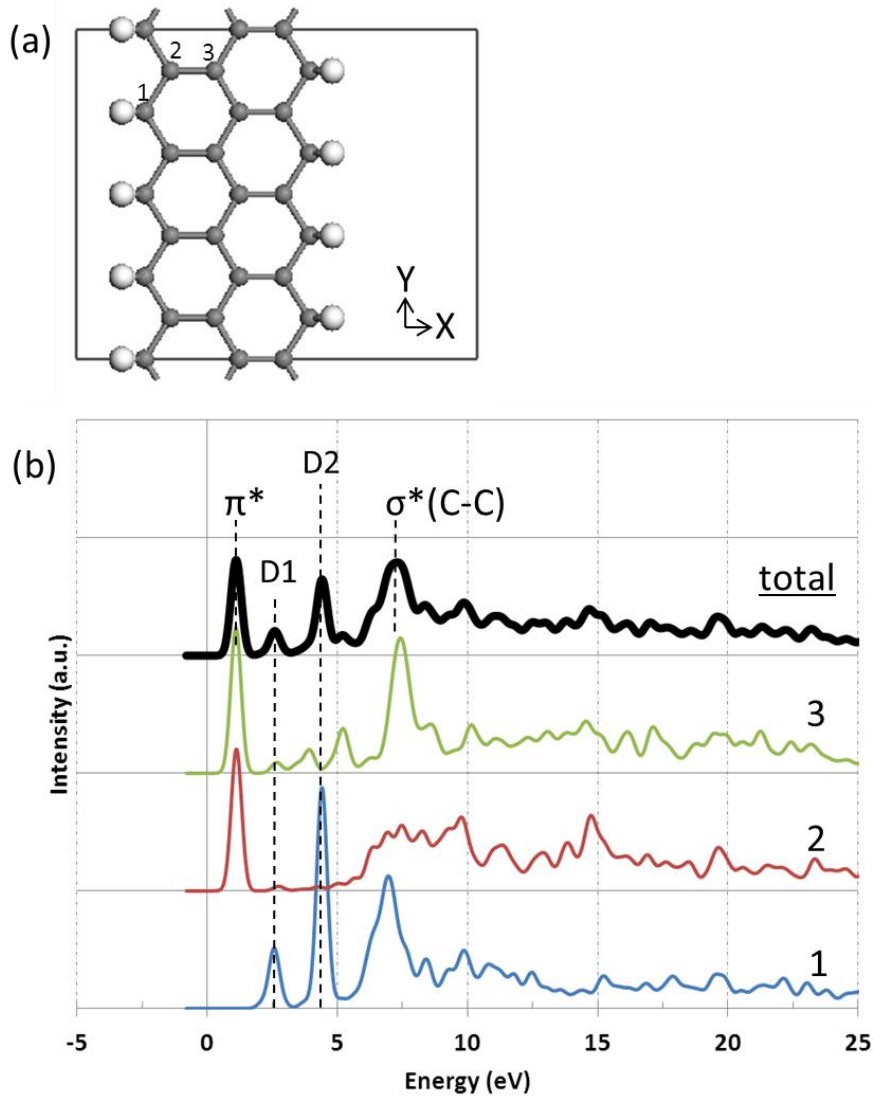

Figure 5.21: (a) Relaxed structure of di-hydrogenated 3-ZGNR (b) the atom-resolved EELS spectra. The top plot shows the total spectrum averaged over all possible core-hole sites.

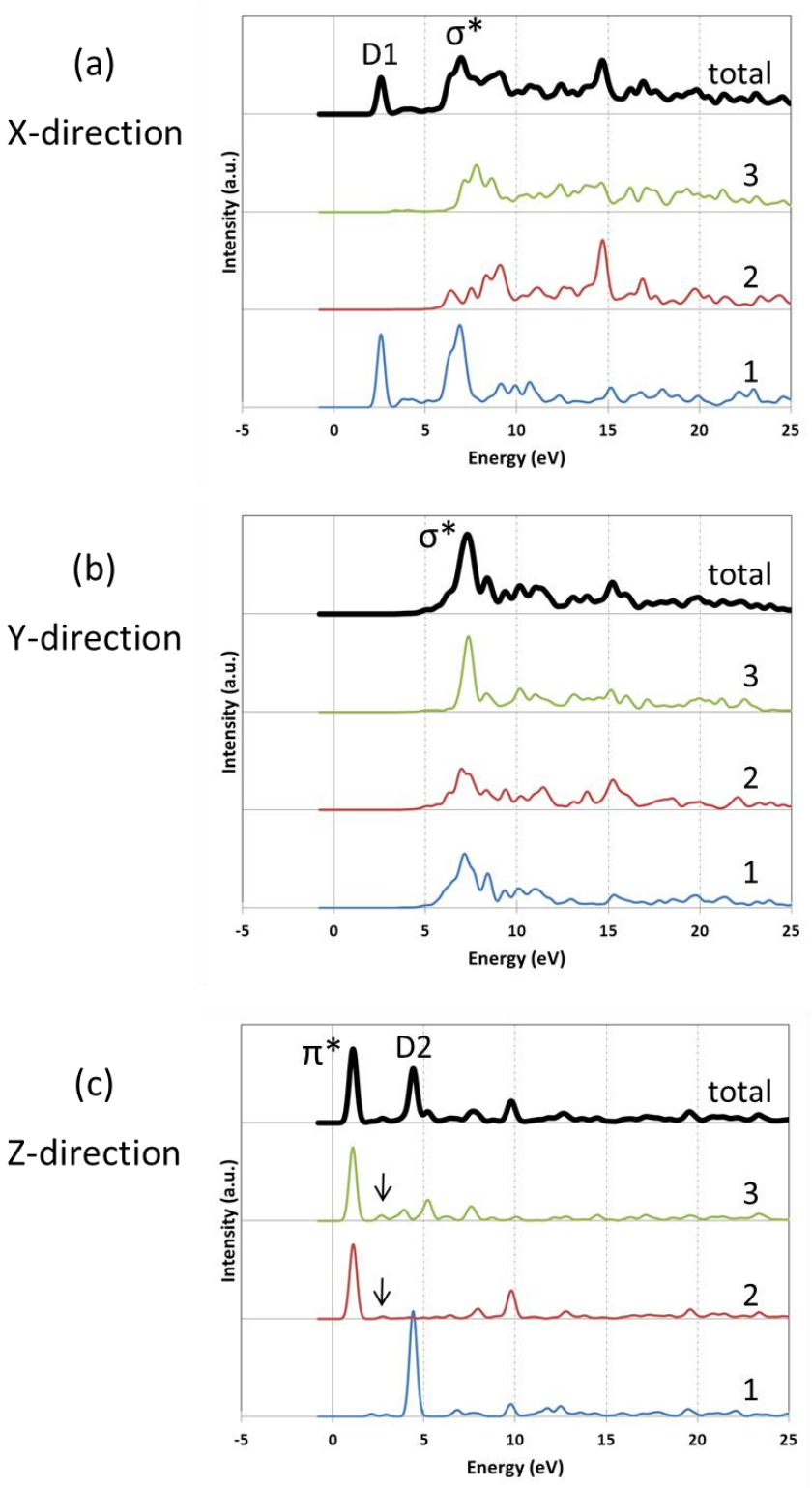

Figure 5.22: Polarised EELS spectra of di-hydrogenated 5-ZGNR with (a) X-axis, (b) Y-axis, (c) Z-axis. The top plots show the total spectra averaged over all possible core-hole sites.

5.2.4. Klein edge GNRs

As described in section 4.2.4, the trihydrogenated edge is the most stable Klein edge. In this section, we report the EELS spectra of this most stable Klein edge structure. Figure 5.23 shows (a) the relaxed structure of the 3-ZGNR with trihydrogenated Klein edge and (b) the atomic resolved EELS spectra. In this case, the core-hole was inserted into four distinct atoms in different environments. The EELS calculations were performed for each atom. Each spectrum was normalised by the area under the EELS spectra so that total integrated EELS =1. A total spectrum is obtained by averaging over the individual spectra. Figure 5.24 shows the results of EELS calculations with polarised electric field and orientation in the direction of the (a) X, (b) Y and (c) Z-axis respectively.

The σ* peak is clearly observed in the total EELS spectrum as seen in Figure 5.23. These peaks also can be seen in the X-Y plane in Figure 5.24. The first strong peaks at inner carbon sites labelled 3 and 4 are assigned to π* peaks. The peak at around 2 eV in total EELS spectrum is composed of these π* peaks. Therefore, the peak at around 2 eV in total EELS spectrum can be assigned to π* peak. The two peaks between π* and σ* peak are labelled by K1 and K2 in the total spectrum. These peaks mainly come from edge site atom. At the spectrum from the edge site, the π* peak vanishes because the edge atom is sp3 carbon atom bonded to three hydrogen atoms and one carbon atom. The two prominent peaks corresponding to K1 and K2 appear below the σ* peak. These peaks can be seen in the X-Y plane and mainly (c) Z-direction in Figure 5.24, respectively. These directions correspond to the directions of two C-H bonds connected to the edge carbon atom and assigned to σ*(C-H) peak. The K1 and K2 peak are also related to the inner carbon sites. The corresponding peaks at these atoms are observed only in Figure 5.24

(c) Z-direction. Therefore, these peaks can be assigned to split π* peak. Judging from these results, the K1 and K2 peak in total spectrum can be assigned to transition into the unoccupied mixture state of π and σ(C-H) bond.

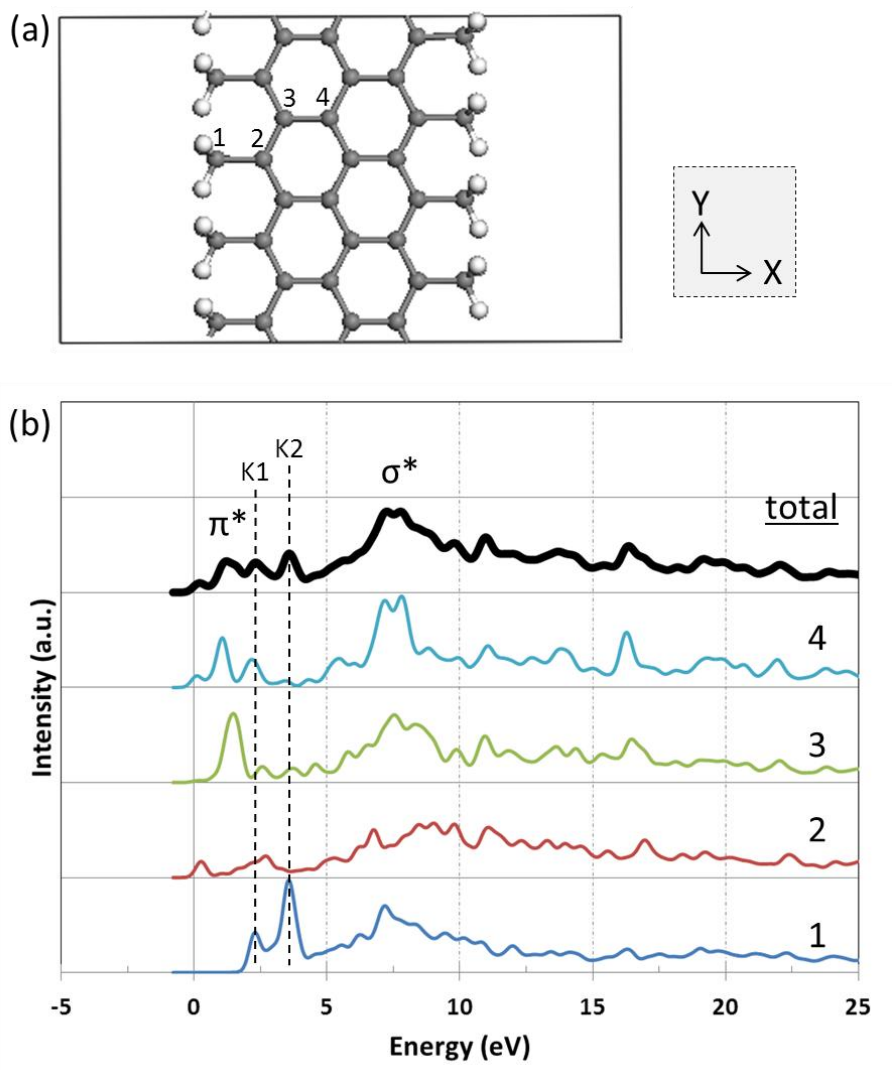

Figure 5.23: (a) A relaxed structure of 3-ZGNR with trihydrogenated Klein edge and (b) the atom-resolved EELS spectra. The top line is the total spectrum.

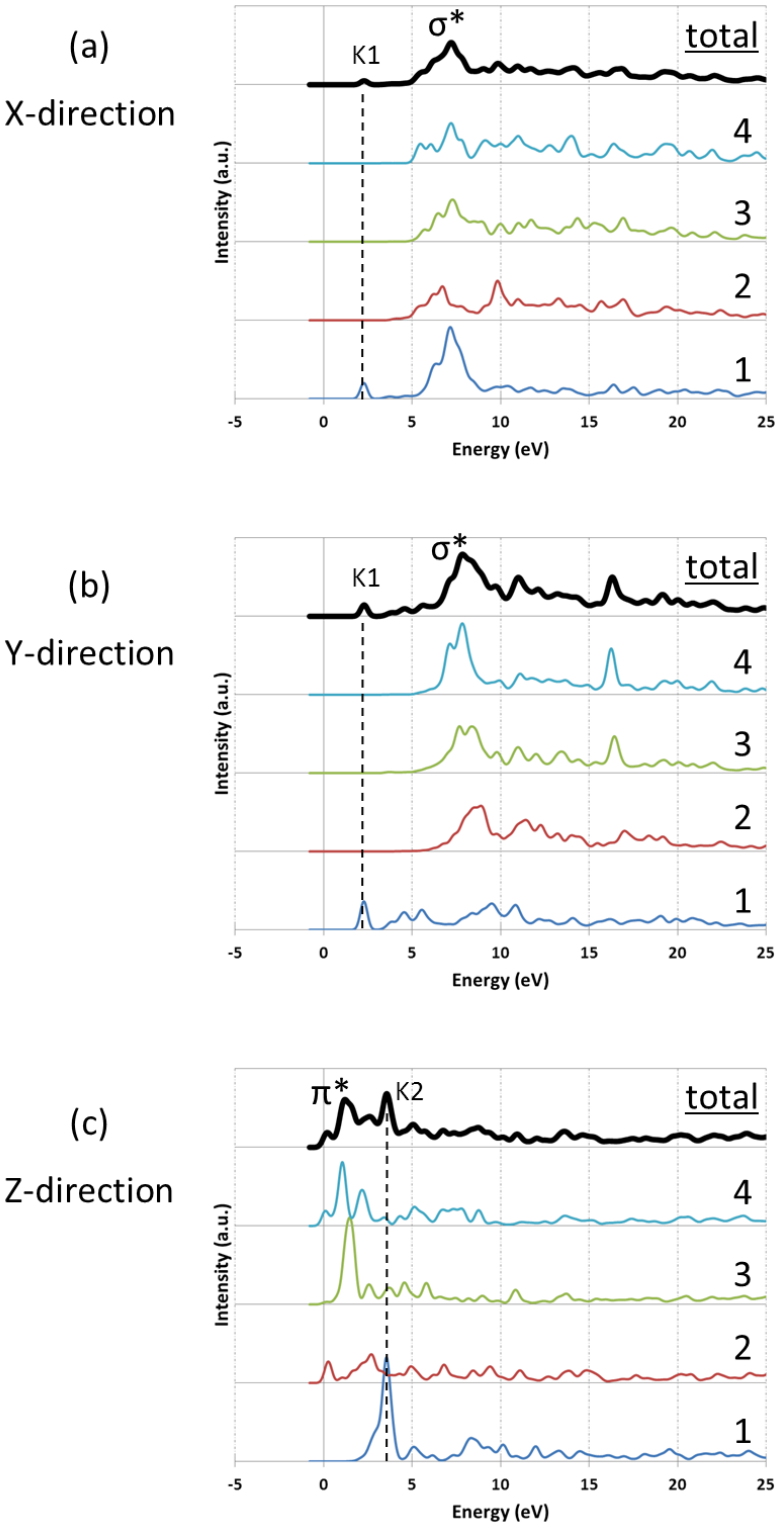

Figure 5.24: Polarised EELS spectra with the direction (a) X-axis, (b) Y-axis, (c) Z-axis.

5.3. Conclusion

In conclusion, we have reported the first systematic study of EELS spectra of GNRs. Our results reveal that spectral features are largely affected by the atomic site, ribbon width, edge-shape and edge modification. Using these spectral differences, EELS spectra can be a useful tool for analysis. In particular, in anisotropic materials such as GNRs, EELS spectra obtained from polarised condition can be used as a fingerprint for detailed information. For instance, in the case of triple bonds, the first sharp peak at the edge carbon atom in polarised EELS along the x-direction is the identifiable feature as seen in Figure 5.3 (a) and Figure 5.16 (a). In case of hydrogenation, the first peak at the edge carbon atom in polarised EELS along the direction corresponding to the orientation of the C-H bonding is the identifiable feature as seen in Figure 5.7 (a) (b), Figure 5.19 (a) and Figure 5.22 (a) (c).

6. Summary and Future Work

6.1. Summary

In this thesis, the detailed EELS data of graphene nano-ribbons (GNRs) based on the atomic and the electronic structure were reported.

In Chapter 4, we initially focused on the bare zigzag and armchair edge as the basic structures. Then, we investigated the effect on both the structures and the magnetism of edge modifications such as hydrogen modification, reconstructed edge and the Klein edge. As a result, in both the AGNRs and the ZGNRs, the edge structures saturated with two hydrogen atoms were found to be the most stable, respectively. In particular, the armchair ribbon modified by two hydrogen atoms was found to be the most stable in all structures investigated within this work. With regard to magnetic properties, only ZGNRs unsaturated by hydrogen exhibit magnetism (antiferromagnetism).

In Chapter 5, the theoretical spectra gained from CASTEP calculations indicate that the spectral features are largely affected by the atomic site, ribbon width, edge-shape and edge modification. As an example, Figure 6.1 shows the EELS spectra of the edge carbon atoms in all types of the GNRs investigated within this work. Each ribbon width is about the same. These spectra are arranged on the basis of the results of the energetic stability in chapter 4, and the top plot is the spectrum of the edge carbon atom in the most

energetically-favourable AGNR with di-hydrogenation. In each spectrum, the characteristic peaks are identified clearly and the differences depend highly on the edge shapes and edge modifications. Using spectral differences such as these, EELS spectra can be a useful tool for structural analysis. In particular, in anisotropic materials such as GNRs, EELS spectra can be used as a fingerprint for detailed information. For instance, in the case of triple bonds, the characteristic feature appears in plane. In case of hydrogenation, the characteristic features appear in the direction corresponding to the orientation of the C-H bonding.

These results will be able to contribute to the analysis of future experimental work on GNRs.

6.2. Future work

The properties of GNRs strongly depend on the edge modification and the defects. This thesis covered non-passivated and hydrogen passivated GNRs. However, for example, GNRs with oxygen also show the property of magnetism and are getting a lot attention as organic half-metallic materials [41] [42], and other experiment shows that GNRs with nanopores have large-magnitude ferromagnetism and promises to be a graphene magnet [43]. For these materials, the EELS analysis is an appropriate tool because this technique is very sensitive to the chemical environment as we reported in this thesis. Further studies of the various ribbons investigated look promising.

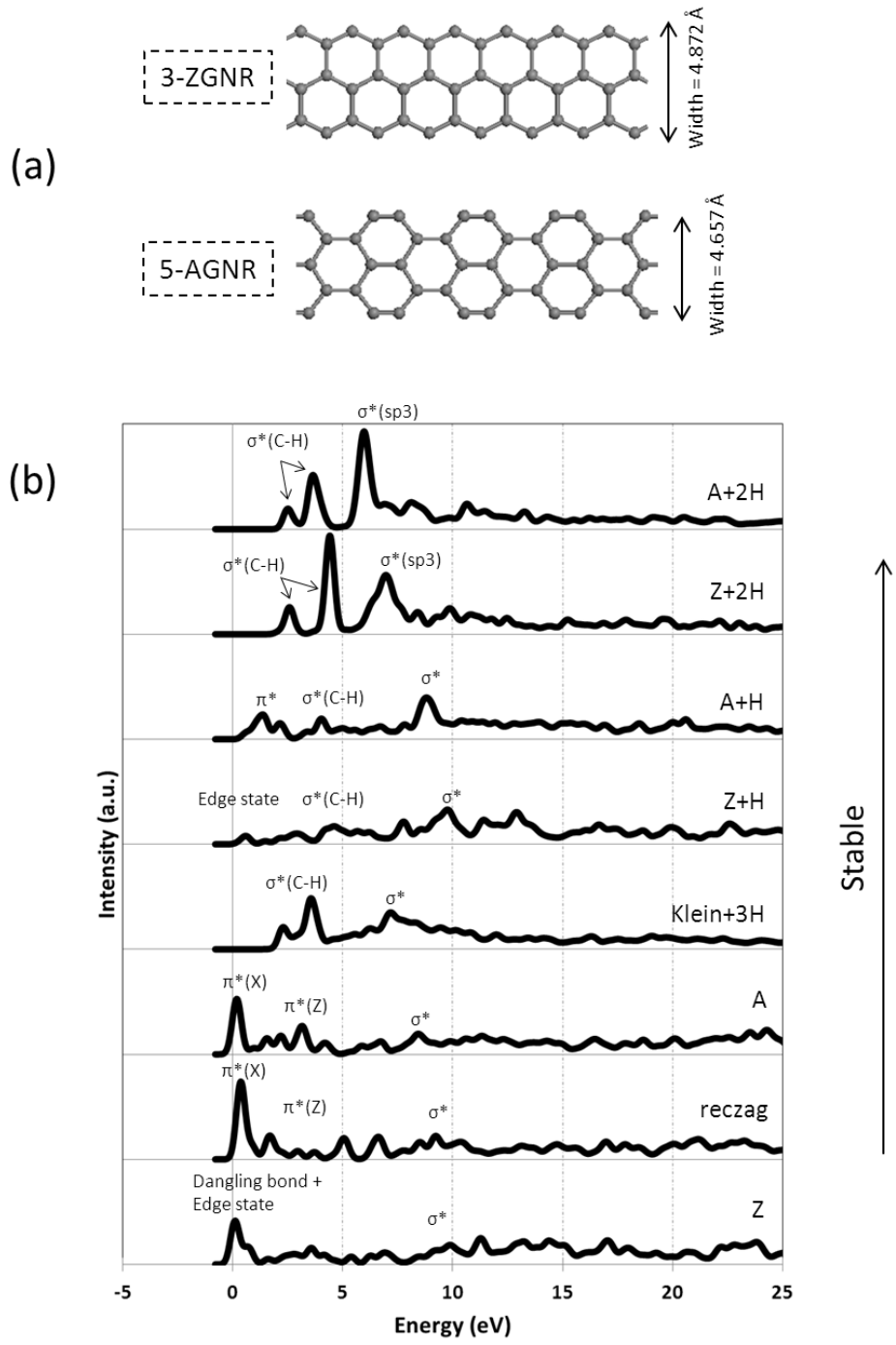

Figure 6.1: (a) A structures of 3-ZGNR and 5-AGNR and (b) the atom-resolved EELS spectra of edge carbon atoms. The spectra are arranged by the energetic stability. Klein, Z, A, reczag represent GNRs with Klein edge, zigzag edge, armchair edge and reconstructed zigzag edge, respectively. H represent hydrogen atoms added on an edge carbon atoms.

Appendix A

EELS spectra of GNRs

A.1 Non-passivated AGNRs

In section 5.1.1. the effect of the ribbon width on the EELS spectra were shown and then we focused on the ribbon width N=9 as an example. Here, we present atom-resolved EELS spectra of ribbon width N=5-8 which could not be shown.

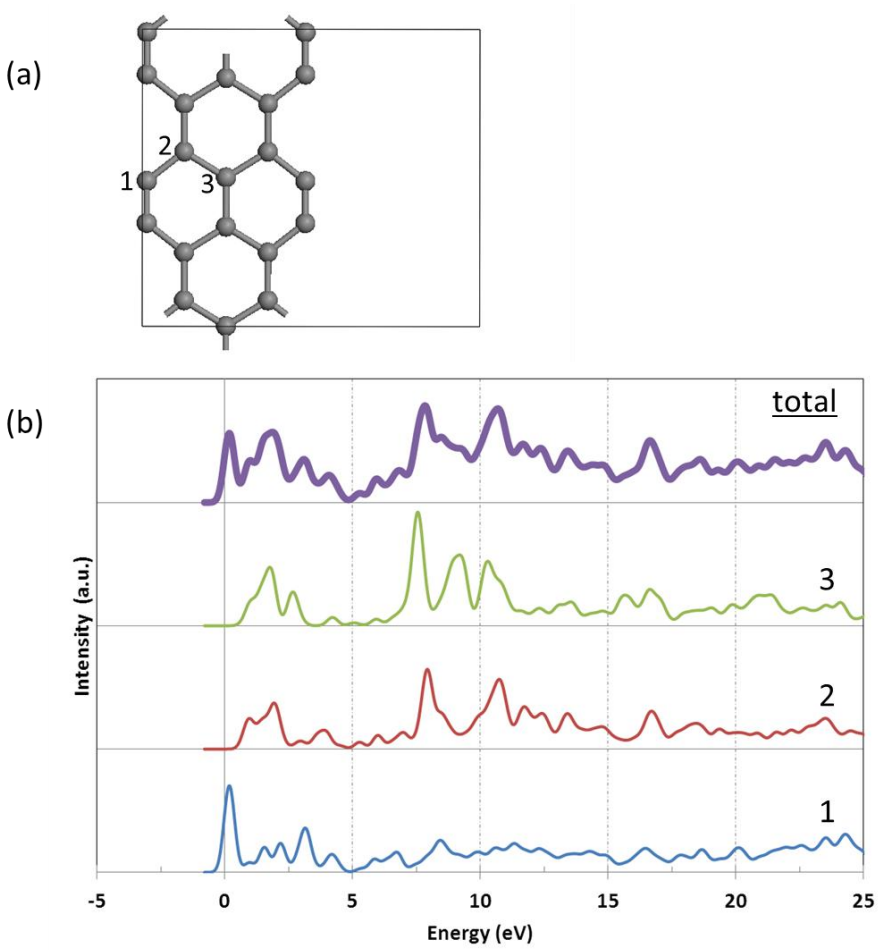

Figure A. 1: (a) The relaxed structure of non-passivated 5-AGNR and (b) EELS spectrum for each core-hole atom. The top plot shows the total spectrum averaged over all possible core-hole sites.

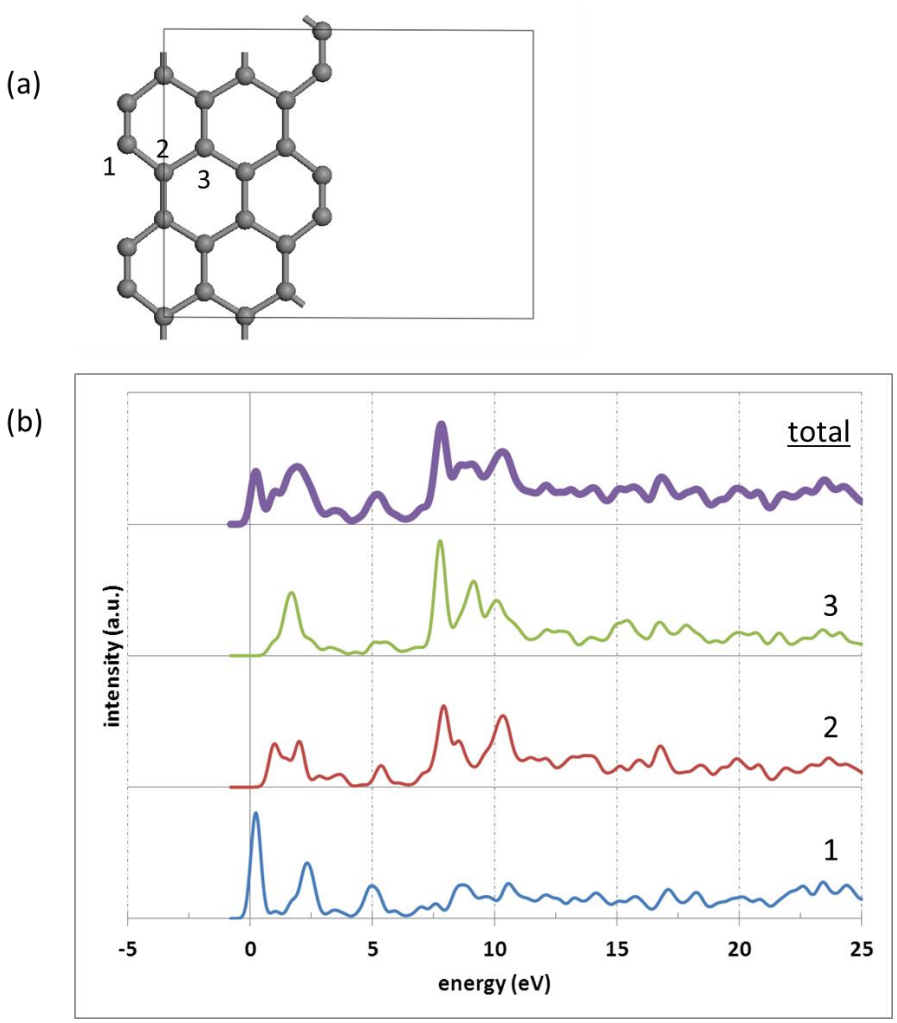

Figure A. 2: (a) The relaxed structure of non-passivated 6-AGNR and (b) EELS spectrum for each core-hole atom. The top plot shows the total spectrum averaged over all possible core-hole sites.

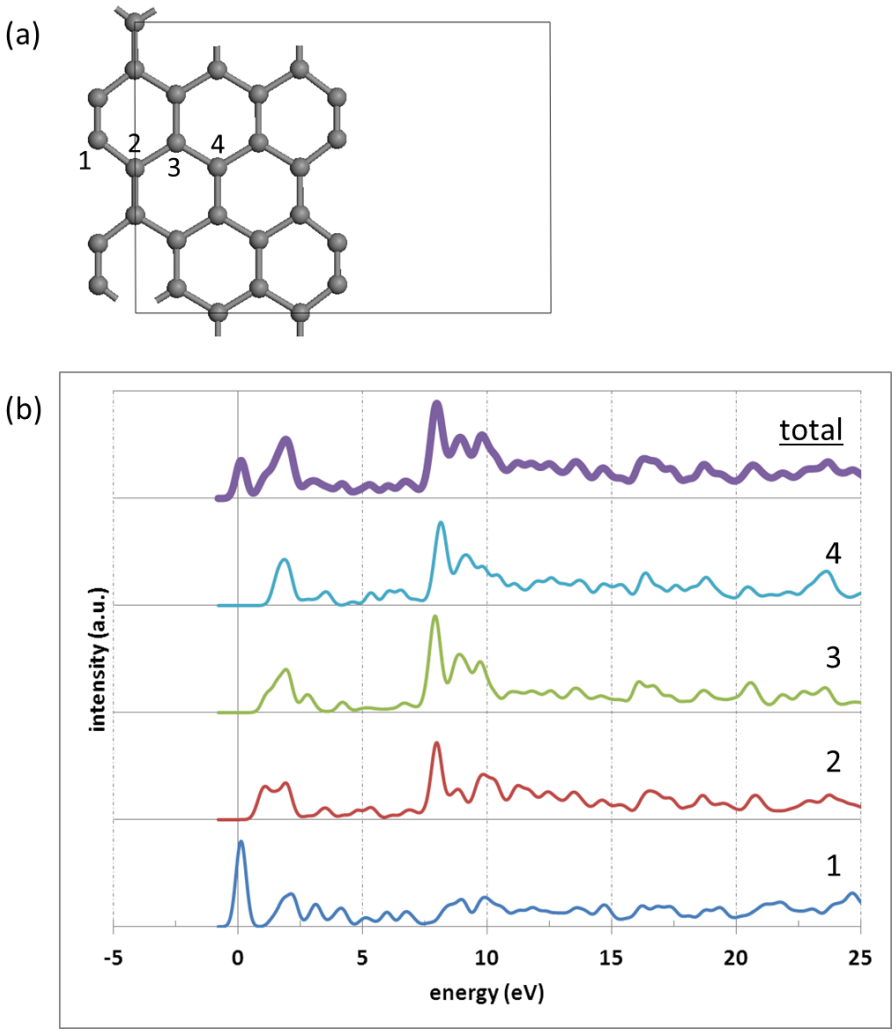

Figure A. 3: (a) The relaxed structure of non-passivated 7-AGNR and (b) EELS spectrum for each core-hole atom. The top plot shows the total spectrum averaged over all possible core-hole sites.

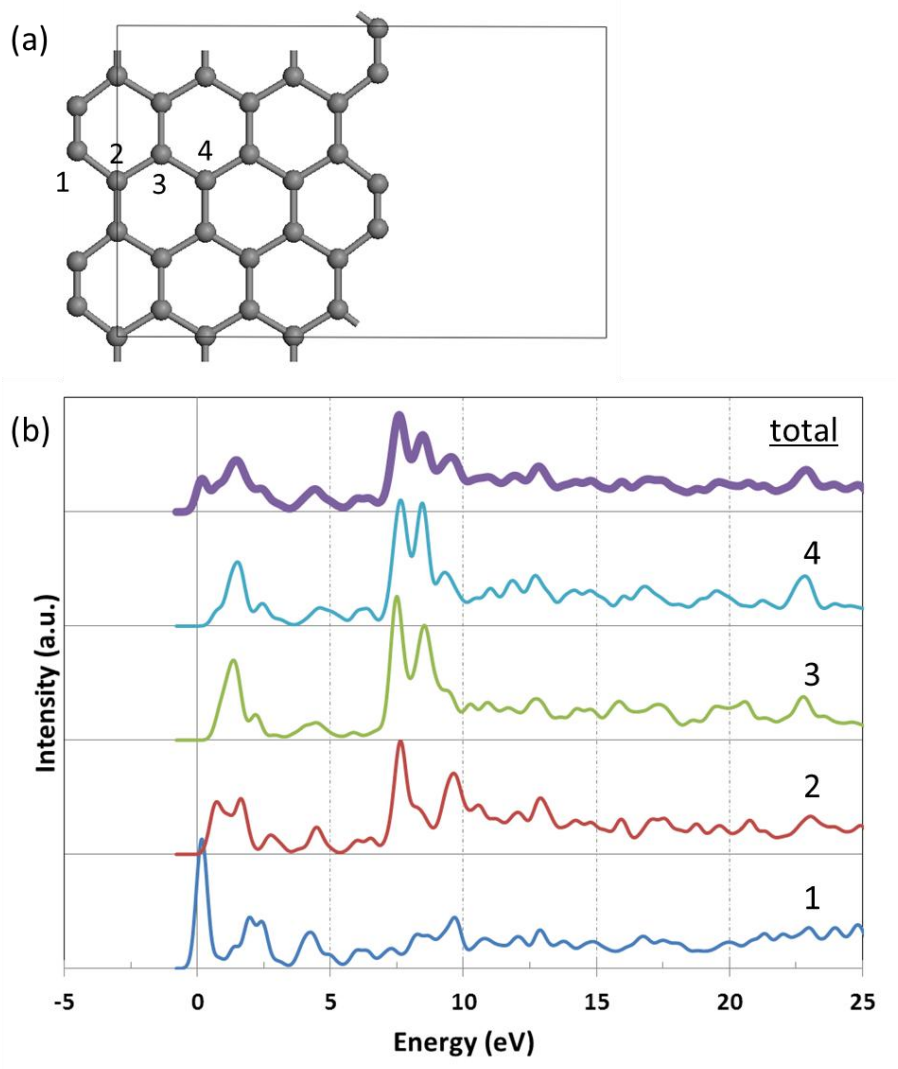

Figure A. 4: (a) The relaxed structure of non-passivated 8-AGNR and (b) EELS spectrum for each core-hole atom. The top plot shows the total spectrum averaged over all possible core-hole sites.

A.2 Non-passivated ZGNRs

In section 5.2.1. the effect of the ribbon width on the EELS spectra were shown and then we focused on the ribbon width N=4 as an example. Here, we present atom-resolved EELS spectra of ribbon width N=3, 5, 6 which could not be shown.

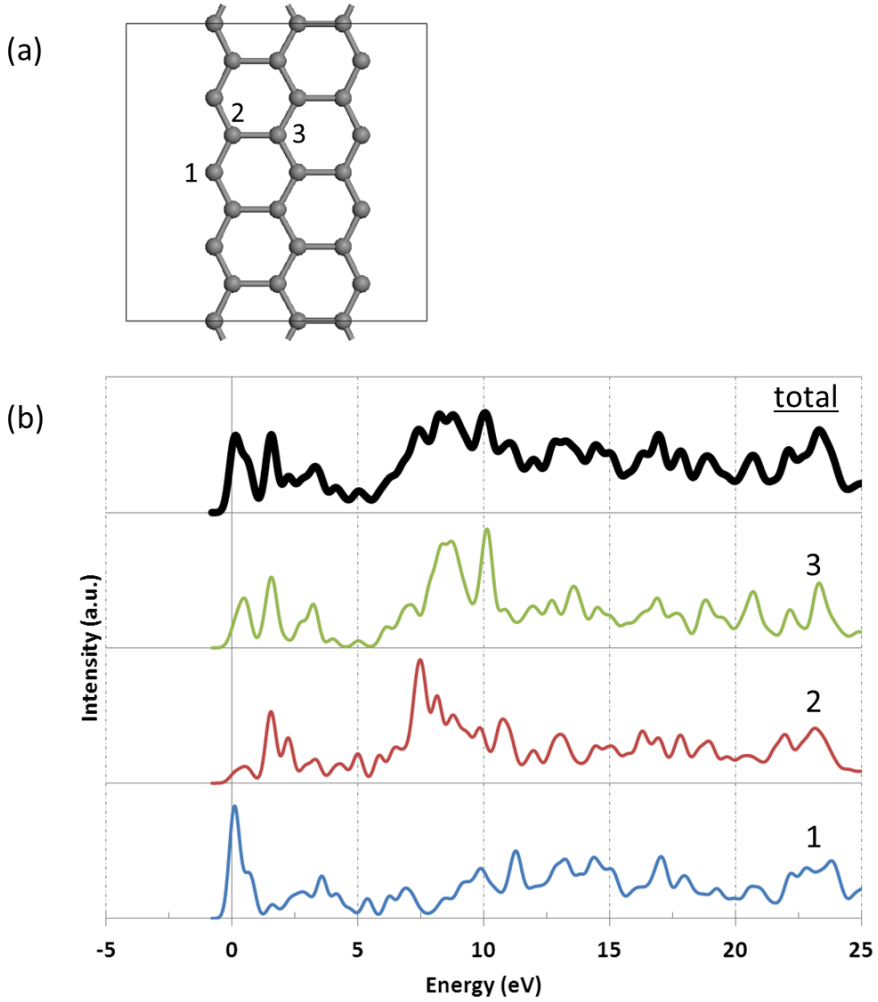

Figure A. 5: (a) The relaxed structure of non-passivated 3-ZGNR and (b) EELS spectrum for each core-hole atom. The top plot shows the total spectrum averaged over all possible core-hole sites.

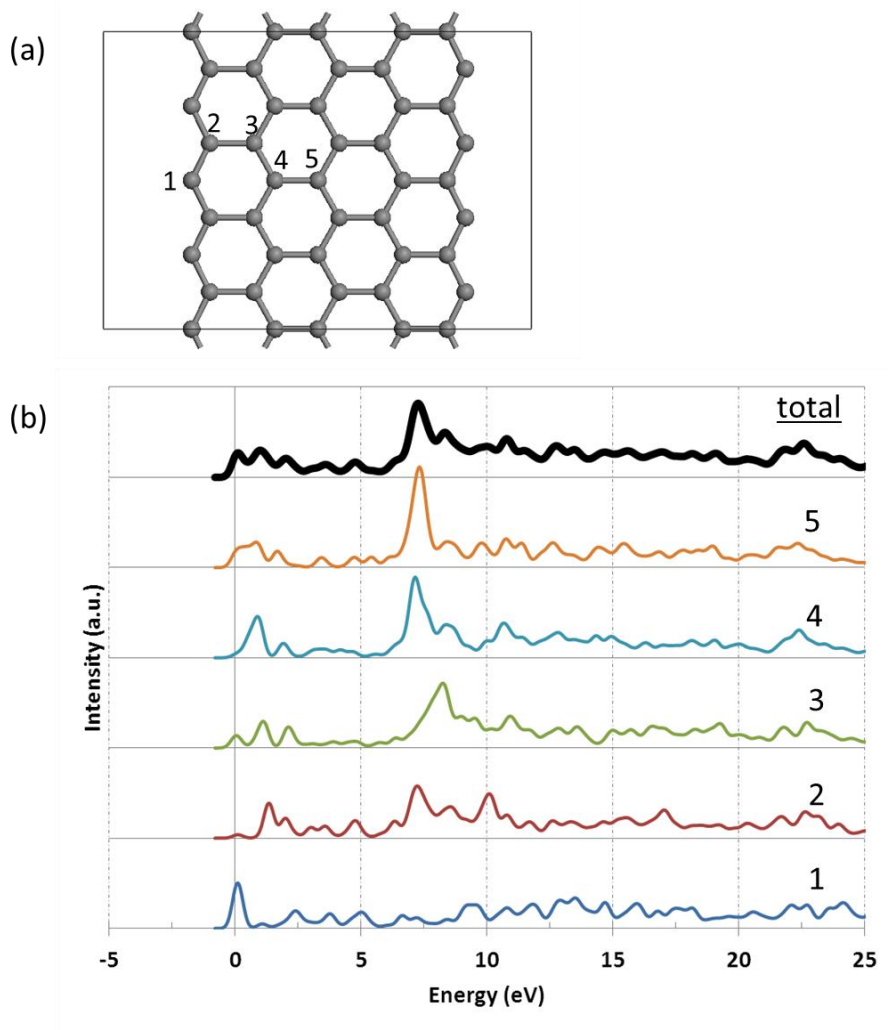

Figure A. 6: (a) The relaxed structure of non-passivated 5-ZGNR and (b) EELS spectrum for each core-hole atom. The top plot shows the total spectrum averaged over all possible core-hole sites.

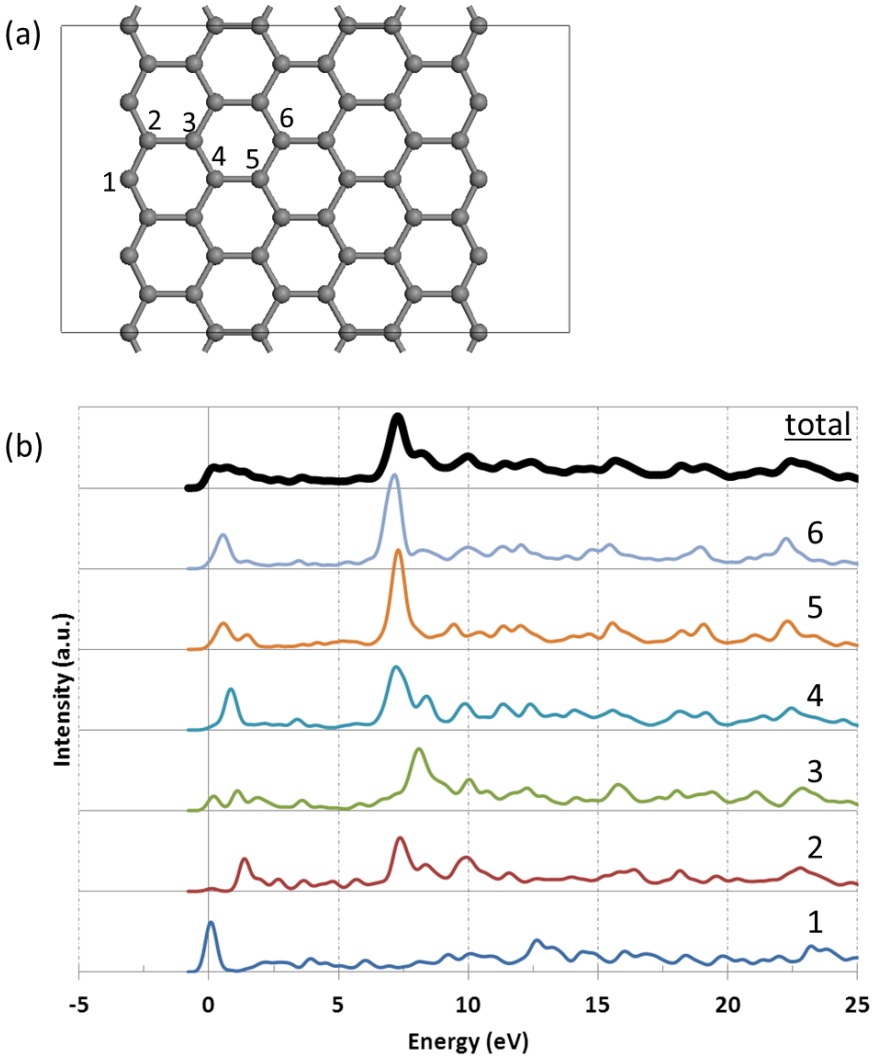

Figure A. 7: (a) The relaxed structure of non-passivated 6-ZGNR and (b) EELS spectrum for each core-hole atom. The top plot shows the total spectrum averaged over all possible core-hole sites.

Appendix B

The modelling of layer separation and vacuum gap

B.1 The effect on the total energy

In order to decide the layer distance (perpendicular to the ribbons) and vacuum gap (in-plane) in unit cells of GNR, the total energy is calculated step by step, while changing the lattice constants. Figure B.1 displays the total energy versus the lattice constants for non-passivated 4-ZGNR. Both total energies show convergence as the lattice constants increase. As a result, the total energy for layer distance and vacuum gap converged at 7 Å and 5 Å, respectively. Hence, in order to calculate isolated GNRs, in this thesis, the layer distance and the vacuum gap were set to be 7 Å and 5 Å, respectively.

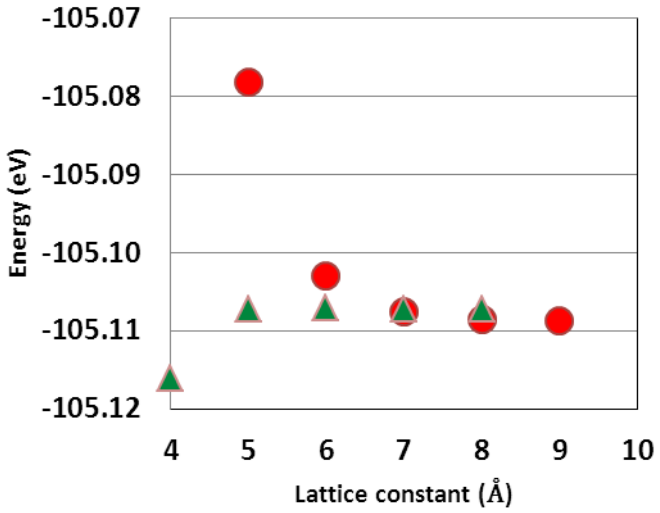

Figure B.1: Total energy versus lattice constant for non-passivated 4-ZGNR. The red circles (green triangles) represent total energy for the lattice constant along the layer (width) direction.

B.2 The effect on the EELS spectra

In this section, we discuss whether the lattice constant determined in section B.1 is also sufficient for EELS calculation. Figure B.2 shows the atom-resolved EELS spectra for non-passivated 3-ZGNR with 5 and 10 Å vacuum gaps. These two spectra at each site show very similar profiles, aside from very slight discrepancies; therefore it has been confirmed that this is also a sufficient vacuum gap for EELS calculations. Figure B.3 indicates the atom-resolved EELS spectra for non-passivated 3-ZGNR with 7 and 14 Å layer distances. These two spectra at each site mostly agree with each other except around 24eV, where some discrepancy persists. The peaks at approximately 24eV in the 7Å-layer distance model disappear in the 14Å-layer distance model. These peaks are therefore considered to be caused by interaction between adjacent layers. In order to

analyse electronic state in this region, it is necessary to further expand the layer spacing.

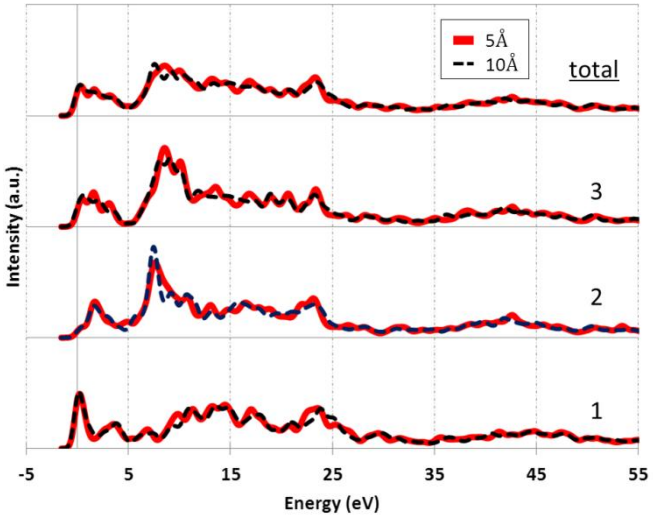

Figure B.2: The atom-resolved EELS spectra for non-passivated 3-ZGNR with 5Å (solid red line) and 10Å (dashed black line) vacuum gap.

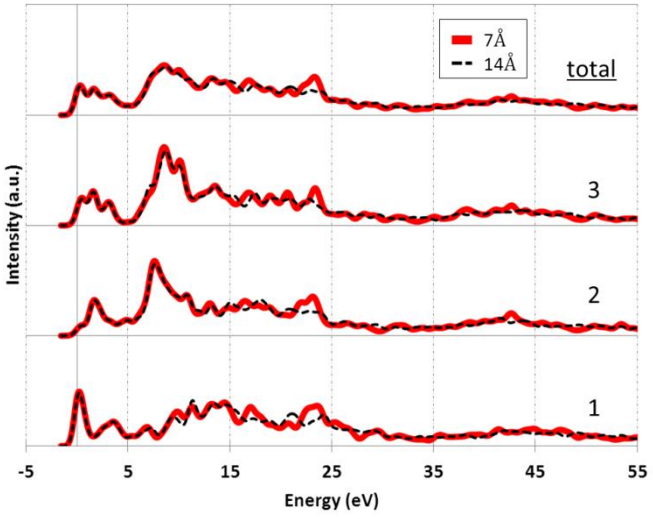

Figure B.3: The atom-resolved EELS spectra for non-passivated 3-ZGNR with 7Å (solid red line) and 14Å (dashed black line) layer distance.

References

1. C. Lee, X. Wei, J.W. Kysar, J. Hone: Measurement of the elastic properties and intrinsic strength of monolayer graphene. SCIENCE 321, 385 (JULY 2008)

2. A. A. Balandin, S. Ghosh, W. Bao, I. Calizo, D. Teweldebrhan, F. Miao, and C.N. Lau: Superior thermal conductivity of single-layer graphene. NANO LETTERS 8(3), 902-907 (2008)

3. K. I. Bolotin, K. J. Sikes, Z. Jiang, M. Klima, G. Fudenberg, J. Hone, P. Kim, H.L. Stomer: Ultra high electron mobility in suspended graphene. SOLID STATE COMMUNICATIONS 146, 351 (2008)

4. A. K. GEIM AND K. S. NOVOSELOV: The rise of graphene. NATURE MATERIALS 6, 183 (2007)

5. F. Cervantes-Sodi, G. Csányi, S. Piscanec, and A. C. Ferrari: Edge-functionalized and substitutionally doped graphene nanoribbons: Electronic and spin properties. PHYSICAL REVIEW B 77(16), 165427 (2008)

6. F. Cervantes-Sodi, G. Csanyi, S. Piscanec, and A. C. Ferrari: Electronic properties of chemically modified graphene ribbons. PHYSICA STATUS SOLIDI 245(10), 2068 – 2071 (2008)

7. J. Kunstmann, C. Ozdogan, A. Quandt, and H. Fehske: Stabilities of edge states and edge magnetism in graphene

nanoribbons. PHYSICAL REVIEW B 83 (2011)

8. Z. Liu, K. Suenaga, P. J. F. Harris, and S. Iijima: Open and Closed Edge of Graphene Layers. PHYSICAL REVIEW LETTERS 102, 015501 (2009)

9. C O.Girit, Jannik C. Meyer, Rolf Erni, Marta D. Rossell, C. Kisielowski, Li Yang, Cheol-Hwan Park, M. F. Crommie, Marvin L. Cohen, Steven G. Louie, A. Zettl: Graphene at the edge : stability and dynamics. SCIENCE 323, 1705-1708 (2009)

10. Y. Kobayashi, K. Fukui, T. Enoki, K. Kusakabe, and Y. Kaburagi: Observation of zigzag and armchair edges of graphite using scanning tunneling microscopy and spectroscopy. PHYSICAL REVIEW B 71, 193406 (2005)

11. K. Suenaga, M. Koshino: Atom-by-atom spectroscopy at grapehene edge. NATURE 468, 1088-1090 (2010)

12. Pickard, C.: Ab Initio Electron Energy Loss Spectroscopy., University of Cambridge (1997)

13. M. D. Segall, Philip J. D. Lindan, M. J. Probert, C. J. Pickard, P. J. Hasnip, S. J. Clark and M. C. Payne: First-principles simulation: ideas, illustrations and the CASTEP code. JOURNAL OF PHYSICS: CONDENSED MATTER 14, 2717–2744 (2002)

14. J. Fink: Transmission electron energy-loss spectroscopy. Topics in Applied Physics 69, 204-241 (1992)

15. R. F. Egerton: Electron Energy-Loss Spectroscopy in the Electron Microscope Third Edition edn. Springer (2011)

16. Chris G. Van de Walle, P. E. Blöchl: First-principles calculations of hyperfine parameters. PHYSICAL REVIEW B 47(8), 4244-4255 (1993)

17. P. Hohenberg and W. Kohn: Inhomogeneous electron gas. PHYSICAL REVIEW 136(3B), 864-871 (1964)

18. Richard M. Martin: Electronic Structure 1st edn. Cambridge University Press (2004)

19. D. M. Ceperley, B. J. Alder: Ground State of the Electron Gas by a Stochastic Method. PHYSICAL REVIEW LETTERS 45(7), 566-569 (1980)

20. W. Kohn and L. J. Sham: Self-Consistent Equations Including Exchange and Correlation Effects. PHYSICAL REVIEW 140(4A), A1133–A1138 (1965)

21. O. Gunnarsson, M. Jonson, B. I. Lundqvist~: Descriptions of exchange and correlation effects in inhomogeneons electron systems. PHYSICAL REVIEW B 20, 3136 (1979)

22. N. W. Ashcroft and N. D. Mermin: Solid State Physics. Thomson Learning (1976)

23. Hendrick J. Monkhorst and James D. Pack: Special points for Brillouin -zone integrations. PHYSICAL REVIEW B 13(12), 5188–5192 (1976)

24. P. Blaha, K. Schwarz, G. Madsen, D. Kvasnicka, J. Luitz: An Augmented Plane Wave Plus Local Orbitals Program for Calculating Crystal Properties. User's Guide, Vienna University of Technology, Vienna/Austria (2012)

25. H. Adachi, M. Tsukada and C. Satoko: Discrete Variational Xα Cluster Calculations. I. Application to Metal Clusters. Journal of the Physical Society of Japan 45, 875-883 (1978)

26. C. R. Seabourne, A. J. Scott, R. Brydson, R. J. Nicholls: A systematic approach to choosing parameters for modelling fine structure in electron energy-loss spectroscopy. Ultramicroscopy 109, 1374-1388 (2009)

27. M. H. Lee, J. S. Lin, M. C. Payne, V. Heine, V. Milman, S. Crampin: Kinetic energy tuning for optimising pseudopotentials and projector reduction. PSI-K NEWSLETTER 67, 145 (1994)

28. Y. Baskin and L. Meyer: Lattice Constants of Graphite at Low Temperatures. PHYSICAL REVIEW 100, 544–544 (1955)

29. K. Haruna, H. Maeta: Thermal expansion of synthetic diamond single crystals at low temperatures. DIAMOND AND RELATED MATERIALS 2, 859-861 (1993)

30. J. Yuan, L.M. Brown: Investigation of atomic structures of diamond-like amorphous carbon by electron energy loss spectroscopy. MICRON 31, 515-525 (2000)

31. M. Fujita, K. Wakabayashi, K. Nakada, K. Kusakabe: Peculiar Localized State at Zigzag Graphene Edge. JOURNAL OF THE PHYSICAL SOCIETY OF JAPAN 65(7), 1920-1923 (1996)

32. T. Wassmann, A. P. Seitsonen, A. M. Saitta, M. Lazzeri, and F. Mauri: Structure, Stability, Edge States, and Aromaticity of Graphene Ribbons. PHYSICAL REVIEW LETTER 101, 096402 (2008)

33. A. M. Saitta, T. Wassmann: Structure and stability of graphene

nanorobbons in oxygen, carbon dioxide, water, and ammonia. PHYSICAL REVIEW B 82, 115425 (2010)

34. T. Kawai, Y. Miyamoto, O. Sugino, Y. Koga: Graphitic ribbons without hydrogen-termination: Electronic structures and stabilities. PHYSICAL REVIEW B 62(24), R16349–R16352 (2000)

35. Stone AJ, Wales DJ: Theoretical Studies of Icosahedral C60 and Some Related Species. CHEMICAL PHYSICS LETTERS 128, 501 (1986)

36. P. Koskinen, S. Malola, and H. Hakkinen: Self-passivationg Edge Reconstructions of Graphene. PHYSICAL REVIEW LETTER 101, 115502 (2008)

37. P. Koskinen, S. Malola, and H. Hakkinen: Evidence for graphene edge beyond zigzag and armchair. PHYSICAL REVIEW B 80, 073401 (2009)

38. Klein, D.: Graphitic polymer strips with edge states. CHEMICAL PHYSICS LETTERS 217(3), 261–265 (1994)

39. Y. Kobayashi, K. Fukui, and T. Enoki: Edge state on hydrogen-terminated graphite edges investigated by scannning tunneling microscopy. PHYSICAL REVIEW B 73, 125415 (2006)

40. Z. Hou, X. Wang, T. Ikeda, S. Huang, K. Terakura, M. Boero, M. Oshima , M. Kakimoto, and S. Miyata: Effect of Hydrogen Terminatin on Carbon K-Edge X-ray Absorption Spectra of Nanographene. THE JOURNAL OF PHYSICAL CHEMISTRY C 115, 5392-5403 (2011)

41. Y. Son, M. L. Cohen & S. G. Louie: Half-metallic graphene

nanoribbons. NATURE 444, 347-349 (2006)

42. Hod O, Barone V, Peralta JE, Scuseria GE: Enhanced half-metallicity in edge-oxidized zigzag graphene nanoribbons. NANO LETTERS 7(8), 2295-2299 (2007)

43. K. Tada, J. Haruyama, H. X. Yang, M. Chshiev, T. Matsui, and H. Fukuyama: Ferromagnetism in Hydrogenated Graphene Nanopore Arrays. PHYSICAL REVIEW LETTERS 107, 217203 (2011)